Investigative Modeling of PM2.5 Episodes in the San Joaquin Valley Air Basin during Recent Years

REPORT TO THE

California Air Resources Board Research Division

Project # 15-301

Prepared by:

Dr. Michael J. Kleeman
Dr. Anikender Kumar
Abhishek Dhiman

Department of Civil and Environmental Engineering
University of California, Davis
One Shields Avenue, Davis, CA, 95616

February 26, 2019

DISCLAIMER

The statements and conclusions in this report are those of the contractor and not necessarily those of the California Air Resources Board. The mention of commercial products, their source, or their use in connection with material reported herein is not to be construed as actual or implied endorsement of such products.

ACKNOWLEDGEMENTS

The authors thank William Vance at the California Air Resources Board for his help with project management.

The authors thank Jeremy Avise, James Chen, and Dazhong Yin at the California Air Resources Board for their help with soil moisture availability parameterizations.

Portions of the current report were completed with support from California Air Resources Board Project #14-753.

TABLE OF CONTENTS

ACKNOWLEDGEMENTS i
LIST OF TABLES iv
LIST OF FIGURES iv
LIST OF ACRONYMS vii
ABSTRACT ix
EXECUTIVE SUMMARY x
1 INTRODUCTION 1
1.1 Motivation 1
1.2 Research Objectives 1
1.3 Hypotheses 2
1.4 Report Structure 2
2 TOTAL REACTIVE NITROGEN PREDICTIONS vs. MEASUREMENTS 4
2.1 Introduction 4
2.2 Methods 4
2.2.1 WRF Model Configuration 4
2.2.2 Air Quality Model Configuration 5
2.2.3 Emissions 6
2.2.4 Boundary Conditions 6
2.2.5 Measurements for Model Evaluation 6
2.3 Results 7
2.3.1 Spatial Distribution of Total Reactive Nitrogen 7
2.3.2 Spatial Distribution of Total Ammonia 9
2.3.3 Spatial Distribution of Nitrate Fraction of Total Reactive Nitrogen 11
2.3.4 Long-Term Trends in Total Reactive Nitrogen 13
2.4 Conclusions 14
3 OPTIMUM BOUNDARY LAYER CONFIGURATION FOR WRF SIMULATIONS DURING WINTER STAGNATION EVENTS 15
3.1 Introduction 15
3.2 Description of three PBL schemes 15
3.3 Description of model configuration and Evaluation of data 16
3.4 Results and Discussion 18
3.5 Conclusions 22
4 EFFECT OF INCREASING SOIL MOISTURE ON HUMIDITY AND PARTICULATE NITRATE FORMATION 23
4.1 Introduction 23
4.2 Methods 23
4.2.1 WRF Configuration 23
4.2.2 Air Quality Model Configuration 24
4.2.3 Emissions 24
4.2.4 Boundary Conditions 25
4.3 Results 25
4.3.1 Meteorological Predictions 25
4.3.2 Nitrate Predictions 28
4.4 Conclusions 31

5 EFFECT OFCANDIDATE SOIL NOx EMISSIONS, MODEL VERTICAL RESOLUTION, AND ORGANIC-NITRATE FORMATION ON PREDICTED .... NITRATE VERTICAL DISTRIBUTIONS 32
5.1 Introduction 32
5.2 Methods 34
5.2.1 Air Quality Model 34
5.2.2 Emissions 35
5.2.3 Meteorology and Initial / Boundary Conditions 37
5.2.4 Gas Phase Chemistry 37
5.2.5 Organic Aerosol Treatment 38
5.2.6 Discover-AQ Field and Aircraft Observations 38
5.3 Results 39
5.3.1 Ground Level Time Series and Diurnal Profiles 39
5.3.2 Vertical profiles 45
5.3.3 Resolving the Nocturnal Residual Layer and Nitrate Late Morning Peak . 48
5.4 Conclusions 57
6 EFFECT OF CANDIDATE SOIL NOx EMISSIONS ON LONG-TERM ..... PREDICTIONS OF PARTICULATE NITRATE AND OZONE..... IN CALIFORNIA 58
6.1 Introduction 58
6.2 Methods 59
6.2.1 WRF Configuration 59
6.2.2 Air Quality Model Configuration 59
6.2.3 Emissions 59
6.2.4 Boundary Conditions 60
6.3 Results 60
6.3.1 Performance Statistics For $PM_{2.5}$ Nitrate In Years 2010, 2013, and 2015 60
6.3.2 $PM_{2.5}$ Nitrate Concentrations in 2010, 2013, and 2015 63
6.3.3 NOx Concentrations in 2010, 2013, and 2015 64
6.3.4 Spatial Distribution of $PM_{2.5}$ Nitrate and NOx in January 2010, 2013, ... and 2015 67
6.3.5 Performance Statistics For Ozone and NOx In July of Years 2010, ... 2013, and 2015 71
6.3.6 Spatial Distribution of O_3 and NOx in July 2010, 2013, and 2015 73
6.4 Conclusions 76
7 CONCLUSIONS 77
7.1 Summary of Results 77
7.2 Future research 78
8 REFERENCES 79

LIST OF TABLES

Table 3-1: Combinations of all the WRF runs which include three PBL schemes, ... two land surface schemes and two different datasets used for initial and boundary conditions 18

Table 5-1: Description of all 4 test cases formulated to test Hypothesis 2 and 3. 34

Table 5-2: Emission spiltiing ratios of added species SOAALK, NAPHTHAL, PROPENE, APIN, 13BDE, ETOH, ARO2MN, OXYL, PXYL, MXYL, B124, and TOLUENE based on standard SAPRC11 species ALK3, ALK4, ALK5, OLE1, OLE2, ARO1, ARO2, and TERP 37

Table 5-3: Measurement data sources for DISCOVER-AQ (http://www-air.larc.nasa.gov/missions/discover-aq/discover-aq.html) field campaign. 39

Table 5-4: Episode-average Mean Fractional Bias (MFB) and Mean Fractional Error (MFE) for CO, NOx, O_3, $PM_{2.5}$, NH_4^+, NO_3^-, and SO_4^{2-} during DISCOVER-AQ..... 43

Table 5-5: Episode-average Mean Fractional Bias (MFB) and Mean Fractional Error (MFE) for CO, NOx, O_3, $PM_{2.5}$, NH_4^+, NO_3^-, and SO_4^{2-} during DISCOVER-AQ for HI-RES_SOIL_MOD case. 54

Table 6-1: Model performance of PM2.5 Nitrate during Jan of year 2010, 2013 and 2015 over SJV 60

Table 6-2: Model performance of NO during Jan of year 2010, 2013 and 2015 over SJV.... 65

Table 6-3: Model performance of NO_2 during Jan of year 2010, 2013 and 2015 over SJV .. 66

Table 6-4: Model Performance for Ozone and NOx during Jul of year 2010, 2013 and 2015 over SJV 71

LIST OF FIGURES

FigureES-1. Total reactive nitrogen concentration (red (first) for observation, blue (second) for with_soil_NOx, green (third) for base_case during Jan of year 2010, 2013 and 2015 over SJV xi

Figure ES-2. Daily Mean Fraction Bias for $PM_{2.5}$ nitrate concentrations with candidate soil NOx emissions (left column) and without candidate soil NOx emissions (right column) xii

Figure 2-5. Total reactive nitrogen concentration (red (first) for observation, blue (second) for with_soil_NOx, green (third) for base_case) during Jan of year 2010, 2013 and 2015 at Fresno, Bakersfield, and Visalia. 13

Figure 3-1.Map of modelled domain 17

Figure 3-2. Comparisons of timeseries of PBL height at Fresno for different combinations of PBL schemes and land surface schemes a) YSU-Noah-MP, b) YSU-Pleim-Xiu, c) MYJ-Noah-MP, d) MYJ-Pleim-Xiu, e) ACM2-Noah-MP and f) ACM2-Pleim-Xiu, and initial and boundary condition data with the aircraft observations from DISCOVER-AQ. 20

Figure 3-3.6-day averaged PBL height fields for NARR, FNL and their difference for a) YSU-Pleim-Xiu, b) MYJ-Pleim-Xiu and c) ACM2-Pleim-Xiu..... 21

Figure 4-1.LU_INDEX from NCLD40 data (Cultivated Crops assigned number is 38) 24

Figure 4-2. Average observed and simulated (base as well as SM cases) relative humidity (%), temperature (ºC) and wind speed (m/s) over SJV during Jan-Feb 2013. (**Note**: Here RH values are dived by 10 to place them on the same scale)..... 26

Figure 4-3. Meteorology evaluation (MFB, MFE and RMSE) (base case and revised soil moisture case) of relative humidity (%), temperature (ºC) and wind speed (m/s) during Jan-Feb, 2013 over SJV. Here, SM represents modified soil moisture case. 27

Figure 4-4.(a) Spatial distribution of base and (b) differences (revised soil moisture – base case) relative humidity(%) t surface level during DISCOVER-AQ episode over 4 km domain 28

Figure 4-5. Spatial distribution of surface PM2.5 nitrate concentration (μg/m^3) during DISCOVER-AQ episode over 4 km domain 29

Figure 4-6. Time series of predicted $PM_{2.5}$ nitrate concentrations under basecase humidity conditions and increased humidity conditions when soil moisture availability is increased.. 30

Figure 5-1. Candidate **s**oil NOx emissions for the month of January, 2013 (left) and non-soil NOx emission for January 16, 2013 (right), over central California. Units are ppm m min^{-1}.36

Figure 5-2. Ground-level pollutant concentrations at Fresno during the DISCOVER-AQ campaign. 42

Figure 5-3. Episode-average diurnal profiles at Fresno during the DISCOVER-AQ campaign. Note that enhanced simulations for diurnal profiles are presented in Section 5.3.3..... 45

Figure 5-4. Episode-average vertical profiles at Fresno at 10:00 AM. The uncertainty bars represent 3 times the standard deviation of the measurements. 47

Figure 5-5. Episode-average vertical profiles at Fresno at 12:00 PM. The uncertainty bars represent 3 times the standard deviation of the measurements. 47

Figure 5-6. Episode-average vertical profiles at Fresno at 2:00 PM. The uncertainty bars represent 3 times the standard deviation of the measurements. 48

Figure 5-7. NO_3^- vertical profiles for BASE_SOIL (left) and HI-RES_SOIL (right) at Fresno during DISCOVER-AQ. 49

Figure 5-8. NO_3^- vertical profiles for HI-RES_SOIL case with Kzz,min = ~0.5 m^{2}s^{-1} (left) and Kzz,min = ~0.01 m^{2}s^{-1}(right) for January 16, 2013 during DISCOVER_AQ at Fresno. 50

Figure 5-9. NO_3^- vertical profiles (01 – 12) for HI-RES_SOIL (left) and HI-RES_SOIL MOD (right) at Fresno. The vertical profiles are generated by averaging over January 16 – 21, 2013. 51

Figure 5-10. Diurnal profiles of $PM_{2.5}$ mass, NO_3^-, NH_4^+, gaseous NOx, O_3 and CO at Fresno for the DISCOVER-AQ campaign. These profiles are generated by averaging measurementsover January 16 – 21, 2013 during DISCOVER-AQ..... 52

Figure 5-11. Diurnal profiles of organic aerosol (OA) at Fresno for the DISCOVER-AQ campaign. These profiles are generated by averaging over 16 – 21 Januaryduring DISCOVER-AQ. 53

Figure 5-12. Averaged vertical profiles of species (name written in the graphs) at Fresno at 10:00 AM. These vertical profiles are averaged over 18, 20 – 21 January, 2013. 55

Figure 5-13. Averaged vertical profiles of species (name written in the graphs) at Fresno at 12:00PM. These vertical profiles are averaged over 18, 20 – 21 January, 2013. 55

Figure 5-14. Averaged vertical profiles of species (name written in the graphs) at Fresno at 2:00PM. These vertical profiles are averaged over 18, 20 – 21 January, 2013. 56

Figure 6-1. Daily mean fractional bias (MFB) (top-row) and mean fraction error (MFE) (bottom-row) of PM2.5 nitrate concentration during Jan of 2010, 2013 and 2015 over SJV. Case with candidate soil NOx emissions shown in left column, and contribution of without candidate soil NOx emissions shown in right column. 62

Figure 6-2. PM2.5 nitrate concentration (Red for observation, Blue for with_soil_NOx, Green for base_case during Jan of year 2010, 2013 and 2015 at Bakersfield, Fresno, and Visalia.. 63

Figure 6-3.NOx concentration (Red for observation, Blue for with_soil_NOx, Green for base_case) during Jan of year 2010, 2013 and 2015 over SJV. Note that Y axis uses a logarithmic scale. 64

Figure 6-4. Spatial distribution of base (without soil nox) (left column) and differences (with soil nox emission – base case) of PM2.5 nitrate concentration (right column) for Jan of year 2010,2013 and 2015. Units are $\mu g\ m^{-3}$ 68

Figure 6-5. Spatial distribution of base (without soil nox) (left column) and differences (with candidate soil NOx emission – base case) of NOx concentration (right column) for Jan of year 2010,2013 and 2015. Units are ppb. 70

Figure 6-6. Measured and predicted diurnal variation of O3 and NOx concentrations during July of year 2010, 2013 and 2015 over the SJV. 72

Figure 6-7. Spatial distribution of base (without soil nox) (left column) and differences (with candidate soil nox emission – base case) of Ozone concentration (ppb) (right column) for Jul of year 2010 2013 and 2015 over 4 km domain 74

Figure 6-8. Spatial distribution of base (without soil nox) (left column) and differences (with candidate soil nox emission – base case) of NOx concentration (right column) for Jul of year 2010 2013 and 2015. Units are ppb. 75

LIST OF ACRONYMS

13BDE – 1,3 Butadiene
ACM – Asymmetric Convective Model
ALK3 – SAPRC11 lumped chemical species representing alkanes
ALK4 – SAPRC11 lumped chemical species representing alkanes
ALK5 – SAPRC11 lumped chemical species representing alkanes
APIN – alpha pinene
ARO1 – SAPRC11 lumped chemical species representing aromatic compounds
ARO2 – SAPRC11 lumped chemical species representing aromatic compounds
ARO2MN – model species ARO2 without naphthalene
ARW – Advanced Research core WRF
B124 – 1,2,4-trimethylbenzen
CTMs – Chemical Transport Model
CRPAQS – California Regional PM10/PM2.5 Air Quality Study
CalNex–California Nexus
DISCOVER-AQ –Deriving Information on Surface Conditions from Column and Vertically Resolved Observations Relevant to Air Quality
EMFAC – Emissions Factor
ETOH - ethanol
FDDA – four dimensional data assimilation
GFED – Global Fire Emissions Database
GFS – global forecast system
IMAGE - Integrated Model for the Assessment of the Global Environment
ISOPNN – isoprene dinitrates from NO_3 reaction
MEGAN –Model of Emission of Gases and Aerosols from Nature
MFB – Mean Fractional Bias
MFE – Mean Fractional Error
MTNO3 – monoterpene nitrate
MOZART - model for ozone and related chemical tracers
MXYL – m-xylene
MYJ - Mellor–Yamada–Janjic
NAAQS – National Ambient Air Quality Standards
NAPHTHAL - naphthalene
NARR - North American Regional Reanalysis
NCEP - National Centers for Environmental Prediction
NOx – oxides of nitrogen
OLE1 – SAPRC11 lumped chemical species representing olefins
OLE2 – SAPRC11 lumped chemical species representing olefins
OXYL – o-xylene
PAN – Peroxy Acetyl Nitrate
POA – primary organic aerosol
PXYL – p-xylene
RH – relative humidity
RRTM – rapid radiation transfer model

SAPRC11 – State Air Pollution Research Center chemical mechanism version 2011SIP – State Implementation Plan
SJV – San Joaquin Valley
SOA – secondary organic aerosol
SOAALK – Secondary Organic Aerosol derived from alkanes
T2 – temperature at an elevation of 2m
TERP – SAPRC11 lumped chemical species representing terpenes
UCD/CIT – University of California Davis/California Institute of Technology
VOCs – volatile organic compounds
WRF – Weather Research & Forecast

ABSTRACT

Particulate nitrate accounts for a significant fraction of the maximum 24-hr average $PM_{2.5}$ mass concentrations in California's San Joaquin Valley (SJV). Two decades ago regional chemical transport models (CTMs) were able to predict maximum 24-hr average $PM_{2.5}$ nitrate concentrations with reasonable accuracy. More recently, CTMs have been unable to reliably predict maximum $PM_{2.5}$ nitrate concentrations during contemporary air pollution episodes with decreased concentrations. This failure may be due to biases in emissions inventories, biases in meteorological conditions that affect nitrate formation, or a shift into a new chemical regime where new chemical formation pathways dominate particulate nitrate formation. The purpose of this project was to investigate each of these possible explanations for the degraded CTM performance with the goal to correct biases in nitrate predictions where possible.

Predicted concentrations of total reactive nitrogen were consistently under-predicted in January of the years 2010, 2013, and 2015 in the SJV. Under-predictions for total reactive nitrogen become progressively more severe with years past 2010 suggesting that emissions inventories for reactive nitrogen are diverging from actual conditions. These trends are consistent with continued reductions in mobile source NOx emissions combined with some unknown source of NOx emissions that is not currently represented in the emissions inventory.

The inclusion of candidate soil NOx emissions from agricultural cropland in the SJV partially addresses the gap in reactive nitrogen emissions in central California. The tested soil NOx emissions strongly increase predicted levels of total reactive nitrogen in rural areas and contribute approximately 20% to concentrations of total reactive nitrogen in urban locations of Fresno and Bakersfield. The conversion efficiency of soil NOx to particulate nitrate is higher than the conversion efficiency of urban NOx emissions to particulate nitrate due to the diffuse nature of the soil NOx emissions which yields more favorable mixing ratios with background ozone. The candidate soil NOx emissions improve the accuracy of predictions for wintertime particulate nitrate at ground level, wintertime particulate nitrate vertical profiles, summertime ozone concentrations at ground level, and NOx concentrations during both summer and winter.

The tests conducted in the current study confirm that a missing source of NOx consistent with the candidate soil NOx emissions would improve the performance of regional chemical transport models in California's SJV, but they do not definitely prove that the missing emissions source is fertilized agricultural soils. Future measurements should be made in the rural portions of the SJV to further test the hypothesis that soil NOx emissions are a significant factor in the air quality cycles within the region.

EXECUTIVE SUMMARY

Background: Particulate nitrate accounts for a significant fraction of the maximum 24-hr average $PM_{2.5}$ mass concentrations in California's San Joaquin Valley (SJV). Two decades ago, mobile sources dominated NOx emissions in the SJV and regional chemical transport models (CTMs) were able to predict maximum 24-hr average $PM_{2.5}$ nitrate concentrations with reasonable accuracy. Mobile source emissions have decreased by more than a factor of two over the past 20 years with a corresponding decrease in maximum $PM_{2.5}$ nitrate concentrations, but CTMs are no longer able to reliably predict the residual maximum $PM_{2.5}$ nitrate concentrations. The evidence suggests that contemporary emissions inventories have become biased, meteorological predictions have become biased, or the atmospheric chemical transformations that produced particulate nitrate have entered a new regime with dominant chemical formation pathways that are not well represented in CTMS. The purpose of this project was to investigate each of these possible explanations with the goal to correct biases in nitrate predictions where possible.

Methods: Total reactive nitrogen concentrations were simulated in January of 2010, 2013, and 2015 and compared to measurements across sites in the San Joaquin Valley. Total reactive nitrogen is conserved in the presence of chemical reactions and so the evaluation of total reactive nitrogen removes the uncertainty associated with new chemical formation pathways and rates of reaction. Positive or negative biases in predicted total reactive nitrogen concentrations explicitly point to biases in the emissions inventory or biases in the meteorology that governs the dispersion of pollutants in the atmosphere.

The effects of increasing soil moisture availability and atmospheric relative humidity (RH) were investigated during the DISCOVER-AQ field study in January and February 2013. Increasing RH promotes the formation of particulate nitrate in CTMs which may correct some of the negative bias in predicted nitrate concentrations.

The effects of adding candidate soil NOx emissions were investigated during the DISCOVER-AQ field study in January and February 2013. The accuracy of predicted particulate nitrate, NO, NO_2, and O_3 vertical profiles was evaluated with and without candidate soil NOx emissions. Consistent improvements in the accuracy during these simulations would build confidence in the candidate emissions, whereas degraded performance would show that the candidate emissions are not accurate.

The effects of adding candidate soil NOx emissions were investigated during January and July of 2010, 2013, and 2015. January simulations were evaluated for predictions of particulate nitrate while July simulations were evaluated for predictions of O_3. Consistent improvements in the accuracy during these simulations would build confidence in the candidate emissions, whereas degraded performance would show that the candidate emissions are not accurate.

Results: Predicted ground-level concentrations of total reactive nitrogen were consistently under-predicted in January of the years 2010, 2013, and 2015 in the SJV. Under-predictions for total reactive nitrogen become progressively more severe with years past 2010 (see Figure ES-1) suggesting that emissions inventories for reactive nitrogen are diverging from actual conditions. These trends are consistent with continued reductions in mobile source NOx emissions combined

with some unknown source of NOx emissions that is not currently represented in the emissions inventory.

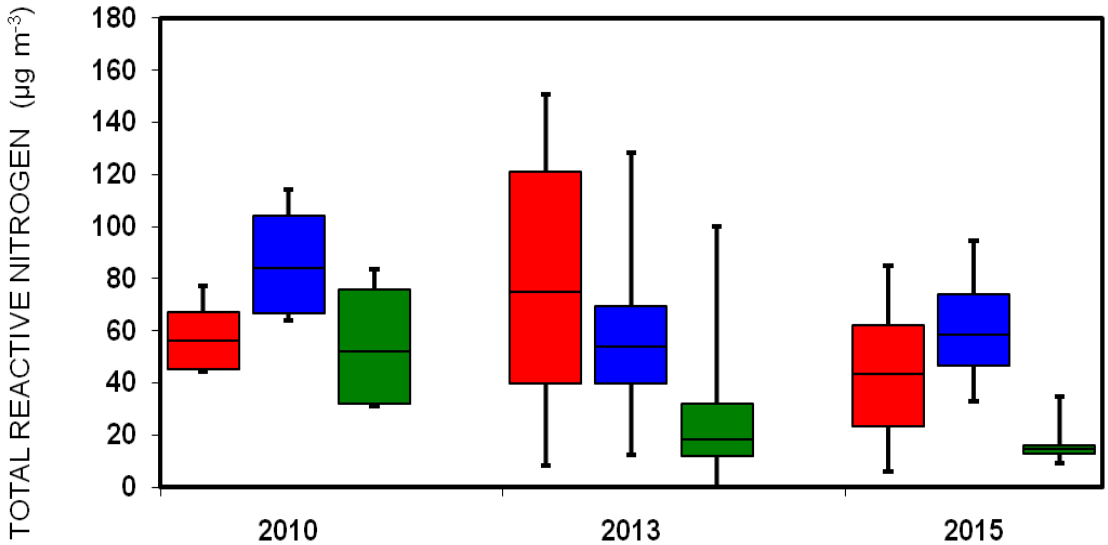

FigureES-1. Total reactive nitrogen concentration (red (first) for observation, blue (second) for with_soil_NOx, green (third) for base_case during Jan of year 2010, 2013 and 2015 over SJV

The inclusion of candidate soil NOx partially addresses the gap in reactive nitrogen emissions in central California. The tested soil NOx emissions strongly increase predicted levels of total reactive nitrogen in rural areas and contribute approximately 20% to concentrations of total reactive nitrogen in urban locations of Fresno and Bakersfield.

Candidate soil NOx emissions in Jan 2010, 2013, and 2015 were efficiently converted to particulate nitrate due to the favorable mixing ratio between diffuse soil NOx emissions and background ozone concentrations. As a result, soil NOx produced approximately half of the particulate nitrate in urban locations of the SJV even though this source accounted for only ~20% of the total reactive nitrogen concentrations.

The inclusion of candidate soil NOx emissions generally increases predicted $PM_{2.5}$ nitrate concentrations in January 2010, 2013, and 2015 which helps correct a consistent under-prediction in concentrations. Despite this general improvement, further research is required to more accurately estimate winter emissions rates of soil NOx and to account for year-to-year variations driven by changes in meteorological conditions, fertilizer application rates, and irrigation practices. Figure ES-2 shows the mean fractional error of predicted $PM_{2.5}$ nitrate concentrations across all simulations with and without candidate soil NOx emissions. The candidate emissions increase predicted concentrations which corrects some of the bias, but they do not change the basic relationship that high concentration events tend to be under-predicted while low concentration events tend to be over-predicted.

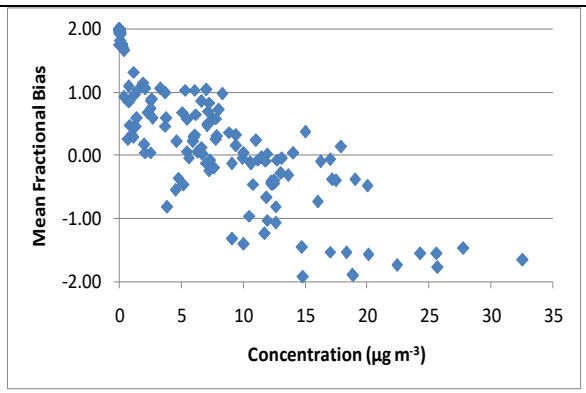

Daily mean fractional bias (MFB) of PM2.5 nitrate with soil NOx case during Jan of 2010, 2013 and 2015 over SJV

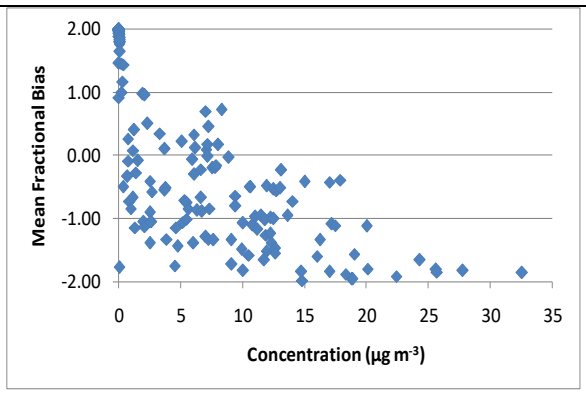

Daily mean fractional bias (MFB) of PM2.5 nitrate without soil NOx (base) case during Jan of 2010, 2013 and 2015 over SJV

Figure ES-2. Daily Mean Fraction Bias for $PM_{2.5}$ nitrate concentrations with candidate soil NOx emissions (left column) and without candidate soil NOx emissions (right column)

The inclusion of candidate soil NOx emissions in July 2010, 2013, and 2015 improved the overall predictions of O_3 and NOx in the SJV by correcting negative biases at the urban locations where the monitors are located.

Conclusions: Candidate soil NOx emissions are consistent with the size of this missing NOx source and their inclusion in regional simulations improves the performance of regional chemical transport models in California's SJV. These results do not definitely prove that the missing NOx emissions source is fertilized agricultural soils.

Future Work: Future measurements should be made in the rural portions of the SJV to further test the hypothesis that soil NOx emissions are a significant factor in the air quality cycles within the region.

INTRODUCTION

1.1 Motivation

Reactive chemical transport models (CTMs) are the primary tools used to develop State Implementation Plans (SIPs) to comply with the National Ambient Air Quality Standards (NAAQS). CTMs must be capable of simulating contemporary air pollution events in order to build confidence in their representation of atmospheric processes and input data before they can be used to design future emissions control strategies. Over the past 20 years, the severity and dominant species in contemporary air pollution events in California has changed significantly. CTMs have been challenged to completely adapt to these changing conditions motivating the continued revisions of CTMs and CTM inputs.

Particulate nitrate accounts for 10-15% of the annual-average $PM_{2.5}$ concentration in California's polluted San Joaquin Valley (SJV), and more than 50% of $PM_{2.5}$ during intensive winter episodes [1, 2]. Precursor emissions and formation processes for $PM_{2.5}$ (especially NO_3^- and NH_4^+) in California have been investigated using air quality models in combination with measurements from multiple field campaigns including, (i) the 2000/2001California Regional $PM_{10}/PM_{2.5}$ Air Quality Study (CRPAQS), (ii) the 2010 California Nexus-Research at the Nexus of Air Quality and Climate Change (CalNex) study and (iii) the 2013 Deriving Information on Surface Conditions from Column and Vertically Resolved Observations Relevant to Air Quality (DISCOVER-AQ) study[1-5]. Nitrate formation is limited by the availability of NOx emissions during cold winter months when background ozone acts as the dominant oxidant[6]. Generally, when provided with approximately precise emissions and meteorology, air quality models do a reasonable job in predicting NO_3^- and NH_4^+ concentrations [7-9], but long-term analysis shows that model predictions for particulate nitrate are falling below measured concentrations during more recent years [10]. This long-term trend suggests that model calculations are missing a nitrate formation pathway, missing an emissions source for nitrate precursors, or have biased meteorological inputs leading to model under-predictions in recent years.

1.2 Research Objectives

The overall objective of this report is to identify and correct (when possible) factors that cause under-predictions of $PM_{2.5}$ concentrations in central and southern California when using regional chemical transport models (CTMs).

The specific project objectives are to:

1. Investigate particulate nitrate formation in California as a function of precursor emissions rates. Summarize total predicted concentrations (gas+particle phase) of reactive nitrogen, sulfur, and ammonia. Compare predicted and measured total concentrations to verify that emissions of reactive species are approximately correct.

2. Investigate particulate nitrate formation in California as a function of meteorological conditions. Identify associations between bias in predicted meteorological variables (wind speed, mixing depth, relative humidity, etc) and bias in predicted nitrate concentrations.

4. Improve emission estimates to remove biases in nitrate precursors.

5. Refine mechanisms for particulate nitrate formation by increasingvertical spatial resolution to better resolve optimal zones of efficient nitrate production in the presences of sharp spatial gradients.

6. Simulate historical (CRPAQS) and current (DISCOVER-AQ and CalNex) air pollution episodes with the latest generation of models and inputs. Determine if the enhanced emissions / meteorology / nitrate formation mechanisms improve model performance for both the historical episodes (that are typically characterized by higher concentrations) and more recent episodes (that are typically characterized by moderate concentrations).

1.3 Hypotheses

The hypotheses that were tested in the research are:

1. Emissions estimates for precursors of particulate nitrate formation in California are biased leading to errors in predicted nitrate formation rates in regional chemical transport models.

2. Meteorological predictions for wind speed, temperature, humidity, etc used as inputs to regional chemical transport models are biased leading to errors in predicted nitrate formation rates.

3. The current conceptual model for nitrate formation is incomplete: increased spatial resolution, new chemical reactions, and/or modified thermodynamic calculations are needed to correct the bias in predicted nitrate concentrations.

4. Modifications needed to improve predicted nitrate concentrations during recent air quality (CalNex, Discover-AQ) episodes also improve predicted nitrate concentrations in historical episodes (CRPAQS).

1.4 Report Structure

This report is comprised of seven chapters, including introduction (Ch 1) and conclusions (Ch7).

Chapter 2 describes the analysis of total reactive nitrogen predictions vs. measurements in order to establish if there is a bias in emissions inventories.

Chapter 3 describes a study to select the optimum boundary layer configuration for WRF simulations during particulate nitrate formation events.

Chapter 4 investigates the effects of soil moisture on ambient humidity and particulate nitrate production in the San Joaquin Valley.

Chapter 5 examines vertical profiles of predicted and measured concentrations of $PM_{2.5}$ nitrate, ozone, and other reactive species with and without the inclusion of candidate soil NOx emissions.

Chapter 6 examines the effects of candidate soil NOx emissions on predicted concentrations of particulate nitrate and ozone.

Chapter 7 summarizes conclusions across the entire project and makes recommendations for future work.

2 TOTAL REACTIVE NITROGEN PREDICTIONS vs. MEASUREMENTS

2.1 Introduction

The majority of the particulate nitrate that forms in the SJV during the winter is emitted as NO that is then oxidized to nitric acid (HNO_3) through various chemical reaction pathways influenced by local meteorological conditions. During this process, the "reactive nitrogen" initially present in NO may be transformed into various forms including NO_2, NO_3, N_2O_5, HNO_2, HNO_3, HNO_4, PAN, PPN, and finally particulate nitrate (inorganic or organic). Evaluations for the predicted vs. measured concentrations of these individual species must simultaneously account for the emissions rates of the precursor NO, the chemical reaction rates for the individual reactions, and the meteorological conditions that influence the system. The uncertainties in these three broad factors often make it impossible to draw definitive conclusions about the issues that contribute to biases in predicted nitrate concentrations.

One method to avoid some the complexity inherent in the analysis of individual reactive nitrogen compounds is to evaluate the sum of all reactive nitrogen compounds together. The sum of reactive nitrogen should not strongly depend on chemical reaction rates which removes a significant fraction of the uncertainty associated with competing chemical pathways and the influence of meteorology on chemical reaction rates and partitioning between the gas and particle phases.

The purpose of this chapter is to compare the total reactive nitrogen predictions to measurements in California's SJV during winter months in the years 2010, 2013, and 2015. The spatial distribution of total reactive nitrogen will be analyzed to determine the representativeness of the monitoring locations. The conversion efficiency of total reactive nitrogen to particulate nitrate will be calculated as a function of location for each target year and notable trends will be discussed. Conclusions will then be made about the accuracy of total reactive nitrogen emissions inventories and the identity of possible missing sources of reactive nitrogen.

2.2 Methods

2.2.1 WRF Model Configuration

Meteorological fields were simulated with the Weather Research & Forecast (WRF) model v3.4 configured with three nested domains centered at 37° N, 120.5° W. The outer domain was divided into 60 × 60 grid cells with 36-km horizontal resolution. The second domain was divided into 112 × 121 grid cells with 12-km resolution. The inner-most domain was divided into 298 × 277 grid cells with 4-km resolution, which covers all of California (as shown in Figure 2-1). The 31 vertical layers from the ground level to the top pressure of 100 hPa were used for all grids. The meteorological initial and boundary conditions were taken from North American Regional Reanalysis (NARR), which has a spatial resolution of 32 km and a temporal resolution of 3 h. The Yonsei University (YSU) boundary layer vertical diffusion scheme was adopted in this study. Four-dimensional data assimilation (FDDA) was applied to anchor model predictions to observed meteorological patterns. The surface friction velocity (u*) was increased by 50% to correct for positive bias during low wind speed events that produce the highest pollution episodes.

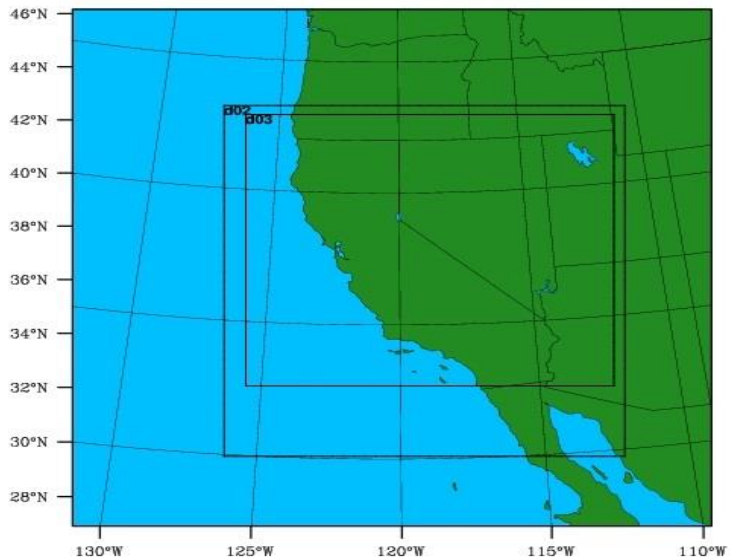

Figure 2-1.WRF Domain Configuration

2.2.2 Air Quality Model Configuration

Simulations for winter conditions in the SJV were carried out using the UCD/CIT regional air quality model. The UCD/CIT model predicts the evolution of gas and particle phase pollutants in the atmosphere in the presence of emissions, transport, deposition, chemical reaction and phase change [11] as represented by Eq. (2-1)

$$\frac{\partial C_i}{\partial t} + \nabla \cdot uC_i = \nabla K \nabla C_i + E_i - S_i + R_i^{gas}(C) + R_i^{part}(C) + R_i^{phase}(C) \qquad (2\text{-}1)$$

where C_i is the concentration of gas or particle phase species i at a particular location as a function of time t, u is the wind vector, K is the turbulent eddy diffusivity, E_i is the emissions rate, S_i is the loss rate, R_i^{gas} is the change in concentration due to gas-phase reactions, R_i^{part} is the change in concentration due to particle-phase reactions and $R_i^{phase}$is the change in concentration due to phase change [11]. Loss rates include both dry and wet deposition. Phase change for inorganic species occurs using a kinetic treatment for gas-particle conversion [12] driven towards the point of thermodynamic equilibrium [13]. Phase change for organic species is also treated as a kinetic process with vapor pressures of semi-volatile organics calculated using the 2-product model [14].

A total of 50 particle-phase chemical species are included in each of 15 discrete particle size bins that range from 0.01-10 µm particle diameter [11]. Artificial source tags are used to quantify source contributions to the primary particle mass for a specific bin size, therefore allowing for the direct contribution of each source of $PM_{2.5}$ and $PM_{0.1}$ mass to be determined. Gas-phase concentrations of oxides of nitrogen (NOx), volatile organic compounds (VOCs), oxidants, ozone, and semi-volatile reaction products were predicted using the SAPRC-11 chemical mechanism [15].

Model simulations were configured using a one-way nesting technique with a parent domain of 24 km horizontal resolution that covered the entire state of California and a nested domain with 4 km horizontal resolution that covered the San Joaquin Valley (SJV). Calculations used 15 telescoping

vertical layers (thickness of first level ~30m, thickness of final level ~1000m) up to a top height of 5km.

2.2.3 Emissions

The emission inventories used in the current study are based on the basecase emissions inventories provided by the California Air Resources Board for the anchor years 2000, 2010, and 2016. General area and point sources were interpolated between these anchor years to capture changes that occurred over time. Several additional updates were made to create day-specific emissions estimates, to correct biases in the basecase emissions, and to improve the representation of long-term trends. Day-specific meteorological information from the WRF model was used with the Model of Emission of Gases and Aerosols from Nature (MEGAN)[16]to estimate day-specific biogenic emissions. The gridded geo-referenced emission factors and land cover variables required for MEGAN calculations were created using the MEGANv2.1 pre-processor tool and the ESRI_GRID leaf area index and plant functional type files available at the Community Data Portal [17]. Daily values of wildfire emissions were generated using the Global Fire Emissions Database (GFED) [18]. Residential wood smoke emissions were updated by considering POA evaporation and wood burning control policies applied in California [19]. These updates reduced the effective residential wood smoke primary organic aerosol (POA) emissions by 50% in all years compared to the basecase inventories, and better represent long-term trends in wood smoke emissions. Mobile source emissions were scaled in 69 regions throughout California based on the Emissions Factor (EMFAC) v2014 using day-specific meteorology from WRF. The source profile for aircraft emissions was updated based on recent measurements. The particulate matter emissions from residential natural gas combustion were set to zero under the assumption that these particles evaporated upon dilution in the atmosphere. Subsequent direct measurements of natural gas combustion emissions at increasing dilution factors revealed that the ultrafine particles emitted by this source will not completely evaporate [20] but this change could not be incorporated into the current study given the long time required for the simulations. Basecase fugitive dust emissions were replaced by an online dust model [21] based on the wind speed, and soil moisture predicted by the WRF model. This change corrects the positive bias in dust emissions and PM2.5 mass noted by Hu et al. [22, 23] and Wang et al. (2016).

2.2.4 Boundary Conditions

The gas and particle phase initial and hourly varying boundary conditions for the UCD/CIT model were taken from the global model MOZART-4/NCEP (a model for ozone and related chemical Tracers). Additional details of MOZART simulations are provided by Emmons et al. [24].

2.2.5 Measurements for Model Evaluation

Total reactive nitrogen species include NO, NO_2, NO_3, N_2O_5, HNO_2, HNO_3, HNO_4, PAN, PPN, and particulate nitrate (inorganic or organic). Of these, NO, NO_2, and particulate nitrate account for virtually all of the nitrogen mass under typical atmospheric conditions. NO, NO_2, and particulate nitrate are routinely measured at multiple locations in the SJV, and so they provide a dataset to evaluate model predictions. The analysis in the current chapter will focus on NO, NO_2, and particulate nitrate as the dominant species in total reactive nitrogen.

2.3 Results

2.3.1 Spatial Distribution of Total Reactive Nitrogen

Figure 2-2 illustrates the spatial distribution to total reactive nitrogen (represented as $NO+NO_2$+particulate nitrate) in central California during January of the years 2010, 2013, and 2015. The left column of Figure 2-2 shows the total reactive nitrogen from all sources, the center column of Figure 2-2 shows the effects of leaving out candidate soil NOx emissions, and the right column of Figure 2-2 shows the direct contribution from candidate soil NOx emissions to ground-level total reactive nitrogen concentrations. Maximum concentrations of total reactive nitrogen in all years occur in urban centers due to the combined effects of transportation emissions and candidate soil NOx emissions. A local maximum in total reactive nitrogen also occurs around the location of peak candidate soil NOx emissions between Fresno and Bakersfield in all years of the analysis. Ignoring this maximum and focusing on regional averages, soil NOx in the SJV is predicted to account for total reactive nitrogen contributions that are approximately 70% of the peak values predicted in urban centers. Soil NOx accounts for only 15-20% of the total reactive nitrogen in urban centers where most of the monitoring is performed.

Predicted NOx emissions decreases consistent from 2010 through 2015 but predicted ground-level total reactive nitrogen concentrations do not follow a consistent downward trend for two reasons. First, year-to-year variation in meteorological conditions has a strong influence on the predicted concentrations of ground level reactive nitrogen, with more stagnant conditions increasing concentrations. Second, the emissions rates of soil NOx are assumed to be constant across the simulation years in the current analysis. In reality, changing agricultural practices are likely modifying the soil NOx emissions over this time period, but this complexity was not captured in the current analysis.

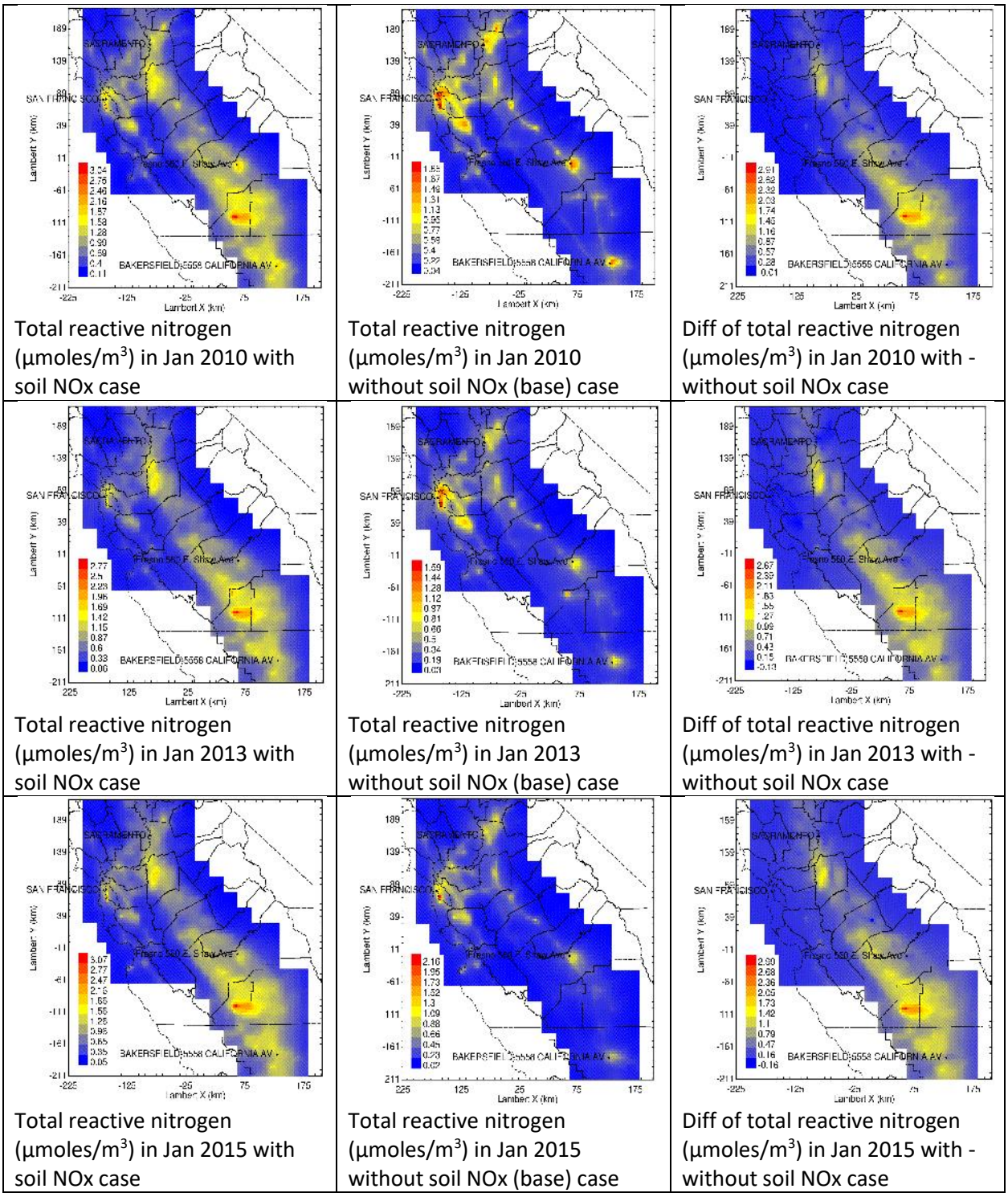

Total reactive nitrogen (µmoles/m^3) in Jan 2010 with soil NOx case

Total reactive nitrogen (µmoles/m^3) in Jan 2010 without soil NOx (base) case

Diff of total reactive nitrogen (µmoles/m^3) in Jan 2010 with - without soil NOx case

Total reactive nitrogen (µmoles/m^3) in Jan 2013 with soil NOx case

Total reactive nitrogen (µmoles/m^3) in Jan 2013 without soil NOx (base) case

Diff of total reactive nitrogen (µmoles/m^3) in Jan 2013 with - without soil NOx case

Total reactive nitrogen (µmoles/m^3) in Jan 2015 with soil NOx case

Total reactive nitrogen (µmoles/m^3) in Jan 2015 without soil NOx (base) case

Diff of total reactive nitrogen (µmoles/m^3) in Jan 2015 with - without soil NOx case

Figure 2-2. Spatial distribution of total reactive nitrogen (N(V)+NO+NO2) in the SJV in Jan 2010 (top-row), 2013 (middle-row), and 2015 (bottom row).Case without candidate soil NOx emissions shown in center column, and contribution of candidate soil NOx emissions shown in right column.

2.3.2 Spatial Distribution of Total Ammonia

Figure 2-3 shows the spatial distribution to total ammonia (represented as NH_3 +particulate ammonium ion) in central California during January of the years 2010, 2013, and 2015. The left column of Figure 2-3 shows the total ammonia from all sources, the center column of Figure 2-3 shows the effects of leaving out candidate soil NOx emissions, and the right column of Figure 2-3 shows the direct contribution from candidate soil NOx emissions to ground-level total ammonia concentrations. Direct agricultural emissions from livestock feeding operations dominate total ammonia emissions in the SJV with little contribution from candidate soil NOx emissions. Maximum total ammonia concentrations occur in the regions with maximum livestock ammonia emissions between Fresno and Bakersfield. The minor changes in total ammonia caused by the omission of the candidate soil NOx emissions are due to changes in the particle size distribution caused by the reduced condensation of particulate nitrate leading to altered deposition rates. Unlike the total reactive nitrogen concentrations illustrated in Figure 2-2, the total ammonia concentrations illustrated in Figure 2-3 show a consistent downward trend over time suggesting the reductions in emissions overwhelm the year-to-year variations in stagnation conditions.

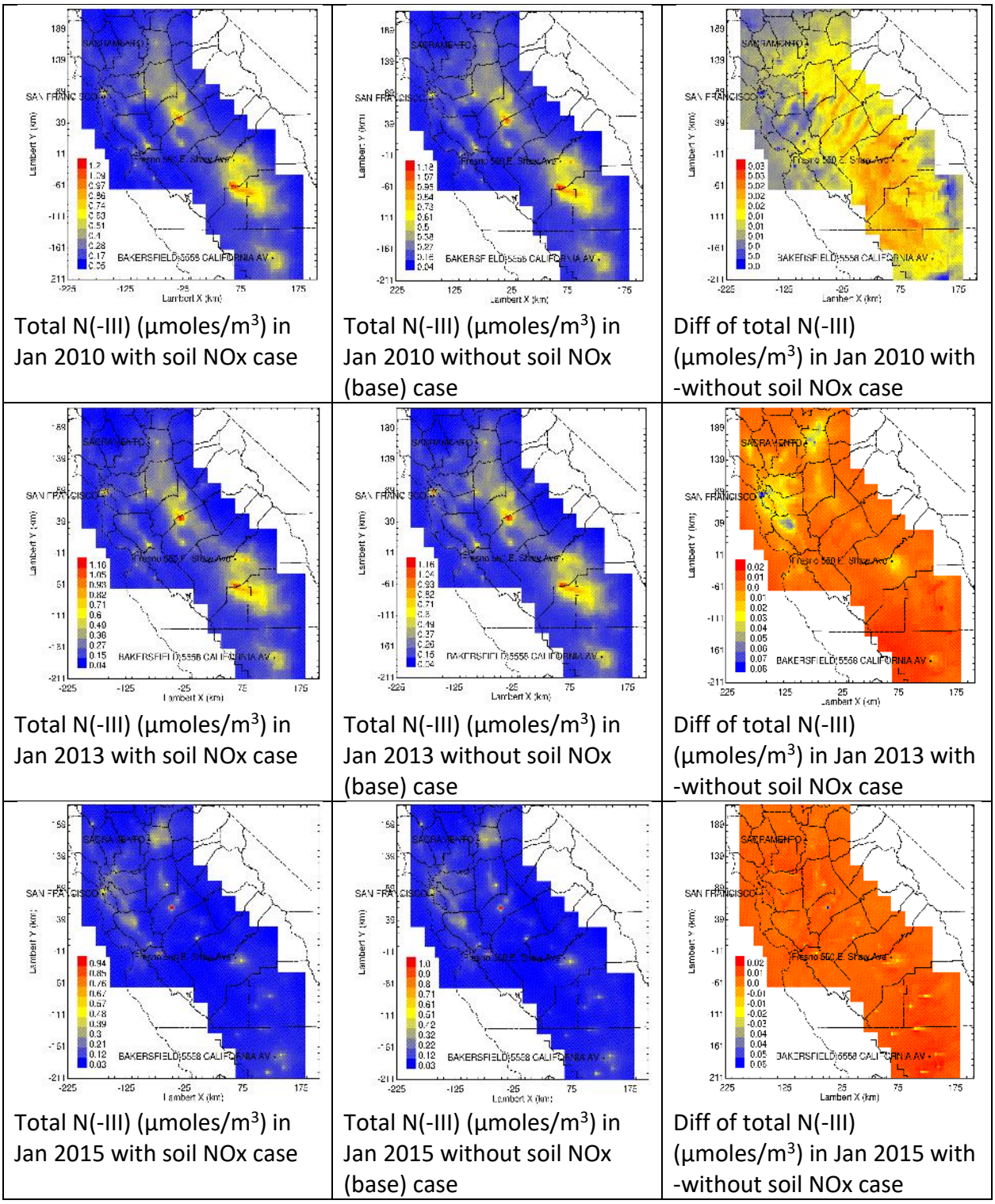

Figure 2-3. Spatial distribution of total ammonia (NH3(g)+NH4+(p)) in the SJV in Jan 2010 (top-row), 2013 (middle-row), and 2015 (bottom row). Case without candidate soil NOx emissions shown in center column, and contribution of candidate soil NOx emissions shown in right column.

2.3.3 Spatial Distribution of Nitrate Fraction of Total Reactive Nitrogen

Figure 2-4 shows the spatial distribution of the fraction of total reactive nitrogen that exists as particulate nitrate in January 2010, 2013, and 2015 in central California. Results are shown for simulations with candidate soil NOx emissions (left column) and without candidate soil NOx emissions (right column). The results suggest that the conversion efficiency to particulate nitrate is a strong function of location, with the lowest conversion efficiency in the locations with the highest NOx emissions. Long-term measurements of total reactive nitrogen and particulate nitrate at a remote location in the SJV could be used to evaluate the plausibility of the candidate soil NOx emissions.

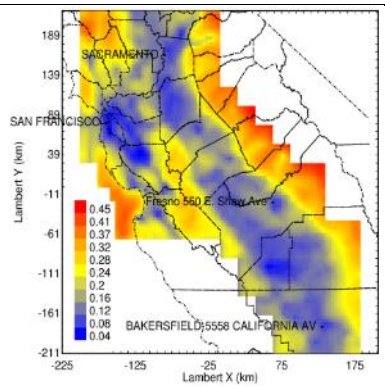

Nitrate/total reactive nitrogen with soil nox case in year 2010

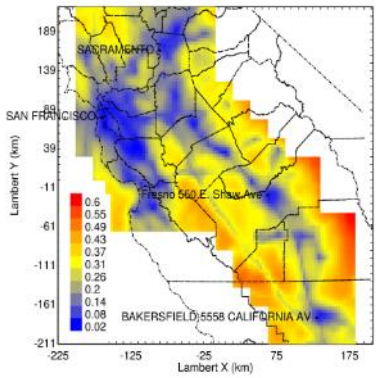

Nitrate/total reactive nitrogen without soil nox (base case) case in year 2010

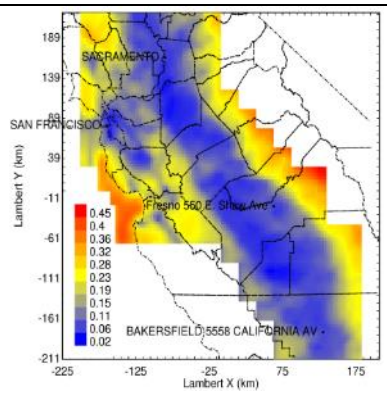

Nitrate/total reactive nitrogen with soil nox case in year 2013

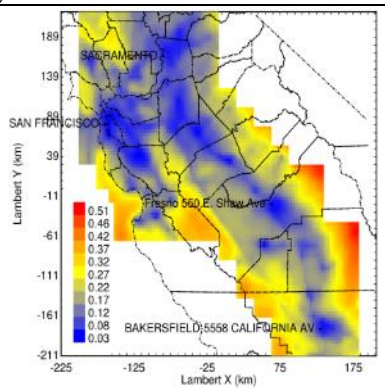

Nitrate/total reactive nitrogen without soil nox (base case) case in year 2013

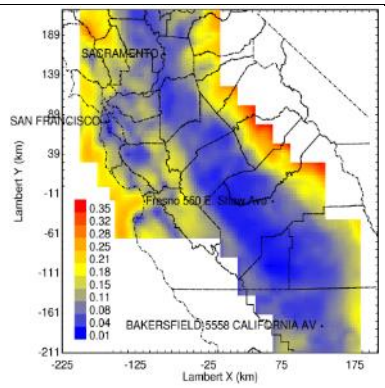

Nitrate/total reactive nitrogen with soil nox case in year 2015

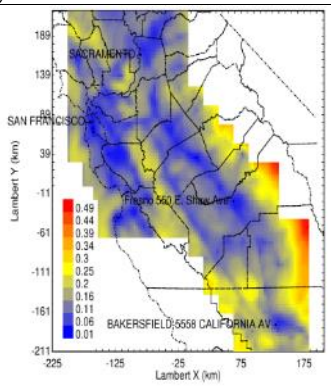

Nitrate/total reactive nitrogen without soil nox (base case) case in year 2015

Figure 2-4. Spatial distribution of the fraction of total reactive nitrogen that exists as particulate nitrate in January 2010, 2013, and 2015.

2.3.4 Long-Term Trends in Total Reactive Nitrogen

Figure 2-5 shows the measured and predicted total reactive nitrogen concentrations during the month of July in the years 2010, 2013, and 2015 at locations across the SJV. The majority of the measurement sites where the comparison is possible are located in urban regions and so each comparison reflects a ~80% contribution from urban sources and a ~20% contribution from candidate soil NOx emissions (for simulations that included soil NOx). In general, concentrations of total reactive nitrogen predicted using candidate soil NOx emissions are higher than concentrations predicted without soil NOx emissions. The simulations without soil NOx emissions predict consistently decreasing total reactive nitrogen concentrations with time. This contrasts with measured concentrations of total reactive nitrogen which increase between 2010 and 2013 before falling in 2015. The measured concentrations suggest that local stagnation conditions play a larger role than emissions reductions in determining ground level concentrations of total reactive nitrogen.

Overall, the trends illustrated in Figure 2-5 suggest that emissions without soil NOx do not adequately capture the measured trends in total reactive nitrogen in the San Joaquin Valley in the years 2010, 2013, and 2015. The constant level of candidate soil NOx emissions evaluated in the current study also does not appear to adequately capture the variations from year-to-year induced by temperature, precipitation, and changing fertilization practices.

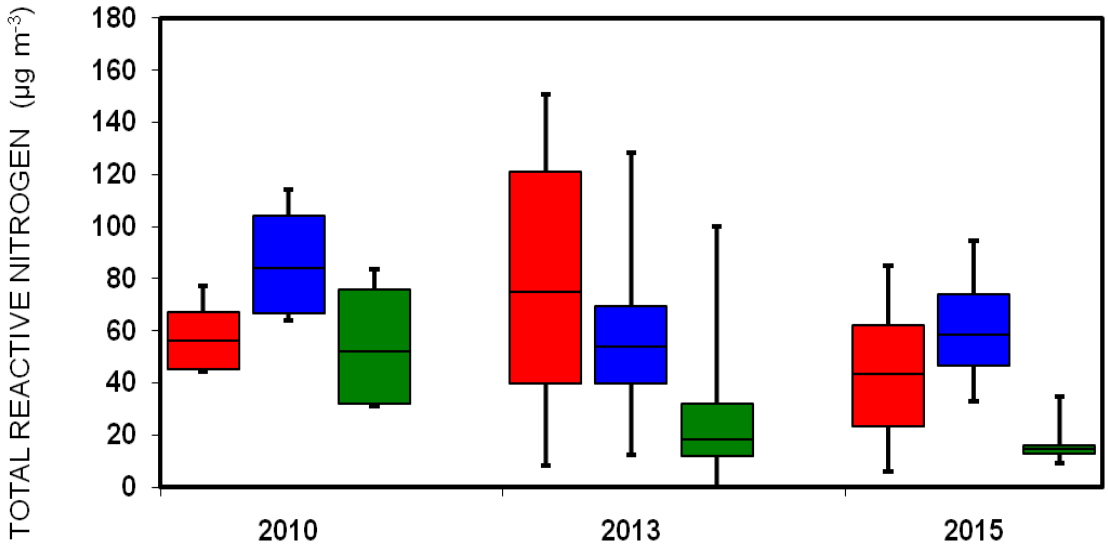

Figure 2-5. Total reactive nitrogen concentration (red (first) for observation, blue (second) for with_soil_NOx, green (third) for base_case) during Jan of year 2010, 2013 and 2015 at Fresno, Bakersfield, and Visalia.

2.4 Conclusions

Simulations conducted for January 2010, 2013, and 2015 in central California show that predicted total reactive nitrogen concentrations are lower than measured concentrations of $NO+NO_2$+particulate nitrate. Under-predictions for total reactive nitrogen become more severe with years past 2010 suggesting that emissions inventories for reactive nitrogen are diverging from actual conditions. These trends are consistent with continued reductions in mobile source NOx emissions combined with some unknown source of NOx emissions that is not currently represented in the emissions inventory. As mobile source emissions decrease, the relative important of this unknown source increases.

Soils are one plausible source of NOx emissions that are not currently represented in CARB emissions inventories. Independent estimates of soil NOx emissions produce significant total reactive nitrogen at the monitoring locations throughout the SJV. Simulations with candidate soil NOx suggest that the urban locations where most monitors are located are still dominated by urban transportation emissions with only a ~20% contribution from soil NOx to total reactive nitrogen. Monitoring at remote locations outside of urban cores would provide better data to evaluate whether the estimates of soil NOx emissions tested in the current study are accurate.

3 OPTIMUM BOUNDARY LAYER CONFIGURATION FOR WRF SIMULATIONS DURING WINTER STAGNATION EVENTS

3.1 Introduction

The Weather Research and Forecasting (WRF) Model is widely used for atmospheric research and operational forecasting needs. It's also used to prepare meteorological inputs for offline air quality models such as UCD-CIT model and EPAs CMAQ model. Many physical processes, such as microphysics of cloud formation and precipitation, the transfer of heat, moisture and momentum at the air-surface interface which cannot be totally described with a certain set of equations, are parameterized. Of all these processes, the evolution of PBL height and WS/WD pattern is not only critical from a meteorological standpoint but also from an air quality perspective as it is important in determining the concentrations of the airborne pollutants like particulate nitrate. Different PBL schemes adopt different assumptions regarding the turbulent transport of mass, moisture and energy which may lead to differences in PBL and subsequently the whole model domain. WRF PBL schemes have been comprehensively evaluated and inter-compared in several different studies. PBL schemes coupled with different land surface schemes for different initial and boundary condition data, however, have not been evaluated and compared (Xie et al, 2012).

In this section WRFv3.4 is used to simulate the PBL heights within San Joaquin Valley region in winter 2013, during the DISCOVER-AQ study and are validated against the flight observations collected during DISCOVER-AQ. The sensitivities of the WRF simulations to the use of three PBL schemes-the YSU scheme, the Mellor–Yamada–Janjic (MYJ) scheme and the (Asymmetric Convective Model version 2 (ACM2) scheme, two land surface schemes-the Noah-MP and PleimXiu land surface model, with two different sets of initial and boundary condition datasets-the North American Regional Reanalysis (NARR) data and National Centers for Environmental Prediction (NCEP) Final (FNL) Operational Global Analysis data are evaluated. We identify differences in model performances with possible consequences for air quality simulations and seek causes of those differences. We also identify the ideal combination of these land surface schemes, PBL schemes and the initialization data which minimized the bias between the predictions and measurements.

3.2 Description of three PBL schemes

PBL schemes are used to parameterize the turbulent mixing of heat, momentum and moisture fluxes within the atmosphere, specifically within the PBL. The PBL processes in WRF are either parameterized by local closure schemes or non-local schemes. The local closure schemes are best suited for shear turbulence in stable conditions. However, convective mixing is achieved by sub-grid scale eddies and large asymmetrical thermals. K-theory, used for local closure schemes, only7 simulates symmetric turbulent mixing between adjacent layers which leads to bias in mixing calculations when turbulent eddies are larger than the layer thickness. Among the three PBL schemes that will be evaluated in this study, the MYJ is a local closure model, the YSU is non-local closure model while ACM2 is a hybrid-model having both local and non-local closure (Hu et al, 2010).

The MYJ PBL scheme uses the 1.5-order (level 2.5) turbulence closure model to represent turbulence above the surface layer. The MYJ scheme determines eddy diffusion coefficients from calculated turbulent kinetic energy (TKE) based on prognostic equations. The scheme works best for all stable and slightly unstable conditions but doesn't work for convective mixing (Hu et al, 2010).

The YSU PBL scheme is a first- order nonlocal scheme, with a counter-gradient flux term in the eddy-diffusion equation. The YSU scheme is modified by increasing the critical bulk Richardson number from zero to 0.25 over land, thereby enhancing mixing in the stable boundary layer (Hong and Kim 2006).

The ACM2 PBL scheme is an improvement over the ACM1 scheme and includes both first order eddy-diffusion component and explicit non-local transport for better shaped vertical profiles near the surface. For stable or neutral conditions, the ACM2 scheme shuts off nonlocal transport and uses local closure thereby making it a hybrid scheme (Hu et al, 2013).

3.3 Description of model configuration and Evaluation of data

Three model domains with one way nesting are used (Figure 3-1) with grid spacing of 36, 12 and 4 km. The 12km domain covers most of California, and the 4km domain covers SJV valley. All model domains have 27 vertical layers with model top set to 1000 hPa. The physical parameterization schemes used in all model domains include Dudhia shortwave radiation, rapid radiative transfer model (RRTM) longwave radiation, WRF Single-Moment 6-Class (WSM6) microphysics and Kain–Fritsch cumulus scheme. The model also uses Noah land surface scheme with multiple parametrization (Noah-MP) and Pleim-Xiu land surface scheme. The NCEP global forecast system (GFS) FNL operational global analyses and NARR analyses are used for initial and boundary conditions.

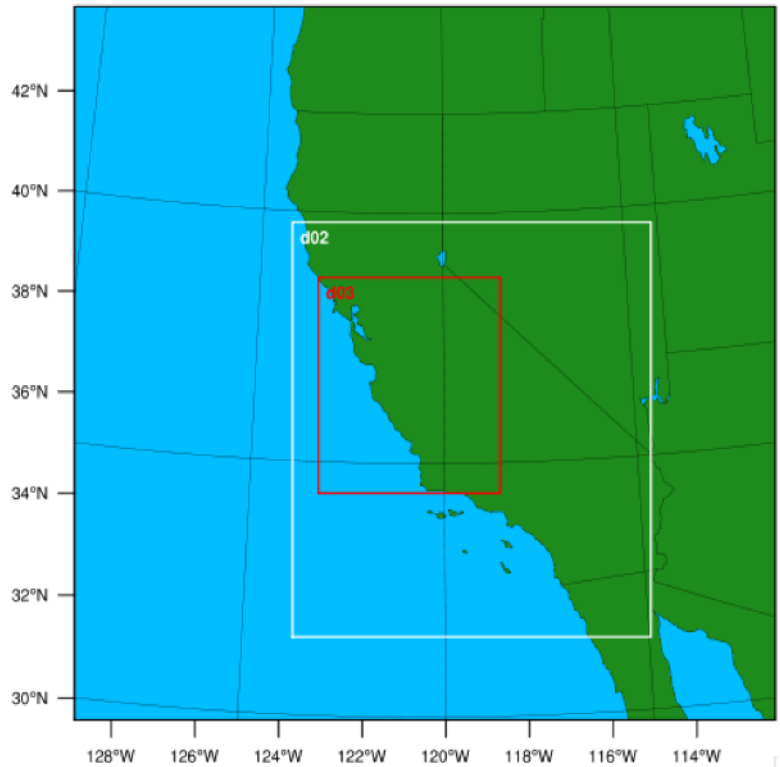

Figure 3-1.Map of modelled domain

Twelve 10-day forecasts, one for the unique combination of three PBL schemes, two land surface schemes and two different datasets (Table 3-1) are initiated at 0000 UTC (1600 PST) every day from 13 January to 22 January. The simulations with YSU use the Monin-Obukhov similarity surface layer scheme, MYJ use ETA similarity surface layer scheme and ACM2 uses Pleim-Xiu surface layer scheme as suggested by NCAR. The first 3 days of model results are treated as spin up, and the remaining 6 days are used for model evaluation.

Data for model validation includes P3B aircraft observation, which took many flights over the SJV valley in spirals above key locations like Fresno to get vertical profiles of temperature and pressure, during the DISCOVER-AQ campaign. The temperature and pressure profiles are converted to theta profiles which are then used to find the PBL height using the 1.0-theta-increase method. Evaluations will focus on the 4-km domain as it houses the city of Fresno with DISCOVER-AQ observations. The observations of vertical profiles are only for a couple of hours during the day due to the inability to fly an aircraft at night.

Table 3-1: Combinations of all the WRF runs which include three PBL schemes, two land surface schemes and two different datasets used for initial and boundary conditions

Case No.	Case Name	PBL Scheme	Land Surface Scheme	Data Source
1/7	NARR/FNL_YSU_NOAH-MP	YSU	Noah-MP	NARR/FNL
2/8	NARR/FNL_YSU_PLEIM-XIU	YSU	Pleim-Xiu	NARR/FNL
3/9	NARR/FNL_MYJ_NOAH-MP	MYJ	Noah-MP	NARR/FNL
4/10	NARR/FNL_MYJ_PLEIM-XIU	MYJ	Pleim-Xiu	NARR/FNL
5/11	NARR/FNL_ACM2_NOAH-MP	ACM2	Noah-MP	NARR/FNL
6/12	NARR/FNL_ACM2_PLEIM-XIU	ACM2	Pleim-Xiu	NARR/FNL

3.4 Results and Discussion

Figure 3-2 shows the time series comparison of all the cases simulated for 6 days from 16January to 21 January 2013 to observations. Figure 3-2a shows the time series comparison for case 1 and 11 with observations. There is no clear diurnal profile to the predicted PBL height in this case as it keeps oscillating from a minimum to maximum every couple of hours which seems abnormal and not representative of real atmospheric behavior. The FNL data in this case also seems to under predict the PBL height as compared to NARR data which seems true while capturing the observations. Both predicted PBL heights don't seem suitable to be used for the air quality model input as the oscillating nature of the PBL height might lead to oscillating pollutant concentration values. This is also true for case 3, 9, 4, 10, 5 and 11 where the oscillating nature of the predicted PBL height persists. However, case 3 and 9 (Figure 3-2c) do a good job at capturing the observations within this oscillating nature. In case 4 and 10 (Figure 3-2d), FNL data does a better job at capturing the observations at its minimums but in general seems worse than every other case for air quality purposes. Case 5 and 10 (Figure 3-2e) are the same but seems less intense in terms of their oscillating nature and do well at capturing the observations.

Case 1, 7, 6 and 12 (Figure 3-2a and 3-2f respectively) do a great job at predicting the PBL height with a nice and clear diurnal profile without oscillating which makes the predicted data with these cases more suitable to be used as meteorological data within an air quality model. These cases also do a good job at capturing the observations and are suitable for air quality modelling purposes.

The MYJ scheme seems to produce the worst PBL height predictions, perhaps because it is a local closure model and thus not able to simulate the unstable conditions within the SJV properly. The YSU scheme being a non-local closure model performs well as it might be better at resolving the unstable conditions within the boundary layer in the central valley. The ACM2 performs the best in terms of predicting the PBL height as well the non-oscillating nature as it a hybrid closure model and can switch between local and non-local closure when the conditions change (Zhang et al, 2004). The Pleim-Xiu land surface scheme seems to be doing a better job at predicting the PBL

height and its diurnal profile when coupled with YSU and ACM2. Noah-MP in general doesn't seem to be working with any of the PBL schemes and data types. MYJ doesn't seem to be working with any of the land surface schemes and data types due to it being a local closure model.

Figure 3-3 shows 6-day averaged PBL height fields of SJV for the case 2, 8 and their difference (Figure 3-3a), for case 4, 10 and their difference (Figure 3-3b) and for case 6, 12 and their difference (Figure 3-3c). The case 2, 8, 6 and 12 perform best in terms of predicting the PBL height and its diurnal profile at Fresno and their field plots also look similar as their difference plot shows the error in SJV PBL heights to be within the range of -25 m to 25 m. Case 4 and 10 which performed the worst have slightly different plots which is corroborated by an error range of -40 m to 160 m in the difference plot.

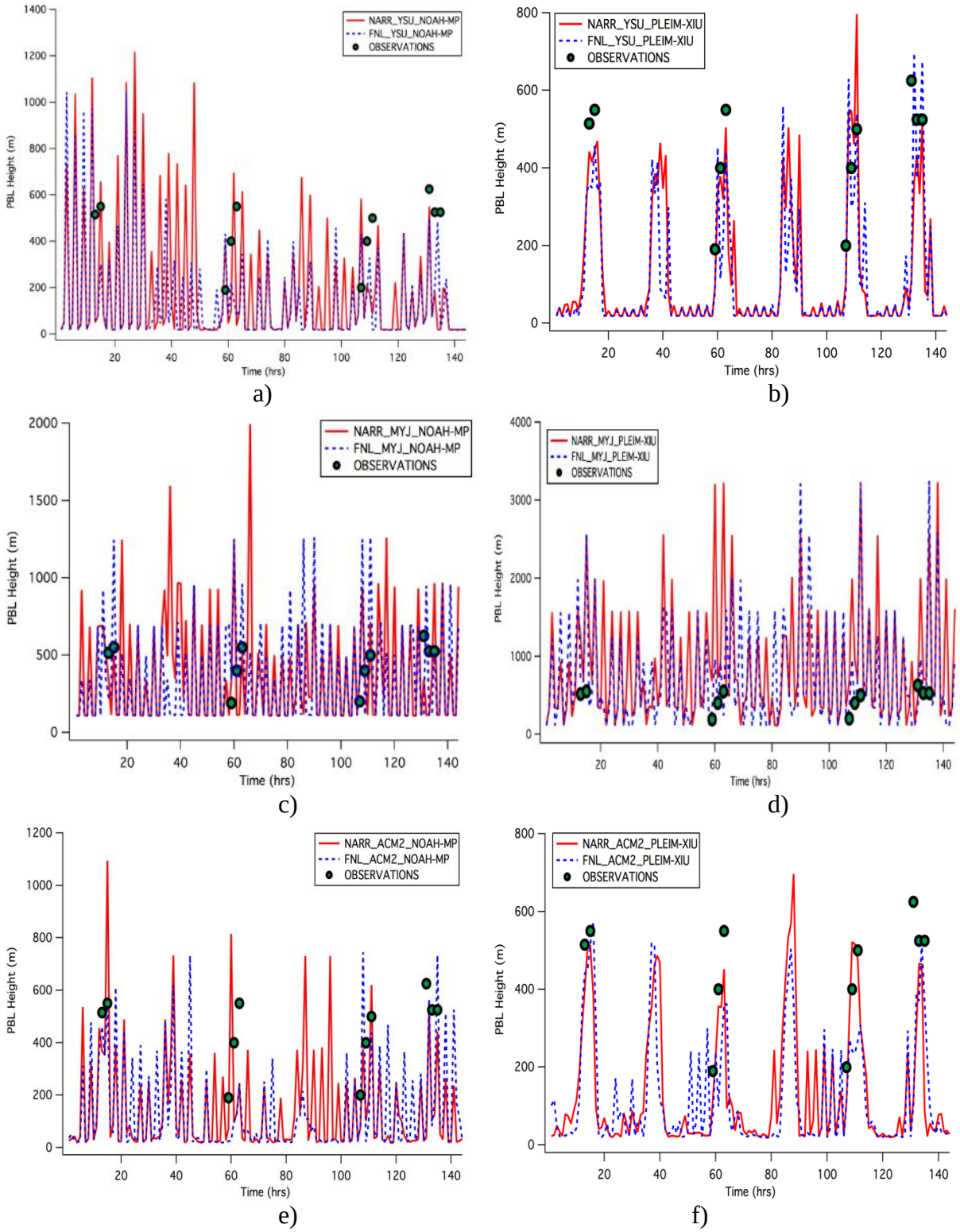

Figure 3-2. Comparisons of timeseries of PBL height at Fresno for different combinations of PBL schemes and land surface schemes a) YSU-Noah-MP, b) YSU-Pleim-Xiu, c) MYJ-Noah-MP, d) MYJ-Pleim-Xiu, e) ACM2-Noah-MP and f) ACM2-Pleim-Xiu, and initial and boundary condition data with the aircraft observations from DISCOVER-AQ.

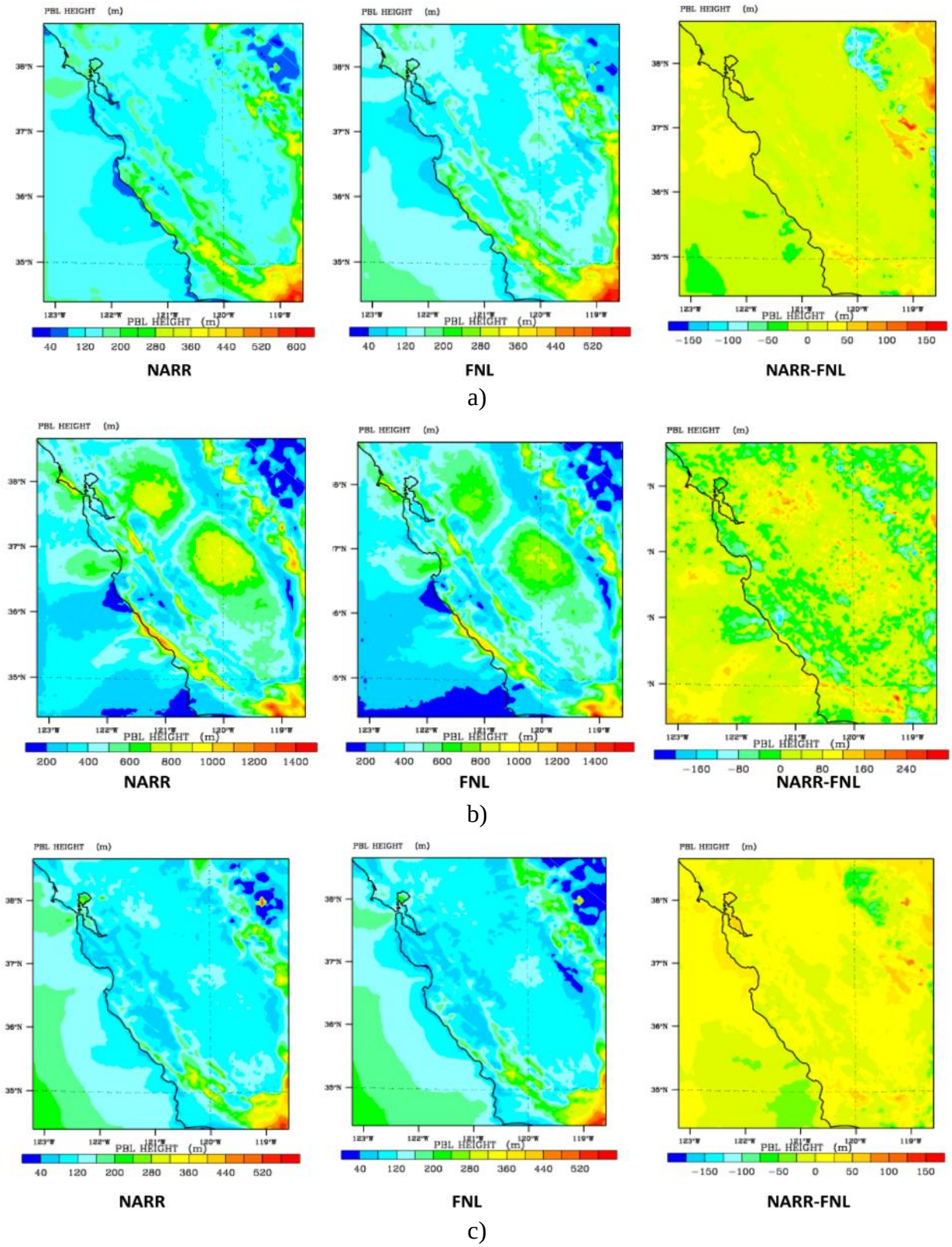

Figure 3-3.6-day averaged PBL height fields for NARR, FNL and their difference for a) YSU-Pleim-Xiu, b) MYJ-Pleim-Xiu and c) ACM2-Pleim-Xiu

3.5 Conclusions

A systematic study was carried out to identify the ideal combination of land surface schemes, PBL schemes and the initialization data that minimizes the bias between measurements and predictions from WRF v3.4 during a winter stagnation event in the SJV with significant nitrate formation. For most cases, NARR initialization data slightly over predicts PBLH in SJV as compared to FNL initialization data. The Noah-MP land surface scheme, in general, performs poorly when combined with any of the tested PBL schemes for winter conditions in the SJV. The Noah-MP scheme is not appropriate for use simulating winter nitrate events in central California. The YSU and ACM2 PBL schemes coupled with PLEIM-XIU land surface scheme produce the most accurate predictions for PBL height which closely match the measurements at Fresno during the DISCOVER-AQ field campaign. The YSU and ACM2 PBL schemes are suitable for nitrate predictions in central California.

In general, PBL height prediction depends more on combination of PBL and land surface schemes used than the type of initial and boundary condition data used. The YSU and ACM2 PBL schemes coupled with PLEIM-XIU land surface scheme produced results that were not strongly sensitive to the choice of initialization / boundary condition data (NARR or FNL).

PBL schemes based on non-local closure models performs much better than the ones based on local closure models. These results are consistent with findings from studies that use air quality models with non-local closure schemes for vertical mixing.

4 EFFECT OF INCREASING SOIL MOISTURE ON HUMIDITY ANDPARTICULATE NITRATE FORMATION

4.1 Introduction

The formation rate of nitrate precursors depends strongly on temperature, humidity, and UV intensity. Likewise, the partitioning of nitric acid to the condensed phase is a strong function of temperature and humidity. Uncertainty in meteorological fields can therefore introduce significant uncertainty into predicted nitrate concentrations. Consistent bias in meteorological fields can introduce consistent bias in those same concentrations.

As part of the development of the California State Implementation Plan (SIP) for airborne particulate matter ($PM_{2.5}$), staff at the California Air Resources Board (CARB) identified a consistent bias in meteorological fields for humidity in their WRF simulations. Humidity was consistently under-predicted by WRF simulations for winter stagnation events, leading to a reduced production rate for $PM_{2.5}$ nitrate. CARB staff hypothesized that the humidity under-predictions were related to inaccuracies in the soil moisture specified in the WRF land-surface model. The correction proposed by CARB staff was to increase the moisture availability for cultivated crops from 0.5 to 0.7 which increases the humidity in the atmosphere immediately above the surface.

The purpose of this chapter is to evaluate the effects of the changes in moisture availability on ambient humidity and predicted nitrate concentrations in the San Joaquin Valley. Soil moisture availability was increased for cropland yielding altered WRF meteorological fields for the time period spanning Jan-Feb 2013. The changes to the accuracy of predicted WRF humidity fields was evaluated. Air quality simulations were then conducted using the new meteorological fields, and the accuracy of the predicted pollutant concentrations was compared to the accuracy of the original calculations. The magnitude of the changes in predicted nitrate concentrations resulting from perturbation in humidity are then compared to the magnitude of changes induced by emissions of soil NOx.

4.2 Methods

4.2.1 WRF Configuration

Meteorological simulations were carried out using the Weather & Research Forecast (WRF) model v3.6 using the Pleim-Xiu land-surface model. Simulations were conducted with the moisture availability of cropland set to the original value of 0.5, and with the moisture availability of cropland increased to 0.7. Moisture availability is a dimensionless parameter related to the volumetric soil moisture content. Moisture availability varies from 1.0 for a water surface to 0.0 for a surface with no potential for evaporation.

Figure 4-1 illustrates the map of soil types in California. Moisture availability was increased to 0.7 in landuse type 38 (cropland) which falls primarily in the Central Valley and the area immediately south of the Salton Sea.

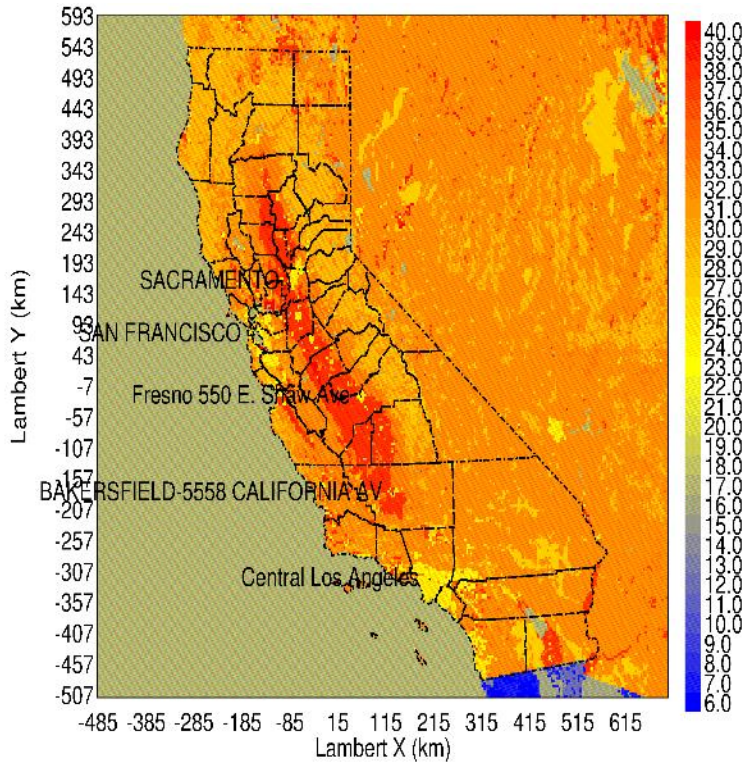

Figure 4-1.LU_INDEX from NCLD40 data (Cultivated Crops assigned number is 38)

Simulations were conducted for Jan-Feb 2013 to support a two-month air quality analysis using three levels of nesting with 36 km, 12 km, 4 km horizontal resolution over central California (see Figure 2-1 for domains). The WRF vertical resolution was 31 telescoping levels up to a height of 100 hPa (approximately 16 km). WRF simulations were initialized from North American Regional Reanalysis (NARR), which has a spatial resolution of 32 km and a temporal resolution of 3 h. Four-dimensional data assimilation (FDDA) was applied to anchor predictions to observed values, and the surface friction velocity (u*) was also increased by 50% in these simulations. The Yonsei University (YSU) boundary layer vertical diffusion scheme was adopted along with the National Land Cover Data (NLCD) 40 category land-use data for this two months simulation.

4.2.2 Air Quality Model Configuration

The configuration of the UCD/CIT air quality model was identical in Chapters 2, 4, and 6. Briefly, model simulations were configured using a one-way nesting technique with a parent domain of 24 km horizontal resolution that covered the entire state of California and a nested domain with 4 km horizontal resolution that covered the San Joaquin Valley (SJV). Calculations used 15 telescoping vertical layers up to a top height of 5km. Further details of the UCD/CIT air quality model are provided in Chapter 2.

4.2.3 Emissions

Basic emissions of criteria pollutants in the current study are identical to those described in Chapter 2 and so only a brief over-view is provided here. Inventories for area sources, point sources, and

mobile sources were provided by the California Air Resources Board for the years 2000, 2010, and 2015. Area and point source emissions for other years were interpolated between these points. Mobile emissions were adjusted for year and local meteorological conditions using EMFAC 2014, biogenic emissions were predicted using MEGAN [16], and wildfire emissions were generated using the Global Fire Emissions Database (GFED) [18]. Fugitive dust emissions were calculated online using the method described by [21]. Candidate soil NOx emissions used in the current Chapter as described in greater detail in Chapters 5 and 6.

4.2.4 Boundary Conditions

The gas and particle phase initial and hourly varying boundary conditions for the UCD/CIT model were taken from the global model MOZART-4/NCEP (a model for ozone and related chemical Tracers). Additional details of MOZART simulations are provided by Emmons et al. [24].

4.3 Results

4.3.1 Meteorological Predictions

Figure 4-2 shows the measured and predicted for relative humidity (RH), temperature at 2m (T2), and wind speed (WS) under base-case (Base) and altered (SM) soil moisture availability. Figure 4-3 shows the mean fractional bias (MFB), mean fraction error (MFE), and root mean square error (RMSE) for these same meteorological variables. These statistics were calculated for meteorological stations location in the Central Valley since this is where the changes to soil moisture primarily occurred. The increased soil moisture availability reduces the mean fractional bias inn RH from -6% to -2% and reduces the mean fractional bias in T2 from 27% to 20% but increases the mean fractional bias in wind speed from 5.5% to 7%.

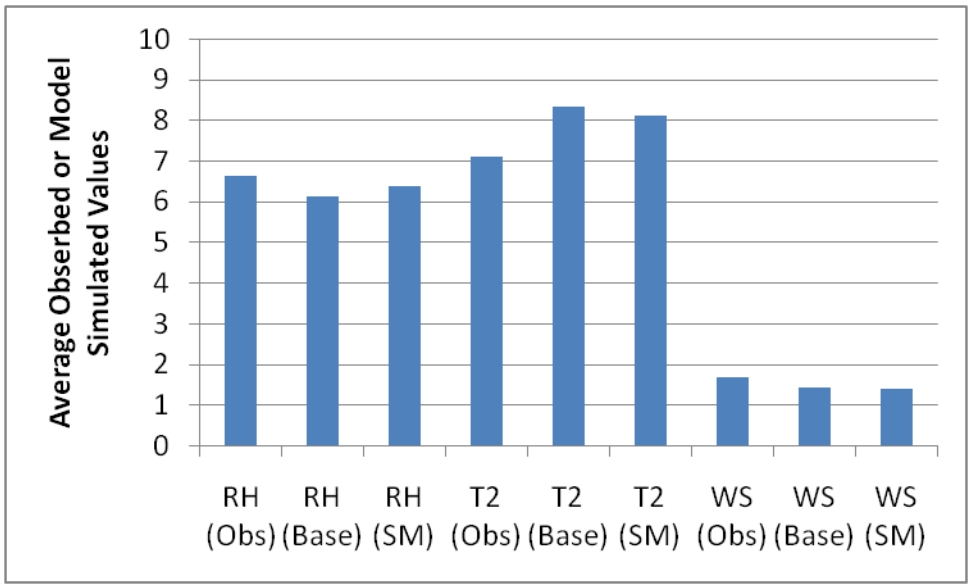

Figure 4-2. Average observed and simulated (base as well as SM cases) relative humidity (%), temperature (ºC) and wind speed (m/s) over SJV during Jan-Feb 2013. (**Note**: Here RH values are dived by 10 to place them on the same scale)

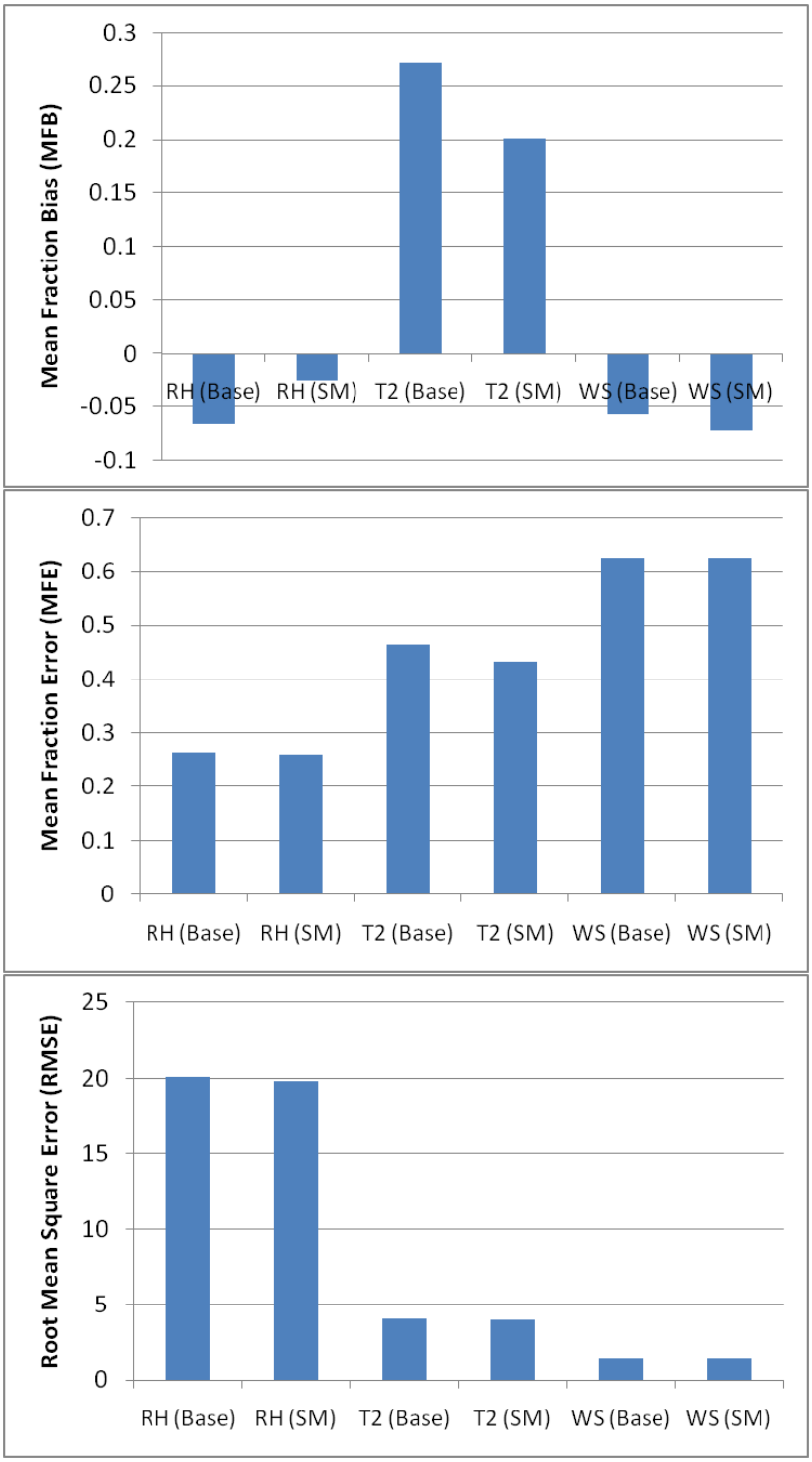

Figure 4-3. Meteorology evaluation (MFB, MFE and RMSE) (base case and revised soil moisture case) of relative humidity (%), temperature (ºC) and wind speed (m/s) during Jan-Feb, 2013 over SJV. Here, SM represents modified soil moisture case.

Figure 4-4 shows the regional ground-level relative humidity plot averaged over the two month simulation period Jan-Feb 2013. Figure 4-4a illustrates the base-case RH, with average values of approximately 83% in the Central Valley. Figure 4-4b illustrates the change in RH when soil moisture availability is increased from 0.5 to 0.7 over cropland. RH increases by approximately 3-6% in response to the increased soil moisture, with the majority of this effect occurring directly over the affected soils.

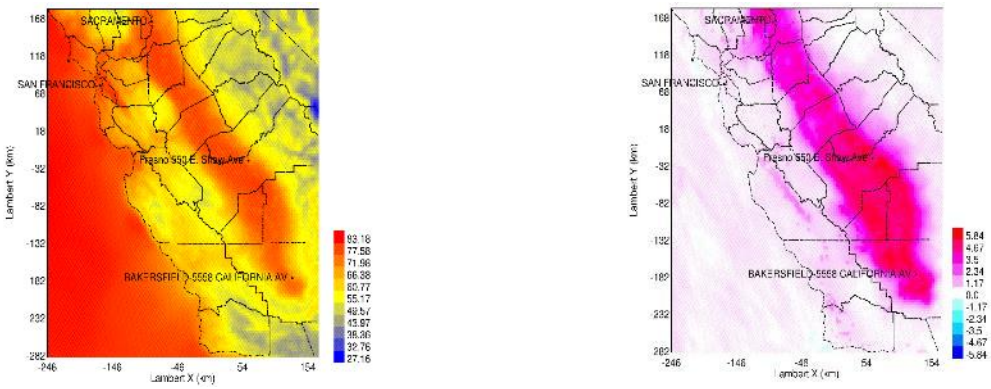

(a) (b)

Figure 4-4.(a) Spatial distribution of base and (b) differences (revised soil moisture – base case) relative humidity(%) t surface level during DISCOVER-AQ episode over 4 km domain

4.3.2 Nitrate Predictions

Figure 4-5 shows the regional ground-level PM2.5 nitrate concentrations predicted over central California during Jan-Feb 2013. Figure 4-5e shows that increasing soil moisture leads to a 0.5 µg m^{-3} increase in predicted nitrate concentrations. In comparison, Figure 4-5g shows that adding candidate soil NOx emissions increases predicted $PM_{2.5}$ nitrate concentrations by 2.8 µg m^{-3} over the simulation period. Figure 4-5h shows that the effects of increasing soil moisture are independent of the soil NOx condition, leading to an additional 0.5 µg m^{-3}.

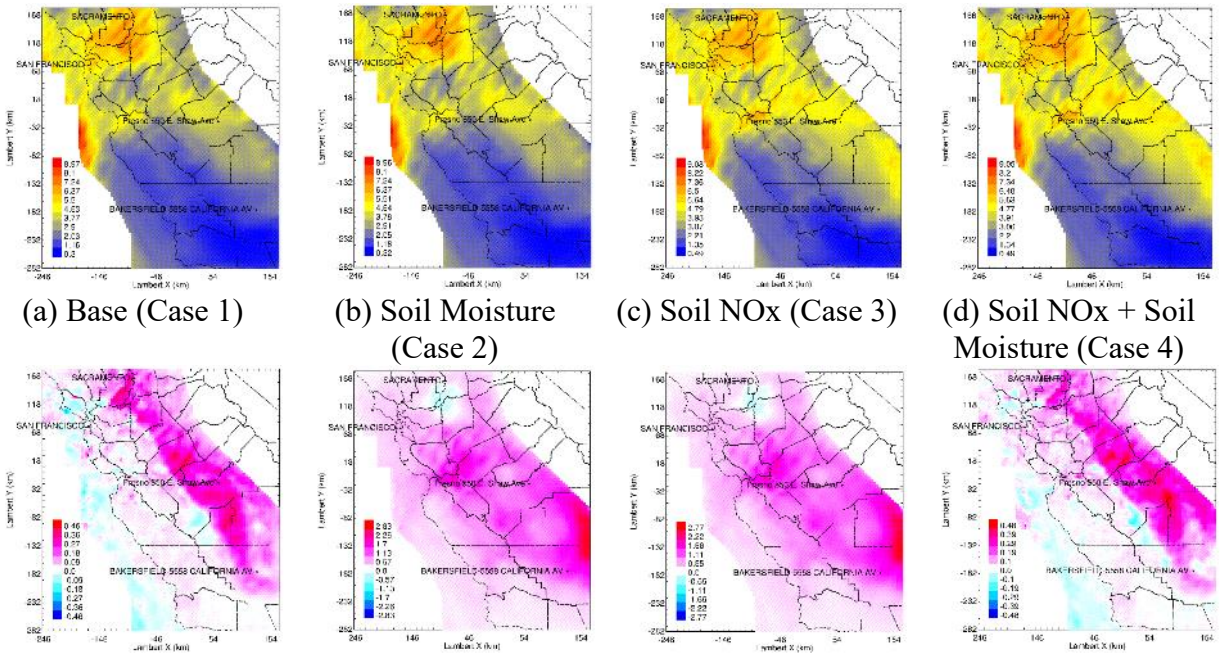

(a) Base (Case 1) (b) Soil Moisture (Case 2) (c) Soil NOx (Case 3) (d) Soil NOx + Soil Moisture (Case 4)

(e) Case 2 – Case 1 (f) Case 4 – Case 2 (g) Case 3 – Case 1 (h) Case 4 – Case 3

Figure 4-5. Spatial distribution of surface PM2.5 nitrate concentration (μg/m^3) during DISCOVER-AQ episode over 4 km domain

Figure 4-6 shows the time-series of predicted $PM_{2.5}$ nitrate concentrations at Fresno from January 16, 2013 – February 11, 2013 with base-case humidity (Base) and increased humidity due to the increase in soil moisture availability (Soil Moisture). The increased soil moisture slightly increases predicted $PM_{2.5}$ nitrate during short time periods but otherwise has little effect. Notably, predicted $PM_{2.5}$ nitrate concentrations are not consistently increased during periods when measured nitrate concentrations reached peak values.

The"nighttime" chemical pathway for nitrate formation thought to dominate during cold winter months in the SJV involves thereactions summarized below:

$$NO + O3 \rightarrow NO2 \quad (4\text{-}1)$$

$$NO2 + O3 \rightarrow NO3 \quad (4\text{-}2)$$

$$NO3 + h\nu \rightarrow NO2 + O(3P) \quad (4\text{-}3)$$

$$NO2 + NO3 \rightarrow N2O5 \quad (4\text{-}4)$$

$$N2O5 \rightarrow NO2 + NO3 \quad (4\text{-}5)$$

$$N2O5 + H2O \rightarrow HNO3 \quad (4\text{-}6)$$

The final reaction in this sequence (4-6) occurs on wet particle surfaces and is therefore limited by relative humidity under dry conditions. The basecase relative humidity predicted by the WRF v3.6 simulations predict relative humidity of approximately 80% in the SJV, which is sufficient to wet

particle surfaces that enable reaction 4-6 to proceed at a rate limited only by the diffusion of N_2O_5 to particle surfaces. As a result, increasing relative humidity has little effect on predicted nitrate formation in the current study.

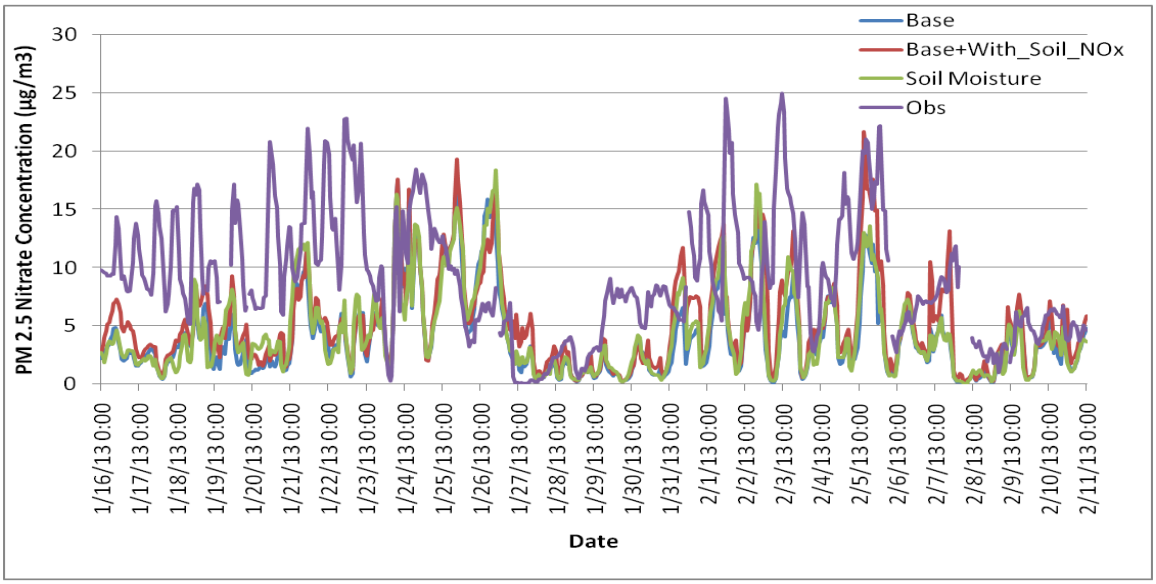

Figure 4-6. Time series of predicted $PM_{2.5}$ nitrate concentrations under basecase humidity conditions and increased humidity conditions when soil moisture availability is increased.

Figure 4-6 also shows the time-series of predicted $PM_{2.5}$ nitrate concentrations at Fresno with base-case humidity plus candidate soil NOx emissions. Results with increased humidity due to the increase in soil moisture availability are also shown for comparison. Increasing soil NOx emissions at the base-case humidity level increases predicted $PM_{2.5}$ nitrate concentrations at Fresno during peak episodes, especially during the latter portion of the simulation period. The inclusion of candidate soil NOx emissions generally improves the accuracy of the model predictions for particulate nitrate during the last half of the simulation period.

The supply of NOx to the mechanism summarized in equations 4-1 through 4-6 appears to have a larger effect on the predicted nitrate concentration than the relative humidity which affects the rate of the final reaction 4-6 under dry conditions. These findings are consistent with previous studies that examined NOx-VOC control isopleths for particulate nitrate formation in the SJV. Kleeman et al. [6] studied the conditions in the SJV during winter 1995 and concluded that particulate nitrate concentrations increased strongly with increasing NOx emissions. Reynolds et al. [25] studied conditions in the SJV during the winter of 2000-2001 and reached a similar conclusion that increasing emissions of NOx lead to increasing levels of predicted $PM_{2.5}$ nitrate.

4.4 Conclusions

Increasing soil moisture availability from 0.5 to 0.7 for cropland in California's SJV increased predicted relative humidity by approximately 5% during Jan-Feb 2013. This change improves the accuracy of WRF predictions for relative humidity and surface temperature, but decreases the accuracy of WRF predictions for wind speed. $PM_{2.5}$ nitrate concentrations predicted by the UCD/CIT air quality model increase by approximately 0.5 $\mu g\ m^{-3}$ in response to the increased humidity. This amount of additional nitrate formation is potentially significant given that basecase nitrate concentrations are typically on the order of 4 $\mu g\ m^{-3}$, but the soil moisture effect is diminished by the fact that basecase humidity in the simulations was already approximately 80% which provides sufficient wet particle surface area for conversion of N_2O_5 to nitric acid.

Adding candidate soil NOx emissions increased predicted $PM_{2.5}$ nitrate concentrations by approximately 2.5 $\mu g\ m^{-3}$ across the SJV during the period January 16, 2013 – February 11, 2013. These changes improve the agreement between model predictions and measurements of $PM_{2.5}$ nitrate during the period January 16, 2013 – February 11, 2013. The finding that regional nitrate concentrations are predicted to increase in proportion to NOx emissions is consistent with previous studies of the SJV.

5 EFFECT OFCANDIDATE SOIL NOx EMISSIONS, MODEL VERTICAL RESOLUTION, AND ORGANIC-NITRATE FORMATION ON PREDICTED NITRATE VERTICAL DISTRIBUTIONS

5.1 Introduction

Anthropogenic sources of NOx such as transportation and industrial activities dominate global emissions (21–28 Tg N yr^{-1}) but natural emissions estimated from 17-37 Tg N yr^{-1} cannot be ignored. These natural sources of NOx include soil emissions in the range of 9–17 Tg N yr^{-1}. NOx emissions from soil are highest in agricultural regions where nitrogen fertilizers are applied. Soil NOx can therefore be an important factor for rural air quality where other sources of NOx are less prominent.

The San Joaquin Valley (SJV) in California is one of the most intensive agriculture areas in the United States. A large variety of crops are grown in the SJV including alfalfa, almonds, citrus, corn, cotton, and wheat. A recent survey determined that nitrogen fertilizers are applied in winter months to alfalfa (18% surveyed applied an average of 27.5 kg-N ha^{-1}), cotton (45% surveyed applied an average of 93.5kg-N ha^{-1}), and wheat (85% surveyed applied an average of 88kg-N ha^{-1}). These fertilizer applications have the potential to contribute to soil NOx emissions during winter months, which can then contribute to particulate nitrate formation.

Previous emissions inventories produced by the California Air Resources Board have not included soil NOx emissions, presumably because these emissions are much lower than anthropogenic NOx emissions from urban areas in the SJV. While the emission rate of soil NOx may be low, the conversion efficiency of this NOx to particulate nitrate can be very high. Nighttime chemistry leading to particulate nitrate formation during winter months is driven by the reaction sequence shown below where O3 is background ozone (not produced locally).

$$NO + O3 \rightarrow NO2 \qquad (5\text{-}1)$$

$$NO2 + O3 \rightarrow NO3 \qquad (5\text{-}2)$$

$$NO2 + NO3 \leftrightarrow N2O5 \qquad (5\text{-}3)$$

$$N2O5 + H2O(liquid) \rightarrow particulate\ nitrate \qquad (5\text{-}4)$$

The nitrate radical (NO3) rapidly photolyzes and so reactions (1-4) above are most effective at producing particulate nitrate at night. Based on stoichiometry, fully converting 1 ppb of NOx to 2.54 µg m^{-3} particulate nitrate requires 2 ppb of background O3. Given that background O3 concentrations are approximately 40 ppb in California, maximum nitrate conversion efficiency will occur in regions with nighttime NOx concentrations ≤20 ppb. Regions with nighttime NOx concentrations between 20-40 ppb will experience decreasing efficiency for nitrate conversion. Regions with ≥40 ppb of NOx will have very low conversion efficiency to particulate nitrate because all of the O3 will be titrated by reaction (1) to produce NO2.

Typical NOx concentrations in SJV cities like Fresno exceed 100 ppb during evening hours making nitrate production at ground level in the urban core highly inefficient. Zones with

nighttime NOx concentrations ≤20 ppb are expected to develop in residual layers above these urban cores, or in rural areas with low level emissions of NOx for sources such as soils. Both of these efficient nitrate production zones will be examined in the current chapter.

Investigation of efficient nitrate production in residual layers above urban cores may require changes to the model configuration. Riemer et al., 2003 determined that mixing and vertical resolution in model calculations may be a critical feature in resolving residual layers of NOx and O3 that lead to efficient particulate nitrate formation. Modern versions of meteorological models which are used to prepare inputs for the regional CTMs already include advanced mixing algorithms beyond simple K theory, such as non-local transport theory that account for the movement of material from ground level directly to elevated model layers due to the action of turbulent eddies that are larger than individual grid cells [26, 27]. Section 3 of this report details the selection of the optimal combination of PBL/land surface/boundary conditions for the SJV. Even with these improvements, however, the telescoping vertical layers typically used by CTMs can dilute concentrations in nighttime residual layers and potentially shift the ratio of NOx / O3 to less optimal conditions for particulate nitrate formation. Thus, tests were conducted using increased vertical resolution in order to properly resolve nighttime residual layers above urban areas in the SJV to determine if they contain zone of efficient nitrate production.

Recently, organic nitrates have been recognized as a significant contributor to PM2.5 OA mass in Alabama, Colorado, and California [28-31]. More than half of that organic nitrate is thought to come from NO3 radical oxidation of monoterpenes. Pye et al. [32] formulated a coupled gas and aerosol system within the CMAQ model to describe the formation of organic nitrates from isoprene and monoterpenes and the subsequent partitioning of these compounds to the particle phase. Tests were conducted with these new reactions added to the SAPRC11 chemical mechanism to determine if the contribute significantly to particulate nitrate formation in the SJV.

In this section, Hypothesis 2, 3, and 4 (described in Section 1.3) are tested using UCD/CIT model for a 4km SJV domain during the DISCOOVER-AQ campaign. Four test cases, namely Basecase, Newmech, BasecaseSoilnox and Hires Soilnox, were carried out and the resulting model predictions were compared with the measurements from the DISCOVER-AQ campaign. The 4 test cases are briefly described in the Table 5-1 with further details provided in the sections below.

Table 5-1: Description of all 4 test cases formulated to test Hypothesis 2 and 3.

CASE		BASE	BASE_NEW	BASE_SOIL	HI-RES_SOIL
Resolution	Horizontal	4km			
	Vertical	16 layers			42 layers
Grid Cells		104 x 116			
Time period		January 16 -February 10, 2013			
Meteorology		WRF v3.4 run with NARR reanalysis data			
Emissions	Anthropogenics	CARB (2010)			
	Wildfires	FINN, NCAR [33]			
	Biogenics	MEGAN [16]			
	Soil NOx	-	-	N-isotope and IMAGE model [34, 35]	
Gas-phase mechanism		SAPRC-11	Expanded SAPRC-11 [32]	SAPRC-11 [15]	
Inorganics		ISORROPIA II [13]			
Initial/Boundary conditions		MOZART-4/NCEP [24]			
SOA model		2-product model [14]			

5.2 Methods

5.2.1 Air Quality Model

The UCD/CIT air quality model used in the current study is a source-oriented regional chemical transport model that simulates the emissions, transport, gas-phase chemistry, aerosol physics and aerosol chemistry (dynamic gas/particle partitioning, coagulation, thermodynamics and deposition) in the lower atmosphere [36, 37]. The model has been successfully applied to predict regional gas and aerosol concentrations in numerous studies [7, 36-52]. A detailed description of the modules used to represent different processes in the model can be found in previous studies: transport [36, 53], gas-phase chemical mechanism [15], inorganic aerosol thermodynamics [54] and deposition [36, 55]. Here, only a brief description of recent updates to UCD/CIT model is provided. For this study, the SAPRC-11 gas-phase chemical mechanism was updated to expanded SAPRC-11; expanded SAPRC-11 differs from the SAPRC-11 used in earlier versions of the UCD/CIT model in that it has an expanded treatment of NOx and OH chemistry of VOCs, which results in formation of ONs, especially for isoprene and monoterpenes. The particle-phase mechanism was updated to include NO_3^- formation from hydrolysis of ONs and SOA formation from glyoxal and methyl glyoxal. The detailed information of these changes to the gas-phase and particle-phase mechanisms can be found in Pye et al., 2015 [32]. The expanded SAPRC-11 chemical mechanism was modified such that it could be compatible with the currently used CARB emissions for SAPRC-11 [56]. The vertical layer structure of current UCD/CIT model atmosphere was also updated; incorporating 42 telescoping levels up to a maximum height of 5 km above the ground as compared to 16 levels used in standard model versions. Vertical mixing in the model, represented with the vertical turbulent diffusion coefficient (Kzz), was updated to better represent the diurnal cycles that occur in the SJV. During the evening hours when the atmosphere is stable, the minimum allowable Kzz (Kzz,min) values were reduced, from 0.5 $m^2\ s^{-1}$ to 0.01 $m^2\ s^{-1}$, in the

stable surface layer to prevent artificial mixing. During the hours immediately after sunrise when the surface layer is in neutral conditions, low Kzz (~0.04 m^2 s^{-1}) values were enforced above the mixing depth to prevent artificial mixing. Both of these changes improved the representation of the vertical concentration profiles in the model calculations, which are critical to testing several theories for particulate nitrate formation.

The UCD/CIT model was used to simulate air quality in the SJV region for the entire DISCOVER-AQ field study which spanned from January 13– February 10, 2013; treating first 3 days as spin up time for the model to avoid any unwanted effects due to initial and boundary conditions (IC/BC). Table 5-1 summarizes all the details of the chemical transport model and modeling system used in this study.

5.2.2 Emissions

NOx emission from California soils (natural and cropland), which are not included in the current CARB emission inventory, were estimated using a soil N-isotope model [57] for natural areas and an Integrated Model forthe Assessment of the Global Environment (IMAGE) model [34, 35] for cropland areas. These models estimated the soil NOx based on surplus nitrogen (N) gases in the environment. The N-surplus was calculated as the difference between N-inputs and N-outputs for natural and cropland areas. This surplus was then partitioned betweenleaching and gaseous losses based on parameters such as temperature, precipitation/irrigation, evapotranspiration, soil texture, soil drainage, soil organiccarbon content, soil total available water content, and land cover. These gaseous losses were then partitioned based on water-filled pore space to provide an estimate of NOx emission. Additional details about the candidate soil NOx emission models can be found in Wang et al.[58] and Bai et al. [57]. The raw candidate soil NOx emissions were acquired directly from the authors, with further details in Almaraz et al., 2018 [35]. These soil NOx emissions, due to their biogenic nature, are appended to the biogenic emissions prepared as an input to the UCD/CIT model.

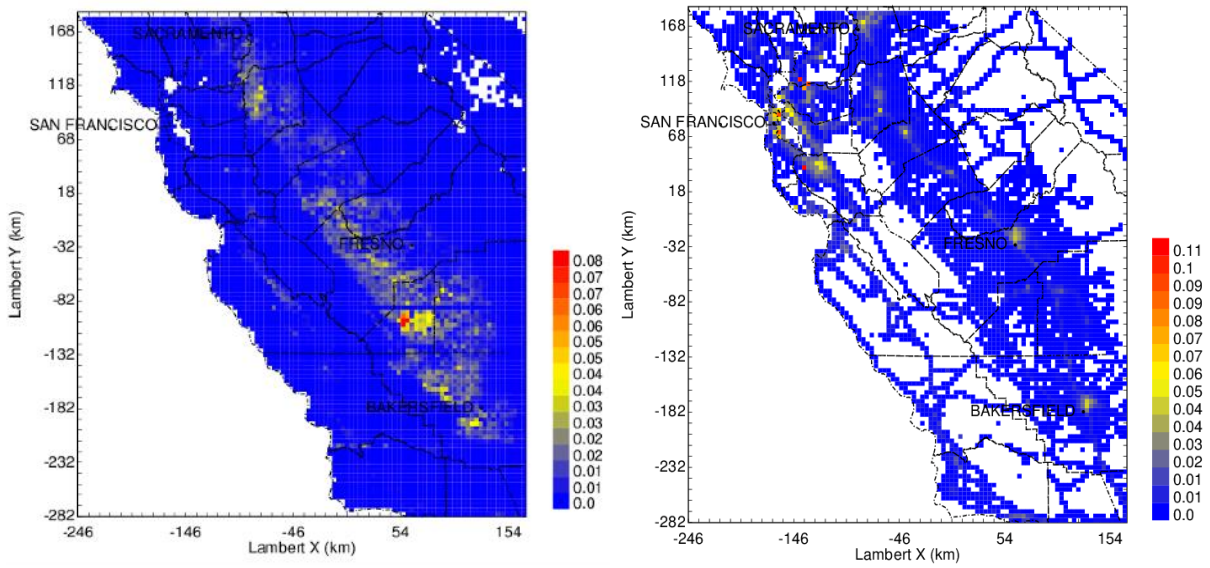

Figure 5-1. Candidate **s**oil NOx emissions for the month of January, 2013 (left) and non-soil NOx emission for January 16, 2013 (right), over central California. Units are ppm m min^{-1}.

Figure 5-1 illustrates candidate soil NOx emissions (left panel) during the month of January, 2013 and non-soil emissions (right panel) for January 16, 2013 over central California. Candidate soil NOx emissions for February and non-soil NOx emissions for other days also have similar spatial variability. All emissions were processed using the University of California, Davis (UCD) emissions processor.

"Newmech" simulations summarized in Table 5-1 were carried out with a modified chemical reaction system that included reactions between NOx and biogenic species that could potentially lead to particulate nitrate formation. Numerous species were added in the expanded SAPRC11 mechanism by splitting the original SAPRC11 species ARO2, OLE1, OLE2, TERP, ALK3, ARO2 and ARO1 into more detailed species as summarized in Table 5-2 below [56].

The expanded SAPRC11 mechanism is only used for the Newmech case while SAPRC11 is used for all the other cases.

Table 5-2: Emission spiltiing ratios of added species SOAALK, NAPHTHAL, PROPENE, APIN, 13BDE, ETOH, ARO2MN, OXYL, PXYL, MXYL, B124, and TOLUENE based on standard SAPRC11 species ALK3, ALK4, ALK5, OLE1, OLE2, ARO1, ARO2, and TERP

1)	SOAALK = O.1 ALK4 + 0.7 ALK5	7)	ARO2MN = 0.96*0.366 ARO2
2)	NAPHTHAL = 0.04 ARO2	8)	OXYL = 0.96*0.171 ARO2
3)	PROPENE = 0.68 OLE1	9)	PXYL = 0.96*0.073 ARO2
4)	APIN = 0.44 TERP	10)	MXYL = 0.96*0.293 ARO2
5)	13BDE = 0.15 OLE2	11)	B124 = 0.96*0.097 ARO2
6)	ETOH = 0.654 ALK3	12)	TOLUENE = 0.804 ARO1

5.2.3 Meteorology and Initial / Boundary Conditions

The Weather Research and Forecasting (WRF) model v3.4was used to generate hourly meteorological fields for the DISCOVER-AQ period. WRF was configured with the Advanced Research core (ARW) with a horizontal resolution of 4 km and 31 vertical layers up to 100mb (~12km) to provide meteorological input to the UCD/CIT model which was interpolated for 16 telescoping levels for the Basecase, Newmech and BasecaseSoilnox up to 5km. For the Hires Soilnox case, WRF was configured with the Advanced Research core (ARW) with a horizontal resolution of 4 km and 51 vertical layers up to 100mb (~12km) to provide meteorological input to the UCD/CIT model which was interpolated for 42 levels up to 5km. The National Center for Environmental Protection's (NCEP) North American Region Reanalysis (NARR) data were used to set the initial and boundary conditions for WRF.

The gas and particle phase initial and hourly varying boundary conditions for the UCD/CIT model were taken from the global model MOZART-4/NCEP (a model for ozone and related chemical Tracers). Additional details of MOZART simulations are provided by Emmons et al. [24].

5.2.4 Gas Phase Chemistry

Reaction rates between NO2+OH and isoprene+OH / ozone were updated in both SAPRC11 and the expanded SAPRC11 mechanisms based on the latest published values. The expanded SAPRC11 mechanism was then modified to include the explicit reactions between NOx and isoprene that are described in the mechanism of Pye at al.[32]. The expanded reactions were then further updated to separately track isoprene dinitrates (ISOPNN) produced from isoprene + NO_3. ISOPNN is a semi-volatile organic nitrate molecule that readily partitions into the particle phase. The formation of organic nitrates from monoterpenes (analogous to PAN) was also tracked explicitly in the expanded mechanism to better represent their role as NOx reservoirs and SOA precursors. Species lumped into TERP (including β-pinene, δ-limonene, α-terpinene, γ-terpinene, camphene, Δ-3-carene, myrcene, pcymene, ocimene, β-hellandrene, sabinene etc.) are reported to form significant aerosol including organic nitrate [59]. TERP chemistry was updated in the expanded SAPRC11 mechanism to represent organic nitrates formed from monoterpenes as a new species named MTNO3. The rate constants of TERP peroxy + HO_2 reactions were updated based on values listed in the Master Chemical Mechanism (MCM v3.3) which increased their reaction rate by a factor of 2.7 at 298 K. Pye et al.[32] also incorporated heterogeneous conversion of NO_3 to nitric acid but this pathway was not included in the present study. Sensitivity tests show that this omission has negligible effects on HNO_3/NO_3^- concentrations since NO_3 concentrations are

very low. The complete list of the expanded reactions in the expanded SAPRC11 mechanism is available in Pye et al. [32].

5.2.5 Organic Aerosol Treatment

The treatment of organic aerosol in the UCD/CIT model version employed in this study follows the scheme of Carlton et al. [60]. Primary organic aerosol (POA) is considered to be non-volatile while semi-volatile secondary organic aerosol (SOA) forms via a 2-product parametrization from precursors such as monoterpenes, sesquiterpenes, isoprene, benzene, toluene, xylene and naphthalenes. These aerosol species then undergo oligomerization to produce non-volatile species. The expanded SAPRC11 model also includes SOA formation from IEPOX and MPAN in the form of AIETET, AIEOS, ADIM etc. Additionally, SOA from isoprene dinitrates and monoterpene nitrates (ISOPNN and MTNO3 respectively) is implemented by treating them as semivolatile species capable of partitioning to the particle phase. ISOPNN was modeled as a C5 dihydroxydinitrate with a molecular weight of 226 g mol^{-1} and saturation vapor pressure (C*) of 8.9 μg m^{-3}[61]. MTNO3 was modeled as a dihydroxy nitrate with a molecular weight of 231 g mol^{-1} and saturation vapor pressure (C*) of 12.1 ug m^{-3} [62]. Temperature effects on partitioning were modeled using an enthalpy of vaporization equivalent to 40 kJ mol^{-1}. ISOPNN and MTNO3 undergo hydrolysis (more of a pseudo hydrolysis designed to maximize the amount of particulate organic nitrate) that converts them to nonvolatile SOA. The sum of particle-phase monoterpene nitrates, isoprene dinitrates, and their hydrolysis products is referred to as particulate organic nitrate-derived aerosol. Previous studies have found that glyoxal and methyl glyoxal can produce ~1 μg m^{-3} of OA [32].

5.2.6 Discover-AQ Field and Aircraft Observations

This study focused on evaluation of the expanded SAPRC11 mechanism by comparing to measurements from the DISCOVER-AQ field campaign in the SJV (Jan 16 - Feb 10, 2013). Measurements were made at multiple locations during this campaigns; the current analysis is focused on the core site of Fresno (Garland) (36.7853°N latitude, -119.7742°W longitude) for DISCOVER-AQ. Vertical profiles were measured with an aircraft-equipped with a HR-ToF-AMS, GCMS, TDILF-MS etc. above Fresno during DISCOVER-AQ to probe the details of local chemistry. These profiles enable a rigorous evaluation of model performance as a function of elevation with a vertical resolution as fine as 20 m.

Table 5-3 summarizes all measurements used in this work. All ground level measurements and averaged diurnal profiles were compared to UCD/CIT model predictions from the first level (representing 0 to about 30 m above ground level). Vertical measurements were compared to model predictions from the 16 vertical levels for Basecase, Newmech and BasecaseSoilnox and 42 vertical levels for the Hires Soilnox case reaching a maximum height of 5 km above ground level.

Table 5-3: Measurement data sources for DISCOVER-AQ (http://www-air.larc.nasa.gov/missions/discover-aq/discover-aq.html) field campaign.

Campaign	Measurement/ Species	Phase	Technique	Location
DISCOVER-AQ	Species measured in an aircraft flight with spirals planned at specific locations (NOx, CO, nitrate, sulfate, benzene, Methanol, Isoprene etc.)	Gas/Particle	HR-ToF-AMS, PILS-AMS, GCMS etc.	Aloft and close to the ground as well
DISCOVER-AQ	Some ground measurements (NOx, CO, PM2.5, O3 etc.)	Gas/Particle	ARB Air Quality Now database with station measurements	Ground

5.3 Results

5.3.1 Ground Level Time Series and Diurnal Profiles

Figure 5-2 summarizes the time series of predicted and measured pollutant concentrations for different test cases at ground level at the Fresno site between Jan 16 – Feb 10, 2013. Periods of special interest include January 14-23 and January 29-February 5, 2013 because PM2.5 concentrations exceeded the 24 h average National Ambient Air Quality Standard for PM2.5 (35 $\mu g\ m^{-3}$) during these times.

BASE and BASE_NEW predictions are essentially identical as demonstrated by the time series plots (Figure 5-2) and performance statistics (Table 5-4) at Fresno, suggesting that the expanded chemical mechanism has limited impact under the conditions experienced during the simulated period. The maximum gas-phase monoterpene and isoprene nitrate concentrations in the BASE_NEW case are ~0.02 ppb and ~0.0004 ppb respectively. If 100% conversion to aerosol phase is assumed, ~0.1 $\mu g\ m^{-3}$ monoterpene nitrate and ~0.003 $\mu g\ m^{-3}$ isoprene nitrate SOA will be formed. This suggests that there is little organic nitrate SOA formation in the model, or formation of SOA in general, due to particularly low biogenic VOC emissions in the SJV during wintertime. The BASE and BASE_NEW cases are therefore used interchangeably in the remainder of the analysis.

Daytime maximum ozone (O_3) concentrations shown in Figure 5-2 are systematically over-predicted on most days for all cases but the HI-RES_SOIL (average = 15.3 ppb) case has the best O_3 performance followed closely by BASE_SOIL (average =17.0 ppb) and BASE (average = 20.9 ppb) as compared to the measurements (average = 10.9 ppb) (see also MFB and MFE values in Table 5-4). The HI-RES_SOIL case captured the daily nighttime concentrations of O_3 (daily minimum) better than the other cases, possibly due to accurate meteorology predicted by WRF as a result of higher vertical resolution.

Simulated daily maximum O_3 concentrations (Figure 5-2) are generally equal to the background O_3 concentration (~40 ppb) reflecting the lack of significant local O_3 production in the winter conditions. O_3 concentration at the ground level reflects the competition between the vertical mixing of background O_3 from the upper atmosphere to the surface versus chemical reactions that

consume background O_3. Both reactive nitrogen species and biogenic VOCs react with O_3. Averaged over the entire episode, nighttime ozone concentrations are slightly over-predicted, likely reflecting the mixing down of O_3 from upper layers due to higher diffusion associated with turbulent eddies. The addition of candidate soil NOx emissions improves the performance of O_3 predictions during both daytime and nighttime hours. Predicted O_3 concentrations begin to increase at 6am approximately 1.5 hours before measured O_3 concentrations start to rise. Sunrise during January 2013 occurred at approximately 7:30 am, which corresponds to the onset of increasing measured O_3 concentrations. The early onset of increased concentrations in model predictions reflects premature mixing that also may have prevented the accurate prediction of enhanced ground-level concentrations of CO and NOx in morning to afternoon hours. The predicted ozone concentrations peak at around 12 – 1 pm but the measured ozone peaks at around 2 – 3 pm, with maximum predicted O_3 concentrations of ~35 ppb (HI-RES_SOIL case) and ~42 ppb (BASE case) as compared to a maximum measured concentration of ~28ppb. This offset in maximum O_3 (model versus measurements) could be explained by the higher starting concentrations of O_3 at the beginning of the day due to the under-prediction of NOx concentrations during morning hours before sunrise.

Ground-level concentrations of pollutants with major contributions from primary emissions (CO) are significantly under-predicted by model calculations, especially in the morning, suggesting that either the emissions strength is too low (more likely) or the model experiences inappropriate mixing leading to dilution rates that are too high. The performance statistics including the average, mean fractional bias (MFB) and mean fractional error (MFE) are provided in Table 5-4.

Predicted NOx concentrations (Figure 5-2) are in reasonable agreement with measurements for all test cases except a few days (19-20 and 21-22 January) where the NOx concentrations are in excess of the measurements. The HI-RES_SOIL (average = 46.8 ppb) and BASE_SOIL (average = 45.4 ppb) cases perform better than the BASE (average = 37.5 ppb) case in comparison to the measurements (average = 49.5 ppb). The BASE_SOIL (MFB= 0.06) predicts NOx concentrations with slightly less bias than the HI-RES_SOIL (MFB = 0.09) as summarized by the performance statistics in Table 5-4. Early morning concentrations of NOx, associated with the rush hour period, are constantly under-predicted in the model calculations. This is also confirmed by the diurnal profile of NOx concentrations shown in Figure 5-2. The measured NOx diurnal profile peaks at around 8 – 9 am while the predictions peak at around 6 – 7 am which suggests premature mixing in the model calculations. Both HI-RES_SOIL and BASE_SOIL cases seem to do an equally good job at predicting NOx diurnal profiles, with greater nighttime concentrations in HI-RES_SOIL case.

Particulate nitrate (NO_3^-) and ammonium (NH_4^+) concentrations exhibit similar timeseries pattern reflecting the formation of ammonium nitrate (NH_4NO_3). The BASE_SOIL and HI-RES_SOIL cases predict significantly higher nitrate concentrations compared to the BASE case. The episode-average concentration of NO_3^- in Fresno is 7.84 µg m^{-3} for BASE_SOIL case and 10.9 µg m^{-3} for HI-RES_SOIL case, both of which are closer to measurements (average = 9.05 µg m^{-3}) than the BASE (average = 5.13 µg m^{-3}) case. Thus, the addition of candidate soil NOx emissions increased the NO_3^- concentration by ~50% for the BASE_SOIL case and ~110% for the HI-RES_SOIL case as compared to the BASE case. The BASE_SOIL case (MFB = -0.09) performs better than HI-RES_SOIL case (MFB = 0.17).

As discussed above, the NH_4^+ performance trends mirror NO_3^- trends. The average concentration of NH_4^+ is 2.60 µg m^{-3} for BASE_SOIL and 3.60 µg m^{-3} in the HI-RES_SOIL cases, both of which are closer to observations (average = 3.23 µg m^{-3}) as compared to the BASE (average = 1.80 µg m^{-3}) case. Thus, the addition of candidate soil NOx emissions increased the NH_4^+ concentration by ~45% for the BASE_SOIL and ~100% for the HI-RES_SOIL as compared to BASE case. The MFB results show that the BASE_SOIL case (MFB = -0.12) under-predicts NH_4^+ concentrations while the HI-RES_SOIL case (0.14) over-predicts NH_4^+ concentrations.

NO_3^- concentrations are under-predicted (for all cases) on January 21 – 22 due to the transport towards the northern part of central valley in the model. WRF predicted daytime winds blowing northward at high speeds that disrupted the stagnation conditions actually observed during this time period. Under-predictions in NO_3^- are mirrored for NH_4^+ and SO_4^{2-}. Stagnation conditions are established again in the model on January 25 – 26 and January 31 – February 4. The NO_3^-, NH_4^+ and SO_4^{2-} concentrations are over-predicted on January 25 – 26 (for all cases) and January 31 – February 4 (mainly HI-RES_SOIL). During the former time period, huge over-predictions for O_3 as compared to measurements (~10 ppb) and the inability of WRF meteorology (possibly wind speed) to represent the partial disruption of the stagnation episode are responsible for NO_3^-over-predictions. During the latter time period, the higher vertical resolution used in the HI-RES_SOIL case enhances the model stagnation conditions to a greater extent as compared to the standard vertical resolution used in the BASE_SOIL and BASE cases, thus leading to over-prediction of NO_3^- concentrations.

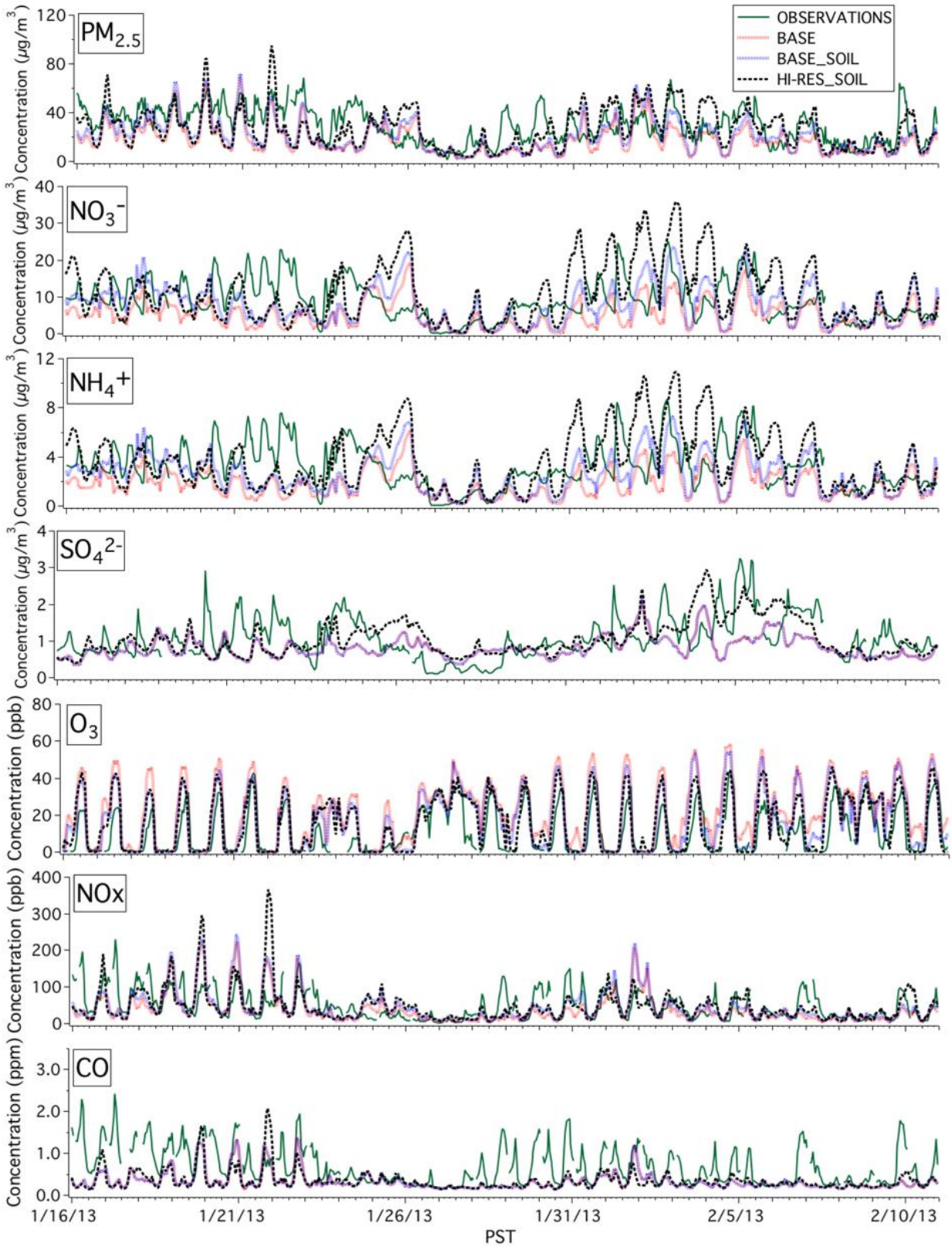

Figure 5-2. Ground-level pollutant concentrations at Fresno during the DISCOVER-AQ campaign.

Table 5-4: Episode-average Mean Fractional Bias (MFB) and Mean Fractional Error (MFE) for CO, NOx, O_3, $PM_{2.5}$, NH_4^+, NO_3^-, and SO_4^{2-} during DISCOVER-AQ.

CASE	Statistic	CO	NOx	NO2	O3	PM2.5	NH4+	NO3-	Sulfate
		ppb				µg m-3			
BASE	Average	325	37.46	24.5	20.91	17.88	1.80	5.13	0.82
	MFB	-0.36	-0.14	0.13	0.32	-0.25	-0.28	-0.28	-0.13
	MFE	0.70	0.71	0.49	1.09	0.64	0.76	0.81	0.55
BASE_NEW	Average	327	37.55	24.3	20.29	17.81	1.76	5.00	0.82
	MFB	-0.36	-0.14	0.13	0.30	-0.25	-0.29	-0.29	-0.13
	MFE	0.70	0.70	0.48	1.11	0.64	0.77	0.82	0.55
BASE_SOIL	Average	326	45.35	-	16.95	21.37	2.59	7.84	0.82
	MFB	-0.45	0.06	-	0.28	-0.36	-0.12	-0.09	-0.09
	MFE	0.70	0.64	-	1.04	0.55	0.65	0.70	0.55
HI-RES_SOIL	Average	340	46.75	27.8	15.33	26.65	3.60	10.91	1.05
	MFB	-0.41	0.09	0.31	0.15	-0.15	0.13	0.17	0.11
	MFE	0.69	0.67	0.53	1.04	0.50	0.64	0.70	0.50
OBSERVATIONS	Average	694	49.52	19.5	10.85	29.82	3.23	9.06	1.07

Figure 5-3 illustrates the average diurnal profile of predicted and measured pollutant concentrations at ground level in Fresno between Jan 16 – Feb 10, 2013. Basecase and Newmech predictions are very similar suggesting that the expanded chemical mechanism has limited impact under the conditions experienced during the simulated period. The Hires Soilnox case seems to move concentrations of all the species in the direction of the measurements followed by BasecaseSoilnox and then Basecase.

The predicted NOx diurnal profile matches well with the measurements except during the morning rush hour period suggesting that either the emissions strength is too low or the dilution is too high. Model calculations also inherently have numerical diffusion associated with instant mixing during the daytime but this artifact is less important at this time because the atmosphere is well mixed below the inversion height. Both BasecaseSoilnox and Hires Soilnox cases seem to do an equally good job at predicting NOx with greater nighttime concentrations in Hires Soilnox.

Local ozone production is weak during the simulated winter conditions represented in Figure 5-3 and so much of ozone measured at the ground level site results from the competition between transport down from background concentrations and chemical reaction. Ozone acts as an oxidant for reactive nitrogen species and biogenic VOCs. Averaged over the entire episode, nighttime ozone concentrations are over-predicted reflecting the under-prediction of NOx concentrations. The addition of candidate soil NOx emission improves the performance of ozone predictions during both daytime and nighttime hours.

Predicted ozone concentrations begin to increase at 6am approximately 1.5 hours before measured ozone concentrations start to rise. Sunrise during January 2013 occurred at approximately 7:30am which corresponds to the onset of increasing measured ozone concentrations. The early onset of increased ozone concentrations in model predictions reflects premature mixing that also may have prevented the accurate prediction of enhanced ground-level concentrations of CO and NOx as discussed above. The predicted ozone concentration peak at around 12-1pm but the measured ozone peaks at around 2-3pm. The delay in the measured ozone peak can also be explained by inappropriate mixing as discussed above. Maximum predicted ozone concentrations are 35 ppb for the Hires Soilnox and 42 ppb for the Basecase while maximum measured concentrations are ~28ppb. This offset appears to be explained by the higher starting concentrations of ozone at the beginning of the day due to the under-prediction of NOx concentrations.

The measured episode-averaged diurnal profiles of NO3-, NH4+ and $SO4^{2-}$ are similar, with a sharp increase between 8am and 10am and peaking around 10-11am, suggesting similar sources and production mechanisms. The daytime peak in concentrations of secondary species has also been observed in previous studies and is primarily attributed to mixing down of these secondary aerosols formed at night in a residual layer aloft [1, 3, 4, 63].

Model calculations predict maximum particulate nitrate concentrations during the evening hours, not during the daylight hours. The diurnal profile of NH4NO3 equilibrium constant as per DISCOVER-AQ measurements [2] matches the predicted NO3- concentrations, which peaks at the time of minimum ambient temperature just prior to sunrise. This finding suggests that model calculations are not able to adequately capture the dynamics of the residual layer. The whole process of nighttime decoupling and post sunrise coupling of the residual boundary layer is explained detail as follows. After sunset at around 5pm, the surface starts cooling thereby suppressing the vertical mixing followed by formation of a shallow nocturnal boundary layer (NBL) and another nocturnal boundary layer (NRL) which forms between the free troposphere and NBL. The initial concentrations of species in NRL is same as that in NBL when the decoupling happens around sunset. After NBL formation, the surface inversion traps fresh emissions but the species in the NRL keep reacting to form secondary aerosols (like NO3-, NH4+, $SO4^{2-}$). Species in the NRL are immune to loss through deposition while species in the NBL deposit throughout the night. The secondary aerosols formed in NRL start to be entrained into the NBL after surface heating and turbulent mixing post sunrise. This is the only time of the day when NRL concentrations are available to be measured by the surface monitors and thus could be a possible reason for the midday peak for secondary organic and inorganic aerosols (NO3-, NH4+, etc.). Further tests are required to determine why these dynamics are not adequately captured by model calculations.

Measured PM2.5 mass diurnal profile peaked primarily at nighttime (contribution from primary aerosols) with two slight peak during the start of rush hour (contribution from secondary aerosols due enhanced oxidation of VOCs and other emissions) and 10-11am (contribution from the NRL coupling post sunrise as discussed above). The model PM2.5 diurnal profile would look much better in sync with the measurements if the model could predict the NRL effect and thereby the midday peak better.

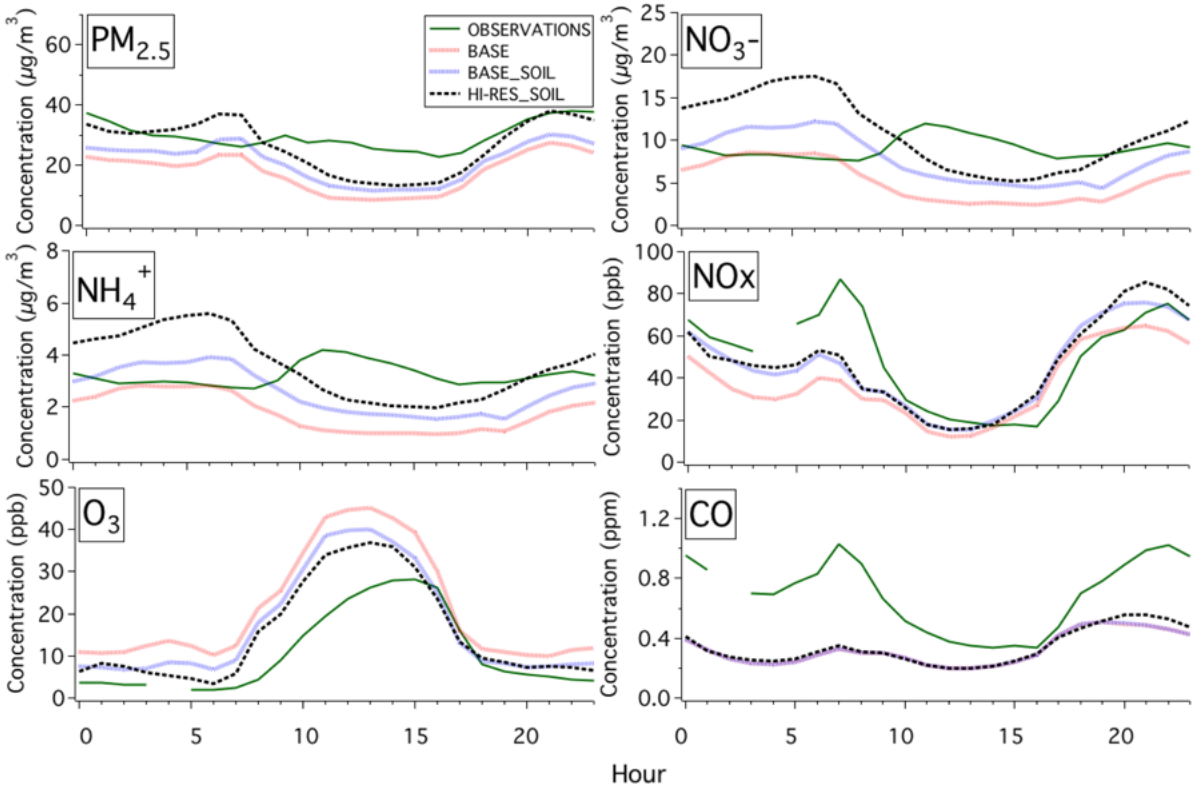

Figure 5-3. Episode-average diurnal profiles at Fresno during the DISCOVER-AQ campaign. Note that enhanced simulations for diurnal profiles are presented in Section 5.3.3.

5.3.2 Vertical profiles

Figures 5-5 through 5-8 illustrate the vertical profiles of measured and predicted pollutant concentrations for all cases up to 1 km from ground above Fresno at different times (10 am, 12 pm and 2 pm respectively) for which P3B aircraft measurements are available. The averaged profiles are calculated by averaging over 7 days (January 18, 20 – 21, 30 – 31 and February 1, 4) during DISCOVER-AQ. It should be noted that the daytime measurements have limited utility because they do not resolve the details of NRL and they do not measure species concentrations during the evening when NO_3^- formation is active. Nevertheless, the vertical profiles help evaluate the model and characterize the overall boundary layer concentrations better than the surface measurements alone.

Approximate PBLH can be estimated by the vertical profiles of primary emissions like CO and NOx. The PBLH estimated from measured vertical profiles is around 250 m, 500 m and 700 m at 10 am, 12 pm and 2 pm respectively. The PBLH estimated from model vertical profiles is around 400 m, 500 m and 700 m at 10 am, 12 pm and 2 pm respectively. This suggests that the model over-predicts mixing during the morning hours by mixing pollutants above the PBLH predicted by WRF.

The morning O_3 vertical profiles are in very good agreement with the measurements from 300 – 500 m but a clear overestimate at lower and higher altitudesis there. The model should be over-predicting at all altitudes as the model always over-predicts O_3 concentrations at the surface during the daytime. However, due to mixing of NOx above the PBLH in the model at 10 am, the predicted NOx concentrations from 300 – 500 m are higher than the measurements which titrates the model otherwise over-predicted O_3 concentrations to match the measured concentrations. However, O_3 predictions improved as the day progressed with HI-RES_SOIL and BASE_SOIL cases producing the best results as shown by the performance statistics summarized in Table 5-4. Similarly, predicted NOx vertical profiles match the measurements well for all test cases in the afternoon hours. This suggests that the mixing problem became less prominent as the day progressed. As a general observation, apart from the 10 am profiles, the addition of candidate soil NOx emissions improved the predicted NOx vertical profiles for HI-RES_SOIL and BASE_SOIL cases as compared to the BASE case.

The CO vertical profiles are heavily under-predicted within the boundary layer suggesting missing emissions as discussed in section 5.3.1. The CO vertical profiles for the BASE and BASE_SOIL cases are identical as addition of NOx should not alter the CO chemistry. The HI-RES_SOIL case moves the CO concentrations close to the surface towards the measurements but the bias in the emissions still dominates the improvements associated with the higher vertical resolution.

Gas-phase NH_3 concentrations were always under-predicted in all cases as compared to measurements, suggesting missing emissions in the CARB inventory. Predicted gas-phase NH_3 concentrations in the soil NOx cases (BASE_SOIL and HI-RES_SOIL) were slightly lower than in the BASE case because the additional NOx gets converted to HNO_3 which combines with additional NH_3 to form NH_3NO_4. Despite this NH_3 under-prediction, gas-phase HNO_3 concentrations are still the limiting precursor for particulate nitrate formation. It is possible that missing NH_3 emissions leading to an under-prediction in gas-phase NH_3 concentrations may also contribute to poor prediction of NO_3^- diurnal profile. To test if NH_3 emissions from soil could play a role, a perturbation simulation is executed for the BASE_SOIL case where soil NH_3 emissions were created at a level equal to ½ of the candidate soil NOx emissions. This perturbation did not improve model morning NO_3^- predictions (< 5% change). Thus, it appears that NH_3 concentrations are not the limiting factor in NO_3^- formation. This conclusion also supported by the finding that the NO_3^- and NH_4^+ vertical profiles predicted by the BASE_SOIL and HI-RES_SOIL cases match the measured vertical profiles better than the BASE case. The BASE_SOIL case performs best in the morning hours where HI-RES_SOIL case tends to over-predict NO_3^- and NH_4^+. HI-RES_SOIL performs better in the afternoon hours, but the overall model performance keeps degrading as the day progresses. These trends are consistent with excess mixing in the model atmosphere. The statistics summarized in Table 5-4 show that the vertical profile concentrations of NO_3^- and NH_4^+ predicted using the candidate soil NOx emissions are in better agreement with measurements than predictions generated without candidate soil NOx emissions.

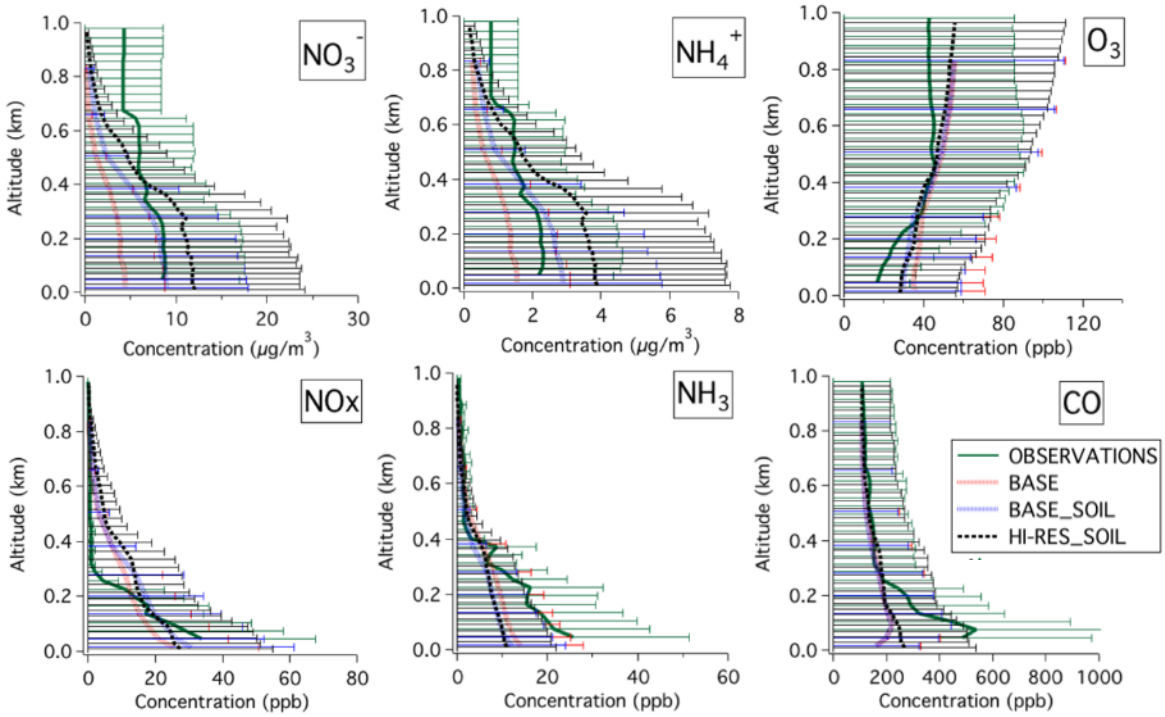

Figure 5-4. Episode-average vertical profiles at Fresno at 10:00 AM. The uncertainty bars represent 3 times the standard deviation of the measurements.

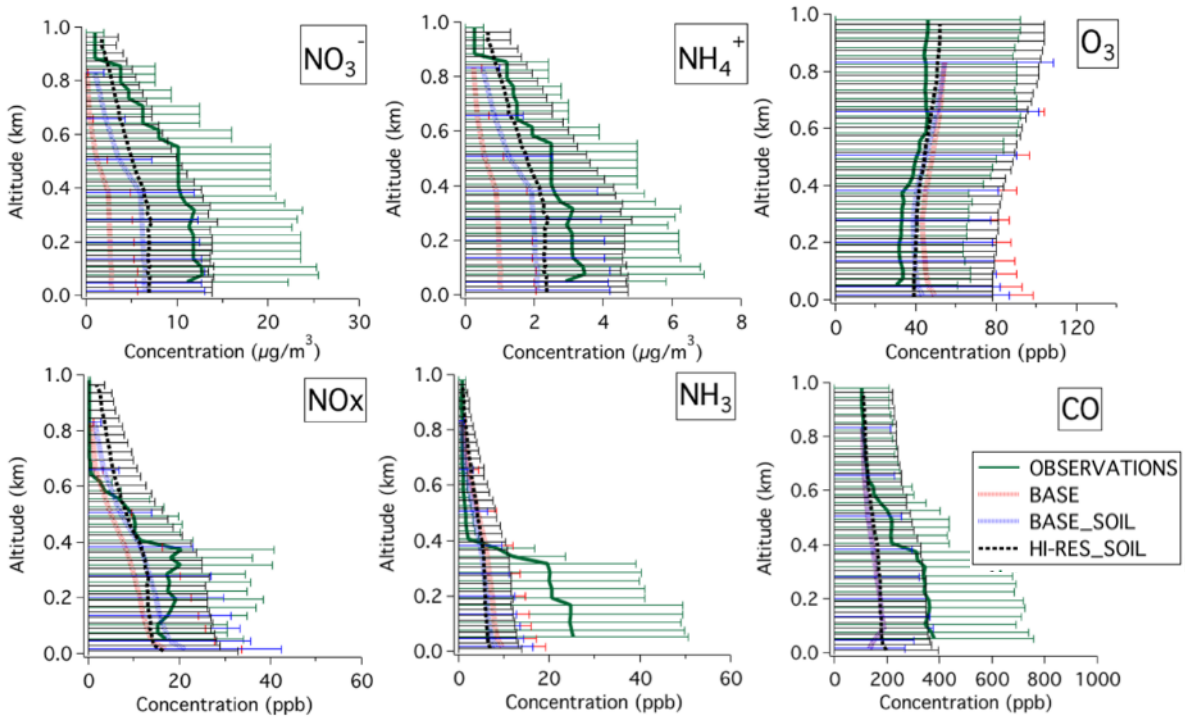

Figure 5-5. Episode-average vertical profiles at Fresno at 12:00 PM. The uncertainty bars represent 3 times the standard deviation of the measurements.

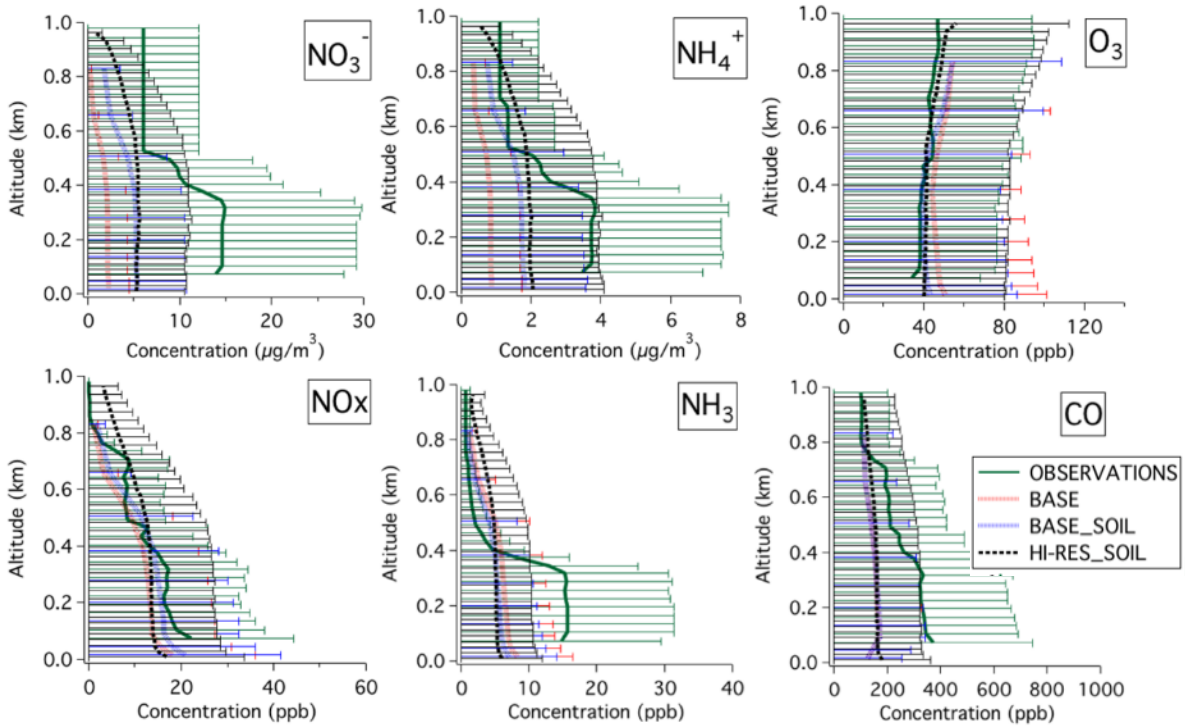

Figure 5-6. Episode-average vertical profiles at Fresno at 2:00 PM. The uncertainty bars represent 3 times the standard deviation of the measurements.

5.3.3 Resolving the Nocturnal Residual Layer and Nitrate Late Morning Peak

Figure 5-7 shows the 4-hour average vertical profiles for BASE_SOIL and HI-RES_SOIL at Fresno. These vertical profiles are averaged over 7 days (16, 18, 20-21, 30-31 January and 1, 4 February, 2013) during DISCOVER-AQ. Both BASE_SOIL and HI-RES_SOIL cases show a clear zone of efficient NO_3^- production aloft during nightime. These profiles are consistent with the hypothesis that there is a zone of optimal concentrations of NOx and O_3 aloft which will lead to greater NO_3^- production. Additionally, this suggests that the zone of efficient nitrate production is only active during nighttime when there is low mixing and the NRL is formed. The HI-RES_SOIL case seems to better resolve this zone of efficient nitrate formation (possibly NRL) much better than BASE_SOIL case, which suggests that HI-RES_SOIL case is able to resolve the boundary layer processes better than the BASE_SOIL.

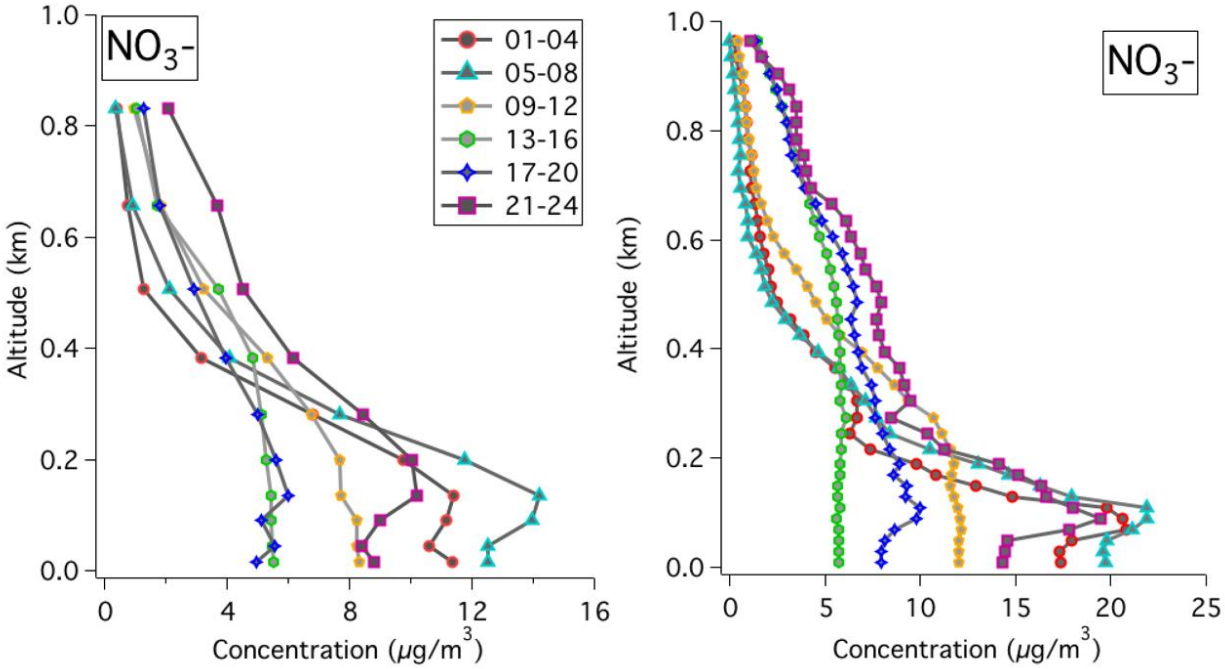

Figure 5-7. NO_3^- vertical profiles for BASE_SOIL (left) and HI-RES_SOIL (right) at Fresno during DISCOVER-AQ.

As discussed in the section 5.3.1, the ground-level concentrations of NO_3^- in HI-RES_SOIL case are overpredicted during nighttime. This could be possibly caused by excess mixing of NO_3^- formed in the the NRL aloft to the surface layer at night in the model calculations or result from direct production of NO_3^- formation in the surface layer (less likely). To check this hypotheis, the model minimum eddy diffusivity (Kzz,min) was lowered from a value of ~0.5 m^2s^{-1} to a value of ~0.01 m^2s^{-1} by modifying the parameterization that calculates Kzz,min. Low Kzz,min values will inhibit mixing down of O_3 from aloft during nightime, thus limiting NO_3^-formation until O_3 concentrations are ~0 ppb as compared to earlier simulations which had non-zero nightime O_3 concentrations. Figure5-8 shows the vertical profiles using the normal and modified Kzz,min for January 16, 2013 at Fresno. The modified Kzz,min decreased NO_3^- concentrations at the surface, leaving an intensified NRL, as compared to original Kzz,min results during nightime (especially from hours 1 – 4 and 20 – 24).

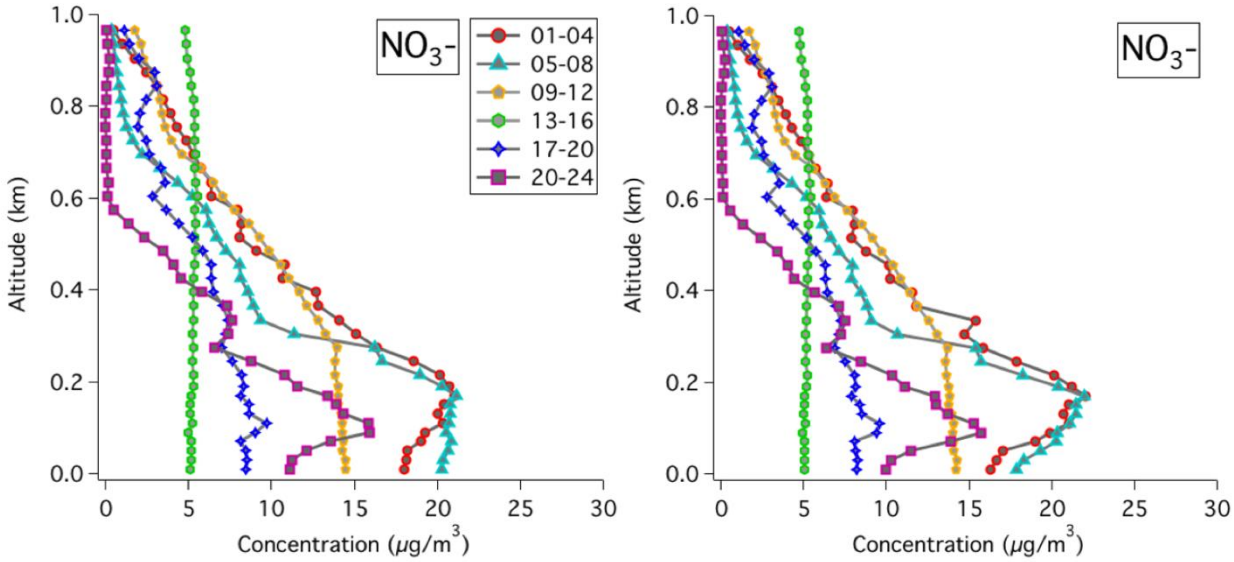

Figure 5-8. NO_3^- vertical profiles for HI-RES_SOIL case with Kzz,min = ~0.5 m^2s^{-1} (left) and Kzz,min = ~0.01 m^2s^{-1}(right) for January 16, 2013 during DISCOVER_AQ at Fresno.

The 4-hour average vertical profiles shown in Figure 5-8 do not illustrate the important progression of the mixing depth into the NRL after sunrise and the resulting entrainment of pollutants into the surface layer. Figure 5-9 therefore plots 1-hour vertical profiles (hours 1 – 12) for NO_3^- for January 16 – 21 at Fresno for the HI-RES_SOIL case to better understand the diurnal pattern. The NO_3^- vertical profiles for hours 1 – 7 show a promient NRL with more concentrations aloft than at the surface. Concentrations in the NRL abruptly mix throughout the entire atmosphere post hour 7, which ignores the effects of elevated subsidence inversion present during this time preiod. The PBLH predicted by WRF at hour 8 in Fresno was ~250 m and the atmospheric stability condition was predicted to be neutral, both of which seem plausible for wintertime conditions. This suggests that the representation of Kzz in the standard model is not behaving as expected above the PBLH during neutral conditions.

The vertical mixing process in the UCD/CIT model are based on turbulent diffusion coefficients (Kzz), which are often parameterized for stable, neutral and unstable atmospheric regimes. The atmosphere is divided into three layers: (i) the surface layer, (ii) the mixing layer and (iii) the free atmosphere. The surface layer is characterized by constant turbulent mixing as a function of height, the mixing layer is characterized by a linear increase in turbulent mixing with height, and the free atmosphere is thought to have little mixing due to non-turbulent flow. Unique Kzz parameterizations are used for each layer to represent the dominance of different processes. The effects of atmospheric stability are determined using the Monin-Obukhov length (L) which is the height at which turbulence is generated more by bouyancy than by wind shear. The three atmospheric regimes are generally defined by: unstable ($L < 0$), neutral ($L = \infty$) and stable ($L > 0$). For unstable conditons, Kzz vertical profiles in surface layer are paramerized by a formulation suggested by Businger, 1971 [64] and Businger et al., 1971 [65] and in other layers by a fomulation suggested by Myrup and Ranzieri, 1976 [66]. For stable conditions, Kzz vertical profiles in surface

layer are parameterized by a formulation suggested by Businger, 1971 [64] and Businger et al., 1971 [65], and in other layers using a formulation suggested by Businger, 1974 [67].

The parameterization of Kzz under neutral conditions merit special attention since the rapid mixing of NRL concentrations throughout the entire model column depth shown in the left panel of Figure 5-9 occurs when the atmosphere shifts from stable to neutral conditions in the early morning hours. For neutral conditons, Kzz vertical profiles are paramertized using a formulation developed by Shir, 1973[68] which does not differentiate between the atmospheric layers and does not recognize the possibility of an elevated subsidence inversion which can inhibit mixing aloft. Other Kzz paramerizations have been developed which do not suffer from this weakness. For example, the neutral Kzz vertical profile paramerization suggested by Myrup and Ranzeiri, 1976 [66] considered different formulations for different layers and suggested very low values of Kzz above the PBLH. This approach was tested in the current study by conducting a sensitivity simulation for January 16 – 21, 2013 (hereafter called HI-RES_SOIL MOD). Kzz was set to a minimum value of ~0.04 m^2s^{-1} as suggested by Myrup and Ranzeiri, 1976 [66]. The HI-RES_SOIL MOD case also maintains the reduced Kzz,min value of ~0.01m^2s^{-1} during stable nightime conditions to avoid excess vertical transport from NRL to the surface. The results from HI-RES_SOIL MOD are discussed below.

The right panel of Figure 5-9 illustrates 1-hour vertical profiles (1 – 12 hours) of NO_3^- averaged over January 16 – 21 at Fresno for the HI-RES_SOIL MOD case. The HI-RES_SOIL MOD predicted the smooth incorporation of the NRL into the surface layer as the mixing height increased throughout morning hours. The artificial mixing is caused by the failure of the original Kzz parameterization for neutral conditions to recognize the elevated subsidence inversion are completely avoided in the updated treatment.

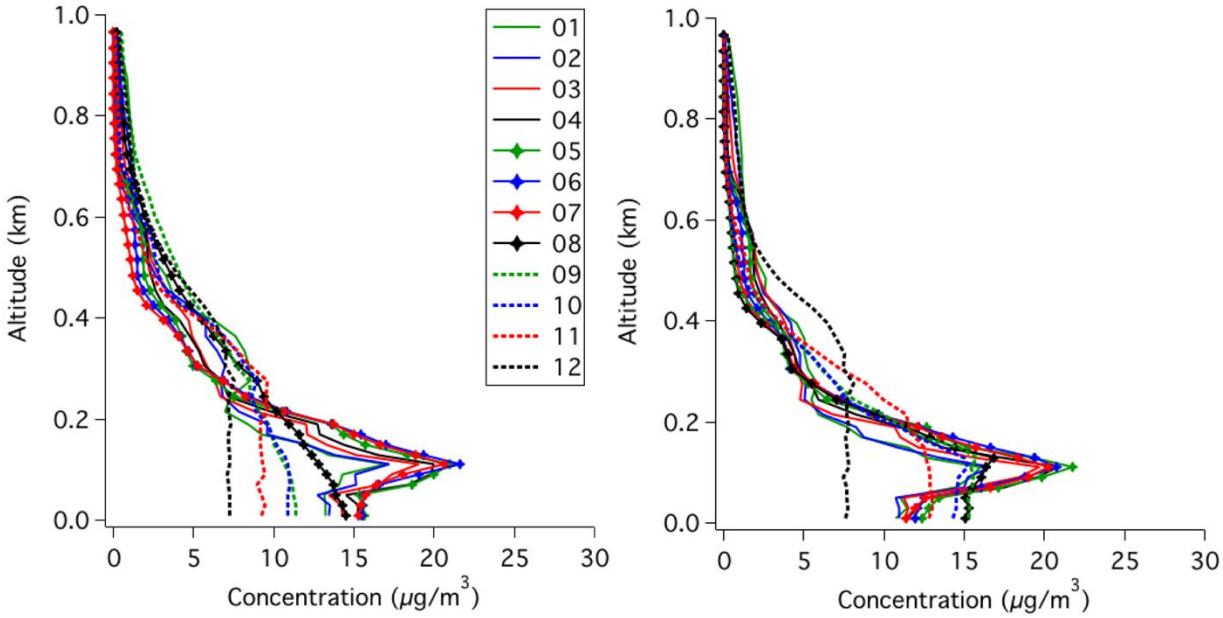

Figure 5-9. NO_3^- vertical profiles (01 – 12) for HI-RES_SOIL (left) and HI-RES_SOIL MOD (right) at Fresno. The vertical profiles are generated by averaging over January 16 – 21, 2013.

Figure 5-10 illustrates the diurnal profiles, averaged over 16 – 21 January, of predicted and measured species at Fresno during DISCOVER-AQ. The HI-RES_SOIL MOD case more accurately predicts the O_3, NOx and CO concentrations, possibly due to enhanced decoupling of the NRL due to lower Kzz,min values. The low Kzz,min value ensured that there is no vertical transport of primary emissions (e.g., CO, NOx) from surface layer to the NRL and mixing down of O_3 from NRL to surface layer. Thus, The HI-RES_SOIL MOD case CO and NOx concentrations increased in the morning and nighttime due to the inability of CO and NOx emissions to escape to the NRL. This is similarly observed for the HI-RES_SOIL MOD case of OA concentrations. Standard metrics of MFB, MFE and average concentrations are all improved in the HI-RES_SOIL MOD case performing best in terms of MFB, MFE and average concentrations. The HI-RES_SOIL MOD case NOx concentrations increased in the morning and nighttime due to the inability of NOx emissions to escape to the NRL.

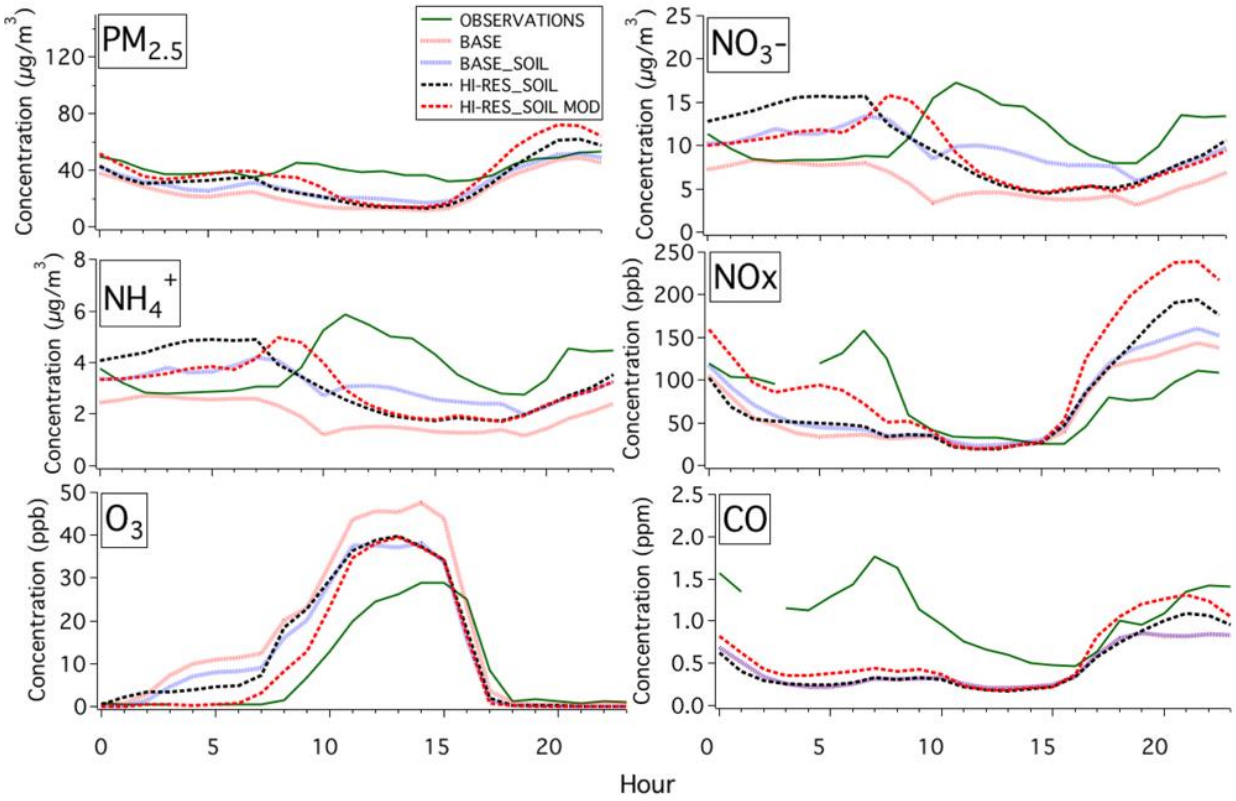

Figure 5-10. Diurnal profiles of $PM_{2.5}$ mass, NO_3^-, NH_4^+, gaseous NOx, O_3 and CO at Fresno for the DISCOVER-AQ campaign. These profiles are generated by averaging measurementsover January 16 – 21, 2013 during DISCOVER-AQ.

The HI-RES_SOIL MOD case predicts that NO_3^- and NH_4^+ concentrations peak later in the day as compared to other cases which is more consistent with the measurements. The BASE_SOIL case NO_3^- and NH_4^+ concentrations peak at around 7 – 8 am followed by HI-RES_SOIL MOD NO_3^- and NH_4^+ concentrations peaking at 9 – 10 am while the measurements peak at 10 – 11 am. The HI-RES_SOIL MOD closely follows the BASE_SOIL NO_3^- diurnal concentrations except during afternoon hours, where BASE_SOIL has a minor peak. This is due to HI-RES_SOIL case PBLH transitioning at the greater gradient in morning to afternoon hours as compared to BASE_SOIL case PBLH. However, there is a clear under-prediction of NO_3^- and NH_4^+ for all cases in the afternoon hours. Recent studies [1, 5] show that daytime photochemical production is also important for NO_3^- production. Thus, the under-predictions in NO_3^- and NH_4^+ during the daytime are also likely related to the model under-predicting daytime photochemical production due to low photolysis rates and OH concentrations during wintertime. However, it may also be that loss processes that are active in the daytime, including dry deposition of HNO_3 and entrainment of cleaner air from above the daytime mixed layer, may be too fast in the model. The BASE_SOIL case performed best in terms of average NO_3^- and NH_4^+ concentrations followed by HI-RES_SOIL and HI-RES_SOIL MOD case in comparison to measurements as summarized by the performance statistics shown in Table 5-5. All the soil NOx cases (BASE_SOIL, HI-RES_SOIL and HI-RES_SOIL MOD) performed similar in terms of MFB and MFE values for NO_3^- and NH_4^+ predictions.

The HI-RES_SOIL MOD case performed best in terms of average $PM_{2.5}$ concentrations followed closely by the BASE_SOIL and the HI-RES_SOIL cases. However, a close look at the diurnal variation shows that majority of that change came at nighttime when the NRL was decoupled from the surface layer. The low Kzz,min value ensured that there is no vertical transport of primary emissions to the NRL, thus resulting in more primary aerosol (e.g., OC and EC) at ground level evident from Figure 5-11. The HI-RES_SOIL MOD case under-predicts $PM_{2.5}$ concentrations in the afternoon when background concentrations from the aloft mix down to the ground. Concentrations of NO_3^-, NH_4^+ and OA are all under-predicted during these hours, likely in part due to less daytime photochemical production in model calculations as discussed earlier.

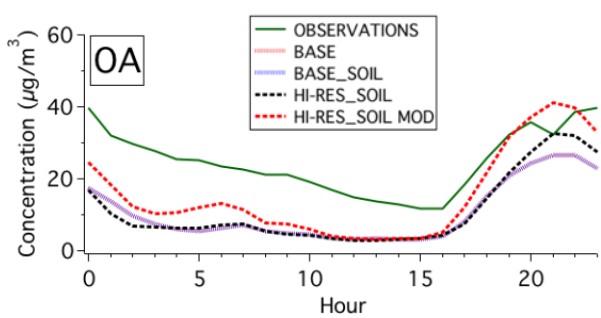

Figure 5-11. Diurnal profiles of organic aerosol (OA) at Fresno for the DISCOVER-AQ campaign. These profiles are generated by averaging over 16 – 21 Januaryduring DISCOVER-AQ.

Table 5-5: Episode-average Mean Fractional Bias (MFB) and Mean Fractional Error (MFE) for CO, NOx, O_3, $PM_{2.5}$, NH_4^+, NO_3^-, and SO_4^{2-} during DISCOVER-AQ for HI-RES_SOIL_MOD case.

CASE	Statistic	CO	NOx	O_3	$PM_{2.5}$	NH_4^+	NO_3^-	SO_4^{2-}	OA
		ppb			µg m^{-3}				
BASE	Average	453	64.51	16.24	25.60	1.93	5.71	0.74	10.54
	MFB	-0.56	-0.16	0.20	-0.55	-0.50	-0.49	-0.13	-0.78
	MFE	0.95	0.71	1.18	0.58	0.78	0.79	0.53	1.01
BASE_SOIL	Average	454	72.91	12.73	30.73	3.11	9.69	0.74	10.53
	MFB	-0.55	-0.04	-0.21	-0.34	-0.09	-0.04	-0.13	-0.78
	MFE	0.95	0.65	1.25	0.41	0.53	0.53	0.53	1.01
HI-RES_SOIL	Average	470	75.34	12.82	31.88	3.19	9.77	0.81	11.09
	MFB	-0.56	-0.08	-0.01	-0.34	-0.09	-0.08	-0.06	-0.78
	MFE	0.99	0.67	1.23	0.43	0.62	0.66	0.51	1.03
HI-RES_SOIL MOD	Average	599	105.62	10.49	37.90	3.03	9.04	0.91	15.51
	MFB	-0.40	0.16	-0.49	-0.19	-0.12	-0.12	0.04	-0.54
	MFE	0.89	0.66	1.24	0.41	0.55	0.59	0.53	0.85
OBSERVATIONS	Average	1096	79.70	8.42	41.20	3.83	11.25	0.98	24.62

Figures 5-12 through 5-14 illustrate vertical profiles of predicted and measured species at 10 am, 12 pm and 2 pm in Fresno during DISCOVER-AQ. The vertical profiles are averaged over 18 and 20 – 21 January for which P3B aircraft measurements are available. NO_3^- and NH_4^+ vertical profiles are in reasonable agreement with measurements at 10am; HI-RES_SOIL MOD case is slightly over-predicting as compared to similar BASE_SOIL and HI-RES_SOIL cases. As the day progressed, HI-RES_SOIL MOD case started behaving more like HI-RES_SOIL case due to the atmosphere transitioning from neutral to unstable conditions. Thus, the major change in vertical profiles was only seen at 10 am.

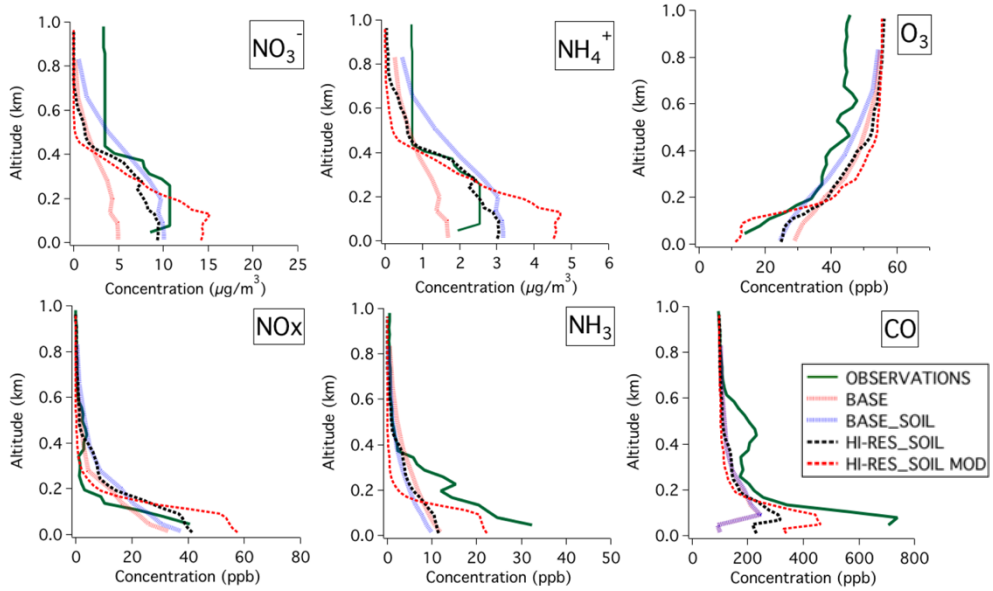

Figure 5-12. Averaged vertical profiles of species (name written in the graphs) at Fresno at 10:00 AM. These vertical profiles are averaged over 18, 20 – 21 January, 2013.

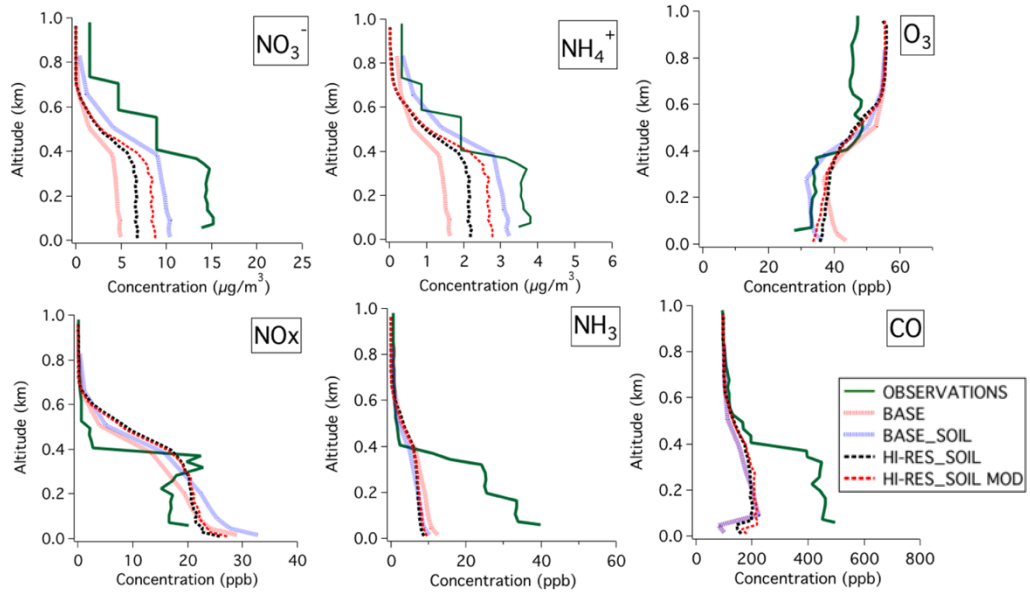

Figure 5-13. Averaged vertical profiles of species (name written in the graphs) at Fresno at 12:00PM. These vertical profiles are averaged over 18, 20 – 21 January, 2013.

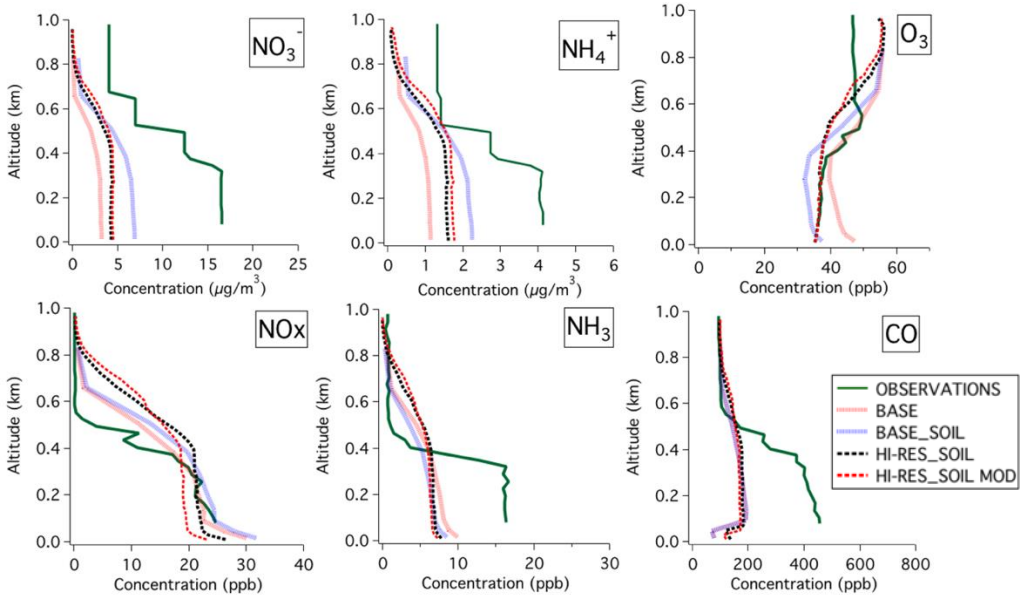

Figure 5-14. Averaged vertical profiles of species (name written in the graphs) at Fresno at 2:00PM. These vertical profiles are averaged over 18, 20 – 21 January, 2013.

5.4 Conclusions

The expanded SAPRC11 mechanism that also considers NO_3-driven chemistry produces little SOA from ONs in this study, likely due to low VOC emissions, in the SJV during wintertime.

Candidate soil NOx emissions have the potential to contribute significantly to formation of NH_4NO_3at ground level and aloft in the SJV. This addition of candidate soil NOx emissions to the original CARB emissions inventory increased the nitrate concentrations by ~50-100% yielding improved agreement with measurements in terms of the average concentrations. Soil NOx is a significant source of NO_3^-, contributing around 10-20% and 25-40% NO_3^- to $PM_{2.5}$ mass in urban and rural areas respectively. Future CARB inventories should consider the incorporation of soil NOx emissions to provide a more accurate starting point for the development of emission control programs.

NRLs that have optimal concentrations of NOx and O_3 concentrations are zones of efficient NO_3^- formation. These NRLs can be resolved more accurately by using higher vertical resolution (especially in the zone between 100 – 300 m above the surface) and accurate vertical diffusion parametrization in model calculations. Increasing the vertical resolution of model calculations increased the predicted ground-level NO_3^- concentrations by approximately around 30%. The original parametrization for Kzz in UCD/CIT model does not consider the limiting effect of upper subsidence inversions under neutral conditions and thus mixes concentrations throughout the model column depth during the early morning and early evening hours. Correcting the parametrization to recognize the presence of the upper subsidence inversion yields more realistic diurnal profiles for NO_3^-concentrations, increasing nitrate concentrations by ~15% during morning hours of the DISCOVER-AQ field study.

The changes to NOx emissions, increased vertical resolution, and vertical mixing in model calculations improved the NO_3^-predictions including the ability to resolve peak concentrations during morning hours, but these changes are still not able to resolve bias in afternoon concentrations. This bias may be attributable to low levels of daytime photochemical production, which can be comparable to nighttime production [1, 5] even during winter conditions when photolysis rates and OH concentrations are low. However, the negative bias may also result from loss processes being too fast, such a dry deposition of HNO_3 or entrainment of cleaner air from above the daytime mixed layer. Further analysis will be required to separate these processes to determine their respective contributions.

6 EFFECT OF CANDIDATE SOIL NOx EMISSIONS ON LONG-TERM PREDICTIONS OF PARTICULATE NITRATE AND OZONE IN CALIFORNIA

6.1 Introduction

Maximum 24-hr average particulate nitrate concentrations in California's San Joaquin Valley have declined over the past two decades due to reduced NOx emissions in the region and the strong relationship between emitted NOx and nitrate production during winter stagnation events [6, 25]. Motor vehicle emissions of NOx that dominated the inventory in the year 2000 have decreased by more than a factor of two and now appear to play a less dominant role in contemporary air pollution episodes.

Recent studies suggest that soil NOx emissions from cropland may be significant in California [34, 35]. The scientific debate around this topic is vigorous, with some researchers stating that point measurements of soil NOx emissions raise questions about the relative importance of soil NOx emissions in general[69]. Whatever the final outcome from this debate, it is becoming clear that soil NOx emissions are not zero (as had been previously assumed in CARB emissions inventories) and the decrease in mobile source NOx emissions has increased the relative importance of other NOx sources, including soils.

In addition to soil NOx emissions estimates from Almaraz et al. [35], Rasool et al. [70] recently added biogeochemical process representations to the CMAQ v5.1 modeling system and predicted soil NOx emissions across the continental United States including California's San Joaquin Valley. Soil NOx emissions in the SJV were predicted to be among the highest in the US depending on the details of the model formulation, with values of ranging from 10 to 40 ng N m^{-2} s^{-1}(3.2 to 12.6 kg ha^{-1} yr^{-1}(0.001 to 0.004 ppm m min^{-1}) during the months of May and July 2011. NO_2 columns simulated with the soil NOx emissions are in better agreement with NO_2 column measurements made with the Ozone Monitoring Instrument (OMI) satellite compared to older models for soil NOx emissions. The model evaluations carried out in the warmer months of May and July were not suitable for evaluating the impact of soil NOx emissions on winter particulate nitrate in the SJV, and the limited evaluation during a single year does not enable an evaluation of soil NOx emissions in the context of long-term trends.

The purpose of the current chapter is to evaluate the effects of candidate soil NOx emissions on predicted ozone (one summer month) and particulate nitrate (one winter month) concentrations in California's San Joaquin Valley during the years 2010, 2013, and 2015.Predicted concentrations are compared to measurements across the SJV during each simulation period so that performance metrics can be calculated. The influence of candidate soil NOx emissions across the years is then interpreted from the overall patterns that emerge from the analysis.

6.2 Methods

6.2.1 WRF Configuration

Meteorological simulations were carried out using the WRF model v3.4 for Jan and July months of year 2010, 2013 and 2015. A complete description of the WRF model configuration is provided in Section 2.2.1.

6.2.2 Air Quality Model Configuration

The configuration of the UCD/CIT air quality model was identical in Chapters 2, 4, and 6. Briefly, model simulations were configured using a one-way nesting technique with a parent domain of 24 km horizontal resolution that covered the entire state of California and a nested domain with 4 km horizontal resolution that covered the San Joaquin Valley (SJV). Calculations used 15 telescoping vertical layers up to a top height of 5km. Further details of the UCD/CIT air quality model are provided in Chapter 2.

6.2.3 Emissions

Basic emissions of criteria pollutants in the current study are identical to those described in Chapter 2 and so only a brief over-view is provided here. Inventories for area sources, point sources, and mobile sources were provided by the California Air Resources Board for the years 2000, 2010, and 2015. Area and point source emissions for other years were interpolated between the anchor years. Mobile emissions were adjusted for year and local meteorological conditions using EMFAC 2014, biogenic emissions were predicted using MEGAN [16], and wildfire emissions were generated using the Global Fire Emissions Database (GFED) [18]. Fugitive dust emissions were calculated online using the method described by [21].

Candidate soil NOx emissions in the current analysis are based on the predictions from the Integrated Model for the Assessment of the Global Environment (IMAGE) [35, 71]. Figure 5-1 illustrates the spatial distribution of the processed emissions inventory used for model calculations in units of ppm m min^{-1}. Maximum NOx emissions rates from soils are in the range of 0.08 ppm m min^{-1}during February which translates to approximately 270 kg-N ha^{-1} $yr^{-1.}$ Average emissions rates across the SJV range from 0.006-0.02 ppm m min^{-1} which translates to approximately 20-80 kg-N ha^{-1} yr^{-1}. These average estimates for soil NOx emissions are approximately a factor of six higher than the estimated soil NOx emissions of 3.2 to 12.6 kg ha^{-1} yr^{-1} made by Rasool et al. [70], reflecting the uncertainty in this newly discovered emissions source.

A constant diurnal profile was used as a first estimate for calculations with candidate soil NOx emissions. More complex profiles specifying higher emissions during the daytime (warmer) hours and lower emissions during the nighttime (cooler) hours did not have a significant impact on predicted pollutant concentrations in urban centers where predictions were compared to measurements.

Monthly-average candidate soil NOx emissions were specified based on historical temperature and rates of rainfall and fertilizer application across California. The biogeochemical processes that

release NOx from soils directly depend on each of these factors and so factors such as the drought that occurred from 2007 to 2015 (excluding 2011 and 2012) would also affect soil NOx emissions. The current analysis therefore represents a first scoping study of the potential effects of soil NOx on long-term particulate nitrate formation and ozone formation, with more detailed analysis to follow.

6.2.4 Boundary Conditions

The gas and particle phase initial and hourly varying boundary conditions for the UCD/CIT model were taken from the global model MOZART-4/NCEP (a model for ozone and related chemical Tracers). Additional details of MOZART simulations are provided by Emmons et al. [24].

6.3 Results

6.3.1 Performance Statistics For $PM_{2.5}$ Nitrate In Years 2010, 2013, and 2015

Table 6-1 summarizes the performance of the UCD/CIT air quality model for particulate nitrate predictions in the SJV for Jan in the years 2010, 2013, and 2015. Similar calculations for 2000 and 2005 are forthcoming but were not available for the current iteration of the final report. Summarizing across the three years, the base simulations without candidate soil NOx emissions underpredict $PM_{2.5}$ nitrate concentrations by and average of 20% while the simulations that include candidate soil NOx emissions over-predict $PM_{2.5}$ nitrate concentrations by 43%.

Table 6-1: Model performance of PM2.5 Nitrate during Jan of year 2010, 2013 and 2015 over SJV

Year	Case	MFB	RMSE	MAE	MFE
2010	Soil	0.98	5.72	4.40	1.10
	Base	0.48	3.81	2.86	0.91
2013	Soil	0.26	7.34	4.68	0.89
	Base	-0.31	8.14	5.15	1.09
2015	Soil	-0.21	10.87	7.21	1.04
	Base	-0.74	12.44	9.23	1.46
All	Soil	0.43	7.39	4.91	0.95
	Base	-0.19	7.99	5.15	1.13

Figure 6-1 illustrates the mean fractional bias and mean fractional error in predicted $PM_{2.5}$ nitrate concentrations as a function of the measured nitrate concentration. The simulations conducted with candidate soil NOx emissions and without candidate soil NOx emissions both exhibit structure in the error terms, with lower concentrations over-predicted and higher concentrations under-predicted. The main effect of the candidate soil NOx emissions is to shift this curve upwards with the result that simulations for episodes with particulate nitrate concentrations of 10 $\mu g\ m^{-3}$ show little bias. This compares to base-case simulations that had little bias when predicting episodes with approximately 1 $\mu g\ m^{-3}$ of particulate nitrate. The inclusion of candidate soil NOx emissions appears to only partially explain nitrate under-predictions in the SJV. It is likely that actual soil NOx emissions have year-to-year variability caused by changes in meterological patterns and fertilization rates that drive the biogeochemical cycles producing NOx. These variations were not represented in the candidate soil NOx emissions inventories, and they may be partially responsible for the bias illustrated in Figure 6-1. It is also possible that some other source of NOx emissions is missing from the inventories leading to the trends illustrated in Figure 6-1.

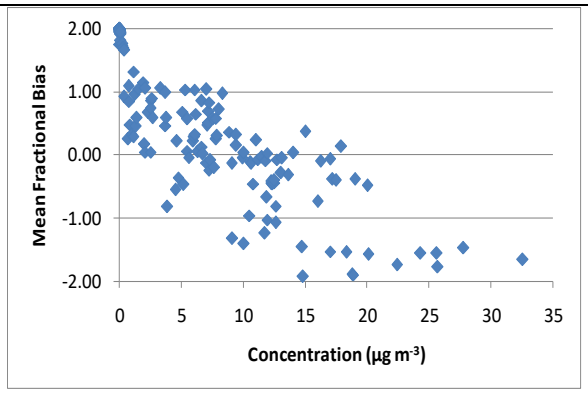

Daily mean fractional bias (MFB) of PM2.5 nitrate with soil NOx case during Jan of 2010, 2013 and 2015 over SJV

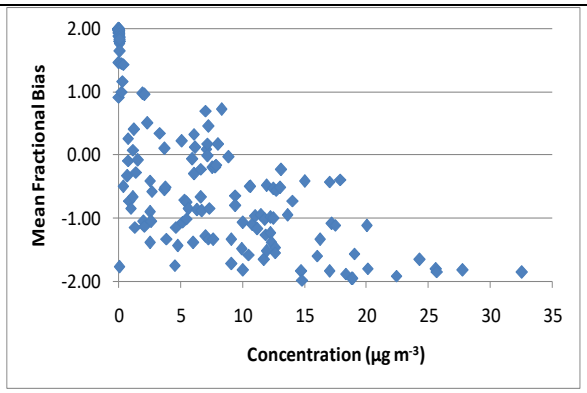

Daily mean fractional bias (MFB) of PM2.5 nitrate without soil NOx (base) case during Jan of 2010, 2013 and 2015 over SJV

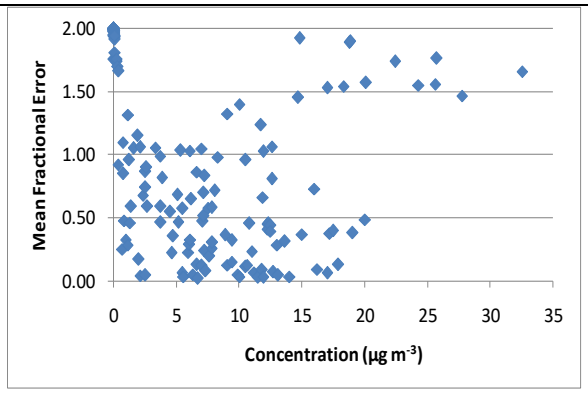

Daily mean fractional error (MFE) of PM2.5 nitrate with soil NOx case during Jan of 2010, 2013 and 2015 over SJV

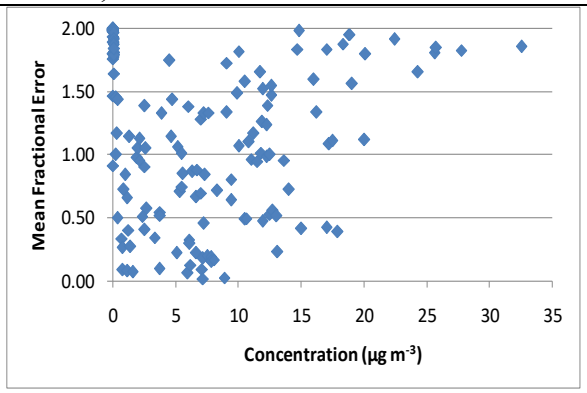

Daily mean fractional error (MFB) of PM2.5 nitrate without soil NOx (base) case during Jan of 2010, 2013 and 2015 over SJV

Figure 6-1. Daily mean fractional bias (MFB) (top-row) and mean fraction error (MFE) (bottom-row) of PM2.5 nitrate concentration during Jan of 2010, 2013 and 2015 over SJV. Case with candidate soil NOx emissions shown in left column, and contribution of without candidate soil NOx emissions shown in right column.

6.3.2 $PM_{2.5}$ Nitrate Concentrations in 2010, 2013, and 2015

Figure 6-2 illustrates the monthly-average measured and predicted $PM_{2.5}$ nitrate concentrations in the SJV. Measured concentrations increase from 2010 to 2015 despite the declining mobile-source NOx emissions during this time period [72]. Model predictions without soil-NOx emissions follow the trend of the mobile-source NOx emissions with concentrations declining in each year. Model predictions with candidate soil NOx emissions start at a higher baseline but also decline in each successive year. This analysis clearly indicates that NOx emissions are directly correlated with monthly-average predicted $PM_{2.5}$ nitrate concentrations, and the ambient measurements suggest that some source of NOx increased between 2010 and 2015. It is unlikely that mobile source or stationary source NOx emissions increased during this time period. A more plausible explanation is that the effects of the drought altered biogeochemical cycles such as those affecting soil NOx emissions leading to the increasing measured $PM_{2.5}$ nitrate concentrations illustrated in Figure 6-2.

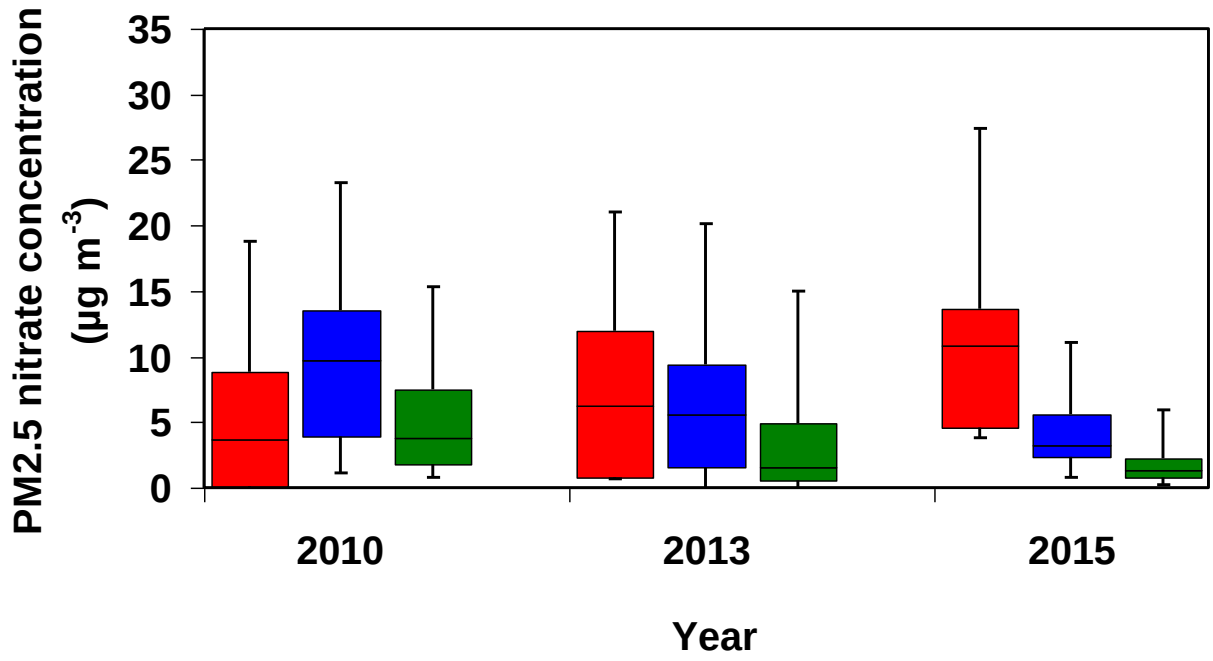

Figure 6-2. PM2.5 nitrate concentration (Red for observation, Blue for with_soil_NOx, Green for base_case during Jan of year 2010, 2013 and 2015 at Bakersfield, Fresno, and Visalia.

6.3.3 NOx Concentrations in 2010, 2013, and 2015

Figure 6-3 shows the monthly-average NOx concentrations in Jan 2010, 2013, and 2015 in the SJV. Concentrations are show on a logarithmic scale reflecting the log-normal distribution that is typical of ambient pollutant concentrations. Although trends are difficult to see on the log-scale, measured NOx concentrations increase slightly from 2010 to 2013 and then decrease slightly in 2015. Predicted concentrations without candidate soil NOx emissions are consistently lower than measured NOx concentrations. Predicted concentrations with candidate soil NOx emissions are higher than measurements in 2010 and 2015, and in good agreement with measurements in 2013. NOx accounts for a significiant fraction of the total reactive nitrogen in the atmosphere and so these trends mirror the long-term trends of total reactive nitrogen display in Chapter 2.

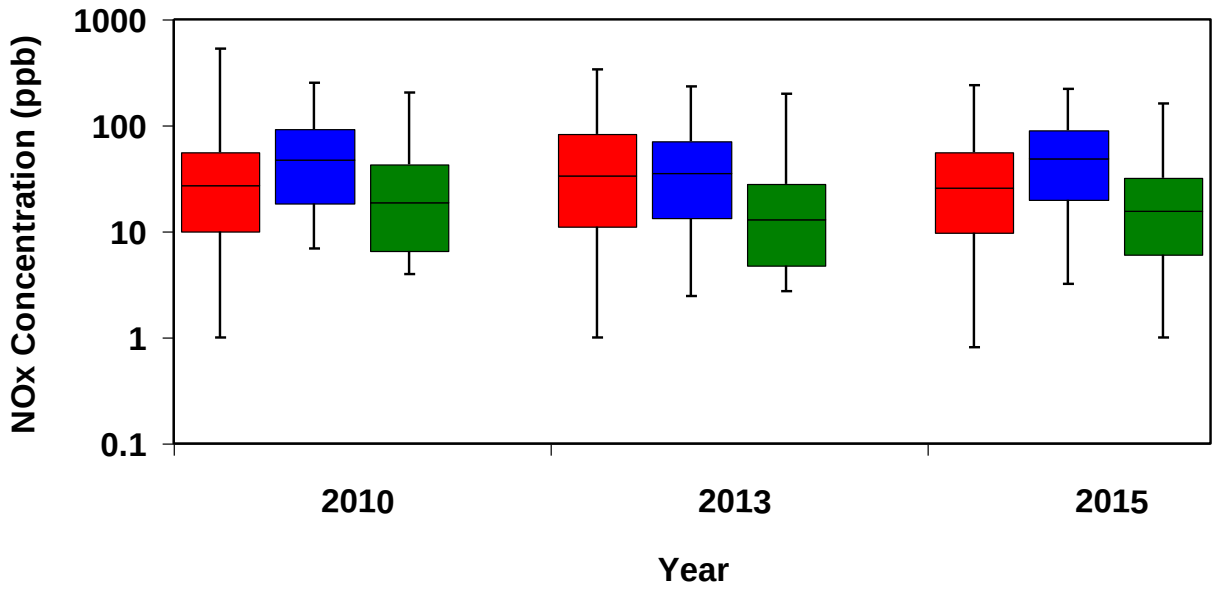

Figure 6-3.NOx concentration (Red for observation, Blue for with_soil_NOx, Green for base_case) during Jan of year 2010, 2013 and 2015 over SJV. Note that Y axis uses a logarithmic scale.

Table 6-2 and 6-3 summarize predicted vs. measured concentrations of NO and NO_2 at sites in the SJV during Jan of 2010, 2013, and 2015. All cases under-predict NO concentrations reflecting bias in the emissions for reactive nitrogen. Base-case simulations under-predict NO_2 at eight out of twelve measurement sites while simulations with candidate soil NOx emissions over-predict NO_2 concentrations at all sites. These findings suggest that the transformation rates that move NO to NO_2 to NO_3 to N_2O_5 to particulate nitrate also have uncertainty, emphasizing the value of the comparisons for predicted vs. measured total reactive nitrogen.

Table 6-2: Model performance of NO during Jan of year 2010, 2013 and 2015 over SJV.

Sites	Cases	Model	Observation	MFB	RMSE	MAE	MFE
Fresno-Drummond	With Soil	5.61	18.83	-0.51	28.99	16.55	1.13
	Base	1.26		-1.22	30.96	17.88	1.55
Visalia-N Church St	With Soil	10.67	15.39	-0.16	23.34	14.04	1.00
	Base	0.72		-1.50	25.88	14.70	1.56
Edison	With Soil	5.95	6.08	-0.24	13.22	7.21	1.05
	Base	1.03		-1.28	11.19	5.58	1.45
Fresno-Sierra Sky	With Soil	3.50	7.14	-0.18	13.53	6.42	1.09
	Base	0.88		-0.88	14.09	6.58	1.49
Fresno-1st Street	With Soil	15.90	15.23	0.21	25.83	15.94	0.97
	Base	10.08		-0.15	24.22	13.63	0.96
Merced-S Coffee Ave	With Soil	1.87	4.71	-0.09	8.18	4.22	1.19
	Base	0.78		-0.48	8.34	4.25	1.40
Clovis-N Vila Ave	With Soil	6.88	14.34	-0.19	24.30	14.19	1.15
	Base	3.73		-0.50	24.39	13.72	1.23
Hanford-S Irwin St	With Soil	10.91	12.36	0.16	16.65	10.64	0.99
	Base	0.51		-1.17	20.90	11.97	1.64
Bakersfield-5558 CA	With Soil	8.87	26.90	-0.42	38.41	22.78	1.11
	Base	2.43		-1.09	42.47	25.33	1.44
Madera-Pump Yard	With Soil	2.64	5.93	0.17	11.91	5.65	1.28
	Base	0.28		-0.62	12.69	5.73	1.75
Fresno-Garland	With Soil	5.17	26.27	-0.66	39.98	23.67	1.15
	Base	2.63		-1.00	41.29	24.42	1.25
Bakersfield-M. Airport	With Soil	7.98	20.09	-0.45	28.45	16.66	1.05
	Base	2.04		-1.11	31.57	18.54	1.32

Table 6-3: Model performance of NO_2 during Jan of year 2010, 2013 and 2015 over SJV

Sites	Cases	Model	Observation	MFB	RMSE	MAE	MFE
Fresno-Drummond	With Soil	22.91	16.37	0.28	13.96	11.55	0.61
	Base	11.45		-0.47	11.76	9.20	0.71
Visalia-N Church St	With Soil	26.53	14.72	0.51	17.05	14.21	0.69
	Base	8.44		-0.55	10.22	7.83	0.69
Edison	With Soil	21.73	9.75	0.62	18.69	15.36	0.94
	Base	12.36		0.07	12.51	9.38	0.83
Fresno-Sierra Sky	With Soil	20.23	11.24	0.48	14.16	11.44	0.71
	Base	9.51		-0.31	9.05	6.68	0.67
Fresno-1st Street	With Soil	29.75	15.08	0.61	18.82	16.39	0.72
	Base	26.35		0.43	17.65	14.27	0.67
Merced-S Coffee Ave	With Soil	17.15	8.02	0.69	12.22	10.07	0.79
	Base	9.07		0.08	6.38	4.76	0.58
Clovis-N Vila Ave	With Soil	24.17	14.60	0.45	15.46	12.64	0.66
	Base	19.56		0.21	13.27	10.08	0.59
Hanford-S Irwin St	With Soil	26.61	12.27	0.69	18.25	15.35	0.78
	Base	6.59		-0.57	8.51	6.45	0.69
Bakersfield-5558 CA	With Soil	25.79	18.35	0.33	13.87	11.33	0.55
	Base	13.99		-0.34	12.15	9.38	0.61
Madera-Pump Yard	With Soil	19.45	9.73	0.57	13.56	11.02	0.73
	Base	4.87		-0.73	7.13	5.59	0.81
Fresno-Garland	With Soil	22.12	17.97	0.15	12.25	9.96	0.53
	Base	16.77		-0.16	10.30	8.09	0.52
Bakersfield-M. Airport	With Soil	24.73	16.16	0.36	14.84	12.10	0.60
	Base	14.07		-0.23	10.62	8.24	0.57

6.3.4 Spatial Distribution of $PM_{2.5}$ Nitrate and NOx in January 2010, 2013, and 2015

Figure 6-4illustrates the predicted spatial distribution of $PM_{2.5}$ nitrate in Jan 2010, 2013, and 2015. Concentrations are displayed without candidate soil NOx emissions in the left column, and the contribution from soil NOx is shown in the right column. Variations from year to year reflect the combined influence of meteorological conditions and emissions trends. The metereorology in 2010 followed classical stagnation conditions with a buildup of nitrate in the SJV obvious for simulations without and with candidate soil NOx emissions. In contrast, the monthly meteorology in 2013 and 2015 did not predict consistent stagnation conditions which prevented the buildup of a valley-wide nitrate event. $PM_{2.5}$ nitrate continues to build up in the urban regions of Fresno and Bakersfield but regional concentrations are greatly reduced relative to 2010 levels.

Soil-NOx contributions to particulate nitrate are predicted to be approximately equivalent to non soil NOx emissions in the regional results displayed in Figure 6-4. This contrasts with the results shown in Chapter 2 where soil NOx accounted for approximately 20% of total reactive nitrogen in the urban areas. Model calculations predict that soil NOx is efficiently converted to particulate nitrate because the more diffuse emissions of soil NOx achieve a more favorable mixing ratio with the background ozone that acts as the main oxidant for the conversion process. The intense NOx emissions in the urban areas quench the background ozone leading to lower conversion efficiency of urban NOx emissions to $PM_{2.5}$ nitrate. This difference in conversion efficiency for soil NOx emissions vs. urban NOx emissions means that the relative importance of sources cannot be judged soley by their total emissions rates. The conversion efficiency must also be considered when judging the impact on population exposure and public health.

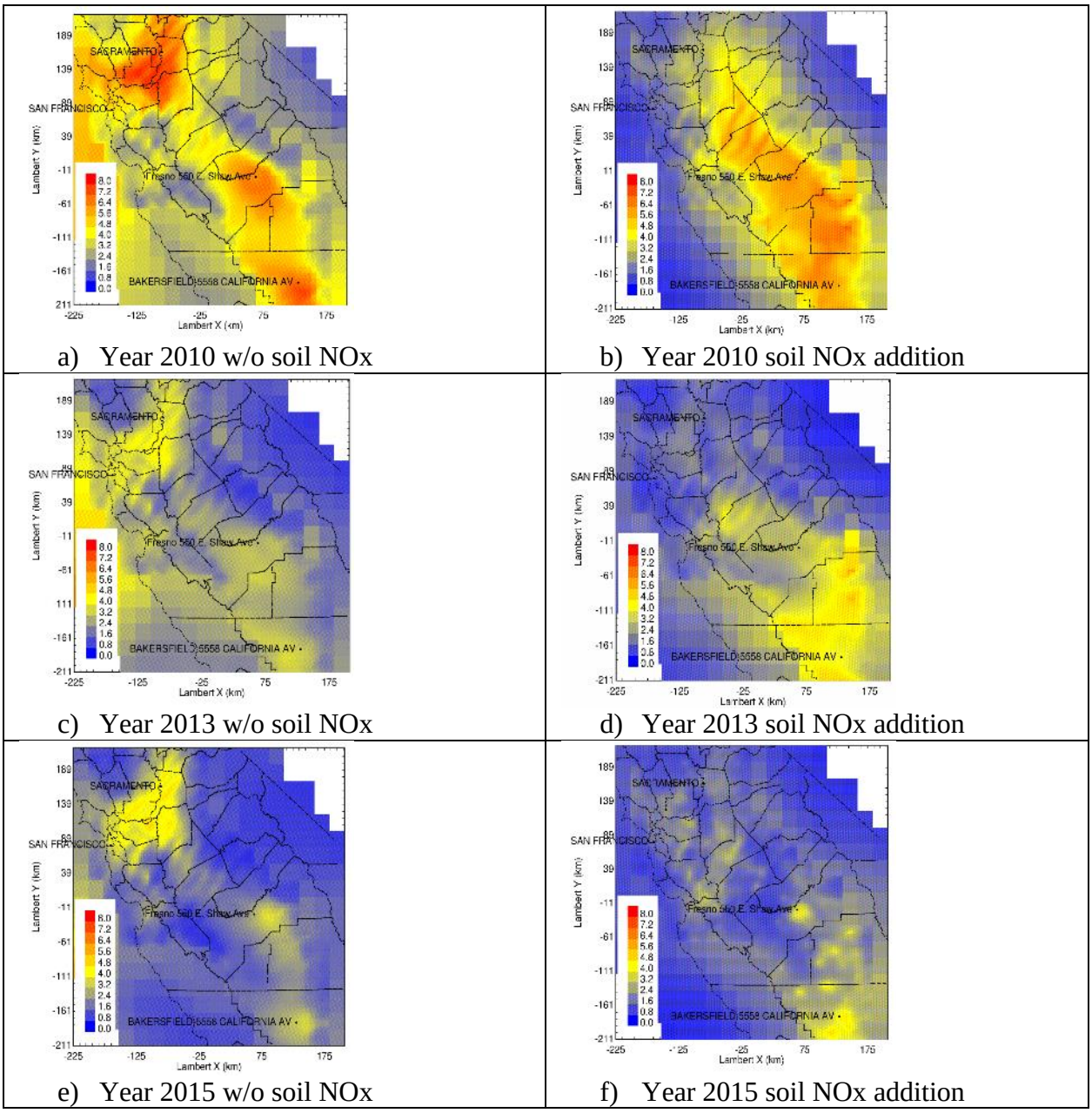

a) Year 2010 w/o soil NOx

b) Year 2010 soil NOx addition

c) Year 2013 w/o soil NOx

d) Year 2013 soil NOx addition

e) Year 2015 w/o soil NOx

f) Year 2015 soil NOx addition

Figure 6-4. Spatial distribution of base (without soil nox) (left column) and differences (with soil nox emission – base case) of PM2.5 nitrate concentration (right column) for Jan of year 2010,2013 and 2015. Units are $\mu g\ m^{-3}$.

Figure 6-5 illustrates the spatial distribution of predicted ground-level NOx concentrations in Jan 2010, 2013, and 2015. Concentrations are displayed without candidate soil NOx emissions in the left column, and the contribution from soil NOx is shown in the right column. Transportation sources dominate non soil NOx emissions with urban areas and major transportation corridors clearly diplayed in the left column of Figure 6-5. Likewise, the spatial distribution of candidate soil NOx emissions reflect the pattern of the emissions, with the highest concentrations over the agricultural soils in the SJV. Variations in stagnation conditions from year to year have little impact on the spatial distributions of the ground level NOx concentrations since these reflect the immediate emissions of NOx rather than the buildup of reaction products requiring several days of stagnation.

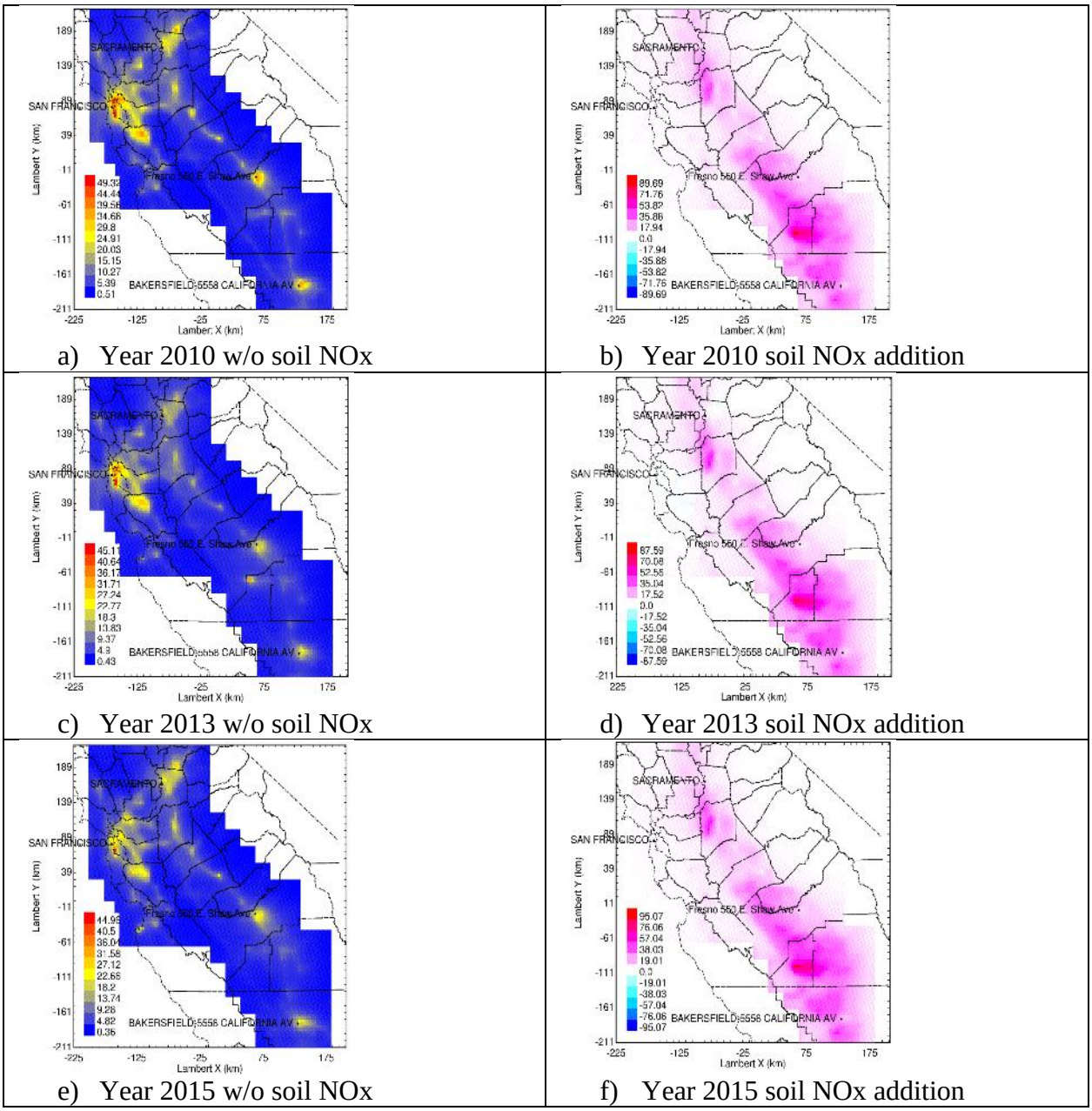

Figure 6-5. Spatial distribution of base (without soil nox) (left column) and differences (with candidate soil NOx emission – base case) of NOx concentration (right column) for Jan of year 2010,2013 and 2015. Units are ppb.

6.3.5 Performance Statistics For Ozone and NOx In July of Years 2010, 2013, and 2015

Table 6-4 shows the performance statistics for predicted O_3 and NOx concentrations with candidate soil NOx emissions (SOIL) and without soil NOx emissions (BASE) in July of 2010, 2013, and 2015. Results are presented for hour 15 corresponding to the typical daily maximum value and for the 24-hr average. Performance statistics for hour 15 predictions of O_3 and NOx are improved with candidate soil NOx emissions relative to the performance statistics without soil NOx emissions. The 24-hr average results show that the implementation of the candidate soil NOx emissions in the current study causes over-predictions of NOx and under-predictions of O_3.

Table 6-4: Model Performance for Ozone and NOx during Jul of year 2010, 2013 and 2015 over SJV

Species	**Case**	**MFB**	**RMSE**	**MAE**	**MFE**
Ozone (hour15)	Soil	-0.01	13.50	10.48	0.15
	Base	-0.19	18.87	15.27	0.23
Ozone (all 24 hours)	Soil	-0.08	15.64	12.05	0.35
	Base	0.04	17.33	13.81	0.36
NOx (hour 15)	Soil	-0.35	4.24	2.84	0.67
	Base	-0.95	4.79	3.53	1.06
NOx (all 24 hours)	Soil	0.18	14.21	8.67	0.66
	Base	-0.68	13.41	8.14	0.97

These variation of model performance as a function of hour is illustrated in Figure 6-6 that displays the average diurnal variation of ozone and NOx measurements and model predictions. Candidate soil NOx emissions cause an over-prediction of NOx concentrations during the evening hours of 20 to 4 which suggests that the constant diurnal variation of the candidate soil NOx emissions may not be accurate. In contrast, the base-case simulations without candidate soil NOx emissions greatly under-predict the measured NOx concentrations. Overall, the addition of candidate soil NOx emissions improves the prediction of O_3 and NOx during July of 2010, 2013, and 2015, but further improvements could be realized by optimizing the diurnal variation of the emissions.

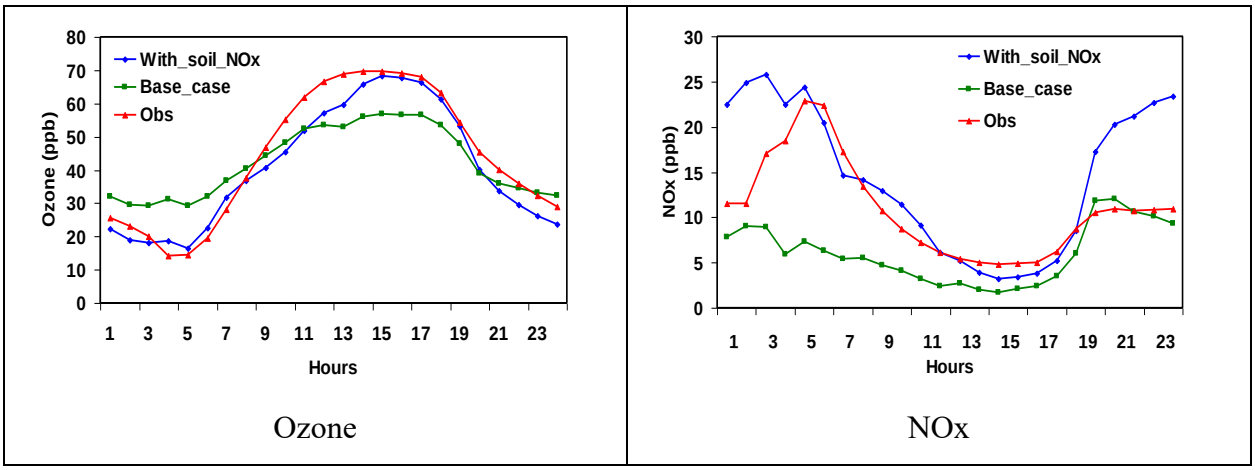

Figure 6-6. Measured and predicted diurnal variation of O3 and NOx concentrations during July of year 2010, 2013 and 2015 over the SJV.

6.3.6 Spatial Distribution of O_3 and NOx in July 2010, 2013, and 2015

Figure 6-7 illustrates the predicted spatial distribution of O_3 averaged during each hour of the day in July 2010, 2013, and 2015. Results are shown separately for simulations without soil NOx emissions (left column of Figure 6-7) and the effects of adding candidate soil NOx emissions (right column of Figure 6-7). The 24-hr average ozone concentrations largely reflect the background ozone advected into the region with maximum concentrations approaching 50 ppb. Regions with lower O_3 concentrations occur in urban areas with intense NOx emissions that quenches O_3. Adding candidate soil NOx emissions to the simulations quenches O_3 immediately above the emissions source but increases O_3 outside this zone. Thus, the addition of candidate soil NOx emissions reduces O_3 concentrations in rural areas and slightly increases O_3 concentrations in urban areas of the SJV.

Figure 6-8 illustrates the predicted spatial distribution of NOx concentrations averaged during each hour of the day in July 2010, 2013, and 2015. Results are shown separately for simulations without soil NOx emissions (left column of Figure 6-8) and the effects of adding candidate soil NOx emissions (right column of Figure 6-8). The non-soil NOx contribution to ground-level NOx concentrations is similar in summer and winter months (compare left column of Figure 6-7 and 6-8) but the soil-NOx contribution to ground-level NOx concentrations is significantly lower in the summer months than the winter months (compare right column of Figure 6-7 and 6-8).

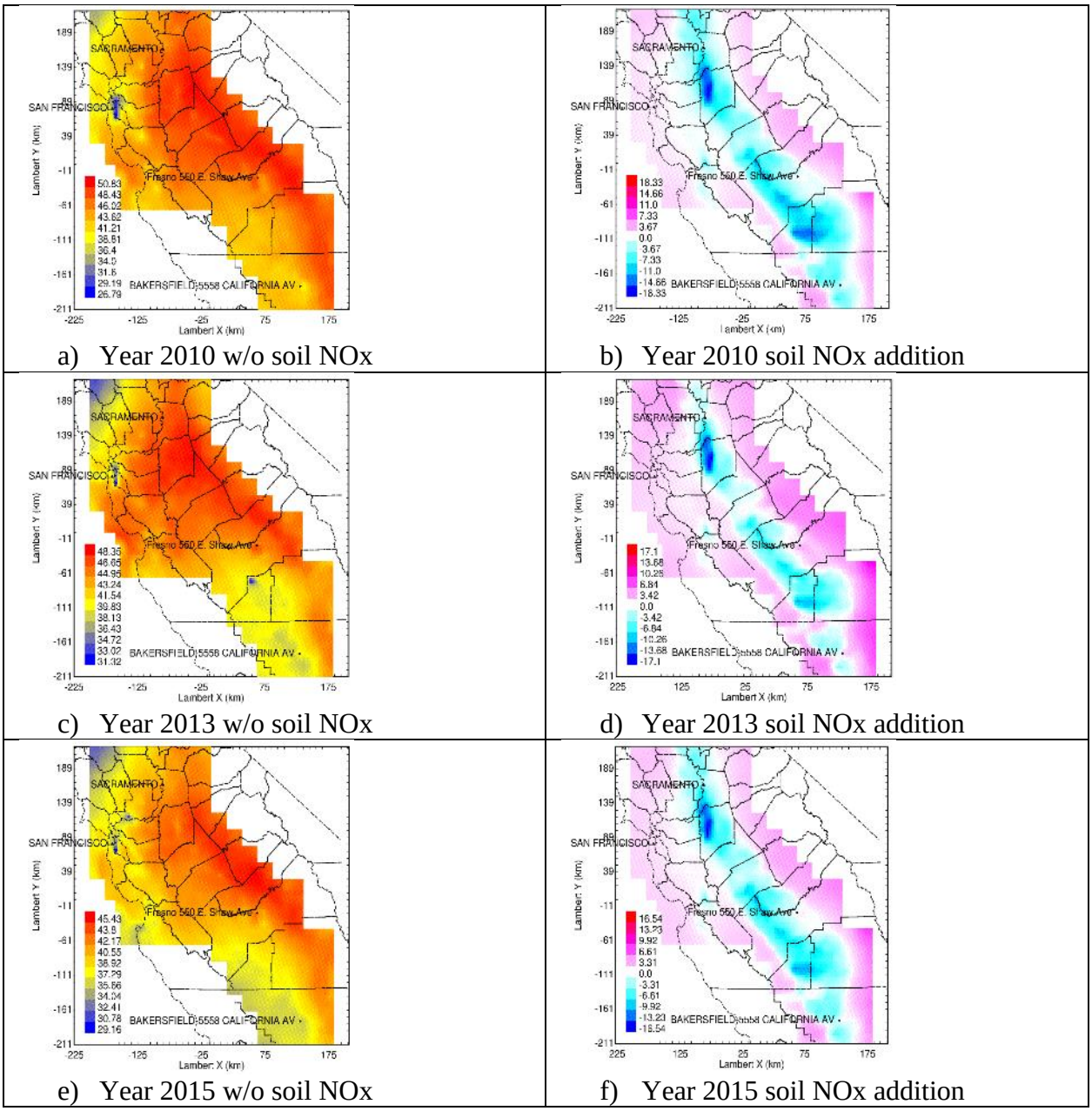

Figure 6-7. Spatial distribution of base (without soil nox) (left column) and differences (with candidate soil nox emission – base case) of Ozone concentration (ppb) (right column) for Jul of year 2010 2013 and 2015 over 4 km domain

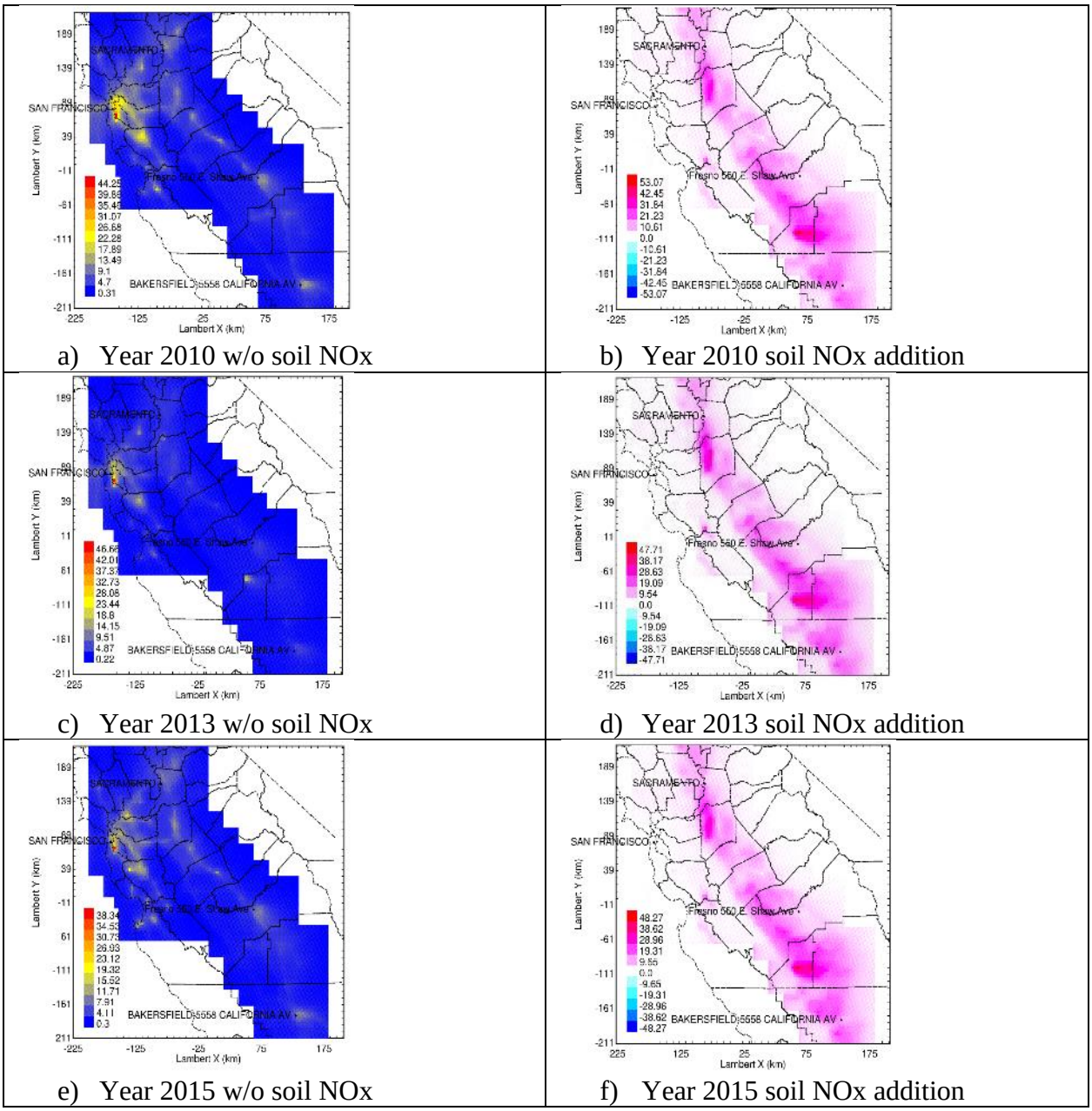

Figure 6-8. Spatial distribution of base (without soil nox) (left column) and differences (with candidate soil nox emission – base case) of NOx concentration (right column) for Jul of year 2010 2013 and 2015. Units are ppb.

6.4 Conclusions

The inclusion of candidate soil NOx emissions generally increases predicted $PM_{2.5}$ nitrate concentrations in January 2010, 2013, and 2015 which helps correct a consistent under-prediction in concentrations when soil NOx emissions are not used. Model predictions without soil-NOx emissions follow the trend of the mobile-source NOx emissions with predicted monthly-average $PM_{2.5}$ nitrate concentrations declining in each year. In contrast, measured monthly-average $PM_{2.5}$ nitrate concentrations increase between 2010 and 2015, suggesting that some source of NOx emissions increases over that time period. Soil NOx emissions that change in response to meteorological conditions (including drought) and fertillizer practices are one potential source of NOx that could explain these trends. The current implementation of candidate soil NOx emissions was constant over each year and a factor of approximately six higher than other estimates for soil NOx emissions based on biogeochemical models. The overall results suggest that winter soil NOx emissions may be over-estimated in the current implementation, but it is likely that soil NOx emissions are non-zero (as had been assumed in previous CARB emissions inventories) and significant in winter months.

Simulations conducted for winter conditions in the San Joaquin Valley suggest that the conversion efficiency for soil NOx to particulate nitrate is higher than the conversation efficiency for urban NOx emissions to particulate nitrate. The diffuse nature of the soil NOx emissions provides a more favorable mixing ratio of NOx to background ozone that increases the efficiency of the reactions converting NOx to nitrate. Future evaluations of the relative importance of NOx emissions sources in the SJV should consider the conversion efficiency when evaluating the potential impacts on public health.

The inclusion of candidate soil NOx emissions generally improves performance statistics for predicted ozone concentrations in July 2010, 2013, and 2015 compared to basecase simulations that omit soil NOx emissions. An analysis of the diurnal profile of O_3 and NOx concentrations suggests that the constant profile for soil NOx emissions used in the current study may not be accurate, but overall the inclusion of the soil NOx emissions improved model performance during the afternoon hours when concentrations reached their daily maximum values.

7 CONCLUSIONS

7.1 Summary of Results

Simulations conducted for January 2010, 2013, and 2015 in central California show that predicted total reactive nitrogen concentrations are lower than measured concentrations of $NO+NO_2$+particulate nitrate. Under-predictions for total reactive nitrogen become progressively more severe with years past 2010 suggesting that emissions inventories for reactive nitrogen are diverging from actual conditions. These trends are consistent with continued reductions in mobile source NOx emissions combined with some unknown source of NOx emissions that is not currently represented in the emissions inventory. As mobile source emissions decrease, the relative important of this unknown source increases.

The inclusion of candidate soil NOx emissions estimated by an independent research group partially addresses the gap in reactive nitrogen emissions in central California. The tested soil NOx emissions strongly increase predicted levels of total reactive nitrogen in rural areas and contribute approximately 20% to concentrations of total reactive nitrogen in urban locations of Fresno and Bakersfield. The tested soil NOx emissions did not account for year-to-year variations in temperature, precipitation, and fertilizer application rates which may influence the magnitude of these emissions.

Candidate soil NOx emissions in Jan 2010, 2013, and 2015 were efficiently converted to particulate nitrate due to the favorable mixing ratio between diffuse soil NOx emissions and background ozone concentrations. As a result, soil NOx produced approximately half of the particulate nitrate in urban locations of the SJV even though this source accounted for only ~20% of the total reactive nitrogen concentrations. Future rankings of NOx emissions sources should account for the conversion efficiency of NO emissions to particulate nitrate.

The inclusion of candidate soil NOx emissions in July 2010, 2013, and 2015 improved the overall predictions of O_3 and NOx in the SJV by correcting negative biases at the urban locations where the monitors are located. The tested soil NOx emissions decreased predicted O_3 concentrations in the rural locations close to the emissions sources but slight increased O_3 concentrations at the urban locations at the eastern edge of the SJV.

The inclusion of candidate soil NOx emissions in January and February 2013 during the DISCOVER-AQ field study improved the prediction of vertical profiles of NOx, particulate nitrate, particulate ammonium ion, and O_3. Increasing the vertical resolution of the model simulations partially helped to refine the zone where conversion of NOx to particulate nitrate is most efficient during the evening hours (approximately 200 m above the surface). Despite this improvement, the model predictions were not able to fully capture the diurnal variation of the ground level concentrations attributed to the downward mixing of the nocturnal residual layer throughout the morning hours of each day.

The inclusion of candidate soil NOx emissions generally increases predicted $PM_{2.5}$ nitrate concentrations in January 2010, 2013, and 2015 which helps correct a consistent under-prediction in concentrations. Despite this general improvement, further research is required to more

accurately estimate winter emissions rates of soil NOx and to account for year-to-year variations driven by changes in meteorological conditions, fertilizer application rates, and irrigation practices.

The inclusion of candidate soil NOx emissions in July 2010, 2013, and 2015 improved the overall predictions of O_3 and NOx in the SJV by correcting negative biases at the urban locations where the monitors are located.

The tests conducted in the current study confirm that a missing source of NOx consistent with the candidate soil NOx emissions would improve the performance of regional chemical transport models in California's SJV, but they do not definitely prove that the missing emissions source is indeed fertilized agricultural soils. Future measurements should be made in the rural portions of the SJV to further test the hypothesis that soil NOx emissions are a significant factor in the air quality cycles within the region.

7.2 Future research

The candidate soil NOx emissions evaluated in the current study generally improve performance statistics for particulate nitrate and ozone in urban locations along the eastern edge of the SJV, but these emissions are predicted to have even larger effects in the rural central portion of the SJV. Long-term measurements should be conducted in the rural central portion of the SJV to directly evaluate the accuracy of the predicted trends and the plausibility of the candidate soil NOx emissions.

The candidate soil NOx emissions evaluated in the current study are approximately six times greater than the soil NOx emissions predicted by a second mechanistic biogeochemical model. Sensitivity studies should be conducted to determine whether reduced estimates of soil NOx emissions during winter episodes would

8 REFERENCES

1. Pusede, S.E., et al., *On the effectiveness of nitrogen oxide reductions as a control over ammonium nitrate aerosol.* Atmospheric Chemistry and Physics, 2016. **16**(4): p. 2575-2596.
2. Young, D.E., et al., *Influences of emission sources and meteorology on aerosol chemistry in a polluted urban environment: results from DISCOVER-AQ California.* Atmospheric Chemistry and Physics, 2016. **16**(8): p. 5427-5451.
3. Chow, J.C., et al., *PM2.5 chemical composition and spatiotemporal variability during the California Regional PM10/PM2.5 Air Quality Study (CRPAQS).* Journal of Geophysical Research-Atmospheres, 2006. **111**(D10).
4. Watson, J.G. and J.C. Chow, *A wintertime PM2.5 episode at the fresno, CA, supersite.* Atmospheric Environment, 2002. **36**(3): p. 465-475.
5. Prabhakar, G., et al., *Observational assessment of the role of nocturnal residual-layer chemistry in determining daytime surface particulate nitrate concentrations.* Atmospheric Chemistry and Physics, 2017. **17**(23): p. 14747-14770.
6. Kleeman, M.J., Q. Ying, and A. Kaduwela, *Control strategies for the reduction of airborne particulate nitrate in California's San Joaquin Valley.* Atmospheric Environment, 2005. **39**(29): p. 5325-5341.
7. Ying, Q., et al., *Modeling air quality during the California Regional PM10/PM2.5 Air Quality Study (CRPAQS) using the UCD/CIT source-oriented air quality model - Part I. Base case model results.* Atmospheric Environment, 2008. **42**(39): p. 8954-8966.
8. Chen, J.J., et al., *Seasonal modeling of PM2.5\ in California's San Joaquin Valley.* Atmospheric Environment, 2014. **92**: p. 182-190.
9. Livingstone, P.L., et al., *Simulating PM concentration during a winter episode in a subtropical valley: Sensitivity simulations and evaluation methods.* Atmospheric Environment, 2009. **43**(37): p. 5971-5977.
10. Hu, J., et al., *Long-term particulate matter modeling for health effect studies in California - Part 1: Model performance on temporal and spatial variations.* Atmospheric Chemistry and Physics, 2015. **15**(6): p. 3445-3461.
11. Held, T., et al., *A comparision of the UCD/CIT air quality model and the CMB source-receptor model for primary airborne particulate matter.* Atmospheric Enviornment, 2005. **39**: p. 2281-2297.
12. Hu, X.-M., et al., *Coupling and evaluating gas/particle mass transfer treatements for aerosol simulation and forecast.* J. Geophys. Res., 2008. **113**(D11208).
13. Nenes, A., C. Pilinis, and S.N. Pandis, *ISORROPIA: A new thermodynamic equilibrium model for multiphase multicomponent marine aerosols* Aquat. Geochem, 1998. **4**: p. 123-152.
14. Carlton, A.G., et al., *Model representation of secondary organic aerosol in CMAQv4.7.* Environmental Science and Technology, 2010. **44**: p. 8553-8560.
15. Carter, W.P.L. and G. Heo, *Development of Revised SAPRC Aromatics Mechanisms.* Atmospheric Environment, 2013. **77**: p. 404-414.
16. Guenther, A., et al., *Estimates of global terrestrial isoprene emissions using MEGAN (Model of Emissions of Gases and Aerosols from Nature).* Atmospheric Chemistry and Physics, 2006. **6**: p. 3181-3210.

17. Guenther, A.B., et al., *The Model of Emissions of Gases and Aerosols from Nature version 2.1 (MEGAN2.1): an extended and updated framework modeling biogenic emissions.* Geoscientific Model Development, 2012. **5**: p. 1471-1492.
18. Giglio, L., J.T. Randerson, and G.R. van der Werf, *Analysis of daily, monthly and annual burned area using the fourth-generation global fire emissions database (GFED4).* Journal of Geophysical Research, 2013. **118**(1): p. 317-328.
19. Xue, J., et al., *Seasonal and annual source appointment of carbonaceous ultrafine particulate matter (PM0.1) in polluted California cities.* Environmental Science & Technology, 2018. **in review**.
20. Xue, J., et al., *Ultrafine particle emissions from natural gas, biogas and biomethane combustion.* Environmental Science & Technology, 2018. **in press**.
21. Su, L. and J.C.H. Fung, *Sensitivities of WRF-Chem to dust emission schemes and land surface properties in simulating dust cycles during springtime over East Asia.* Journal of Geophysical Research-Atmospheres, 2015. **120**(21): p. 11215-11230.
22. United States Department of Health and Human Services (US DHHS), Centers for Disease Control and Prevention (CDC), and National Center for Health Statistics (NCHS), *Compressed Mortality File (CMF) 1999-2013 with ICD-10 Codes on on CDC WONDER Online Database.*, in *The current release for years 1999 - 2013 is compiled from: CMF 1999-2013, Series 20, No. 2S, 2014.* 2014.
23. Hu, J., et al., *Predicting primary PM2.5 and PM0.1 trace composition for epidemiological studies in California.* Environ Sci Technol, 2014. **48**(9): p. 4971-9.
24. Emmons, L., et al., *Description and evaluation of the Model for Ozone and Related chemical Tracers, version 4 (MOZART-4).* Geoscientific Model Development, 2010. **3**(1): p. 43-67.
25. Reynolds, S., et al., *Synthesis of CCOS and CRPAQS Study Findings*. 2012, San Joaquin Valleywide Air Pollution Study Agency.
26. Pleim, J.E., *A combined local and nonlocal closure model for the atmospheric boundary layer. Part I: Model description and testing.* Journal of Applied Meteorology and Climatology, 2007. **46**(9): p. 1383-1395.
27. Pleim, J.E., *A combined local and nonlocal closure model for the atmospheric boundary layer. Part II: Application and evaluation in a mesoscale meteorological model.* Journal of Applied Meteorology and Climatology, 2007. **46**(9): p. 1396-1409.
28. Day, D.A., et al., *Organonitrate group concentrations in submicron particles with high nitrate and organic fractions in coastal southern California.* Atmospheric Environment, 2010. **44**(16): p. 1970-1979.
29. Xu, L., et al., *Aerosol characterization over the southeastern United States using high-resolution aerosol mass spectrometry: spatial and seasonal variation of aerosol composition and sources with a focus on organic nitrates.* Atmospheric Chemistry and Physics, 2015. **15**(13): p. 7307-7336.
30. Rollins, A.W., et al., *Gas/particle partitioning of total alkyl nitrates observed with TD-LIF in Bakersfield.* Journal of Geophysical Research-Atmospheres, 2013. **118**(12): p. 6651-6662.
31. Farmer, D.K., et al., *Response of an aerosol mass spectrometer to organonitrates and organosulfates and implications for atmospheric chemistry.* Proceedings of the National Academy of Sciences of the United States of America, 2010. **107**(15): p. 6670-6675.

32. Pye, H.O.T., et al., *Modeling the Current and Future Roles of Particulate Organic Nitrates in the Southeastern United States.* Environmental Science & Technology, 2015. **49**(24): p. 14195-14203.
33. Wiedinmyer, C., et al., *The Fire INventory from NCAR (FINN): a high resolution global model to estimate the emissions from open burning.* Geoscientific Model Development, 2011. **4**(3): p. 625-641.
34. Almaraz, M., et al., *Extrapolation of point measurements and fertilizer-only emission factors cannot capture statewide soil NOx emissions.* Science Advances, 2018. **4**(9).
35. Almaraz, M., et al., *Agriculture is a major source of NOx pollution in California.* Science Advances, 2018. **4**(1).
36. Kleeman, M.J. and G.R. Cass, *A 3D Eulerian source-oriented model for an externally mixed aerosol.* Environmental Science & Technology, 2001. **35**(24): p. 4834-4848.
37. Kleeman, M.J., G.R. Cass, and A. Eldering, *Modeling the airborne particle complex as a source-oriented external mixture.* Journal of Geophysical Research-Atmospheres, 1997. **102**(D17): p. 21355-21372.
38. Ying, Q., et al., *Modeling air quality during the California Regional PM10/PM2.5 Air Quality Study (CPRAQS) using the UCD/CIT Source Oriented Air Quality Model - Part II. Regional source apportionment of primary airborne particulate matter.* Atmospheric Environment, 2008. **42**(39): p. 8967-8978.
39. Hu, J., et al., *Long-term particulate matter modeling for health effect studies in California – Part 1: Model performance on temporal and spatial variations.* Atmospheric Chemistry and Physics, 2015. **15**(6): p. 3445-3461.
40. Hu, J.L., et al., *Long-term particulate matter modeling for health effect studies in California - Part 2: Concentrations and sources of ultrafine organic aerosols.* Atmospheric Chemistry and Physics, 2017. **17**(8): p. 5379-5391.
41. Chen, J.J., Q. Ying, and M.J. Kleeman, *Source apportionment of wintertime secondary organic aerosol during the California regional PM10/PM2.5 air quality study.* Atmospheric Environment, 2010. **44**(10): p. 1331-1340.
42. Held, T., et al., *Modeling particulate matter in the San Joaquin Valley with a source-oriented externally mixed three-dimensional photochemical grid model.* Atmospheric Environment, 2004. **38**(22): p. 3689-3711.
43. Held, T., et al., *A comparison of the UCD/CIT air quality model and the CMB source-receptor model for primary airborne particulate matter.* Atmospheric Environment, 2005. **39**(12): p. 2281-2297.
44. Hixson, M., et al., *Influence of regional development policies and clean technology adoption on future air pollution exposure.* Atmospheric Environment, 2010. **44**(4): p. 552-562.
45. Hixson, M., et al., *Resolving the interactions between population density and air pollution emissions controls in the San Joaquin Valley, USA.* Journal of the Air & Waste Management Association, 2012. **62**(5): p. 566-575.
46. Hu, J., et al., *Mobile source and livestock feed contributions to regional ozone formation in Central California.* Environ Sci Technol, 2012. **46**(5): p. 2781-9.
47. Kleeman, M.J., et al., *Source apportionment of secondary organic aerosol during a severe photochemical smog episode.* Atmospheric Environment, 2007. **41**(3): p. 576-591.

48. Mahmud, A., Hixson, M., Hu, J., Zhao, Z., Chen, S. H., Kleeman, M. J., *Climate impact on airborne particulate matter concentrations in California using seven year analysis periods.* Atmospheric Chemistry and Physics, 2010. **10**(22): p. 11097-11114.
49. Mysliwiec, M.J. and M.J. Kleeman, *Source apportionment of secondary airborne particulate matter in a polluted atmospbere.* Environmental Science & Technology, 2002. **36**(24): p. 5376-5384.
50. Rasmussen, D.J., et al., *The Ozone-Climate Penalty: Past, Present, and Future.* Environmental Science & Technology, 2013. **47**(24): p. 14258-14266.
51. Ying, Q. and M.J. Kleeman, *Source contributions to the regional distribution of secondary particulate matter in California.* Atmospheric Environment, 2006. **40**(4): p. 736-752.
52. Zhang, H.L. and Q. Ying, *Source apportionment of airborne particulate matter in Southeast Texas using a source-oriented 3D air quality model.* Atmospheric Environment, 2010. **44**(29): p. 3547-3557.
53. Hu, J.L., et al., *Particulate air quality model predictions using prognostic vs. diagnostic meteorology in central California.* Atmospheric Environment, 2010. **44**(2): p. 215-226.
54. Nenes, A., S.N. Pandis, and C. Pilinis, *ISORROPIA: A new thermodynamic equilibrium model for multiphase multicomponent inorganic aerosols.* Aquatic Geochemistry, 1998. **4**(1): p. 123-152.
55. Mahmud, A., et al., *Climate impact on airborne particulate matter concentrations in California using seven year analysis periods.* Atmospheric Chemistry and Physics, 2010. **10**(22): p. 11097-11114.
56. Carter, W.P.L., *Development of a database for chemical mechanism assignments for volatile organic emissions.* Journal of the Air & Waste Management Association, 2015. **65**(10): p. 1171-1184.
57. Bai, E., B.Z. Houlton, and Y.P. Wang, *Isotopic identification of nitrogen hotspots across natural terrestrial ecosystems.* Biogeosciences, 2012. **9**(8): p. 3287-3304.
58. Wang, C., et al., *Growth in the global N-2 sink attributed to N fertilizer inputs over 1860 to 2000.* Science of the Total Environment, 2017. **574**: p. 1044-1053.
59. Fry, J.L., et al., *Observations of gas- and aerosol-phase organic nitrates at BEACHON-RoMBAS 2011.* Atmospheric Chemistry and Physics, 2013. **13**(17): p. 8585-8605.
60. Carlton, A.G., et al., *Model Representation of Secondary Organic Aerosol in CMAQv4.7.* Environmental Science & Technology, 2010. **44**(22): p. 8553-8560.
61. Rollins, A.W., et al., *Isoprene oxidation by nitrate radical: alkyl nitrate and secondary organic aerosol yields.* Atmospheric Chemistry and Physics, 2009. **9**(18): p. 6685-6703.
62. Fry, J.L., et al., *Organic nitrate and secondary organic aerosol yield from NO3 oxidation of beta-pinene evaluated using a gas-phase kinetics/aerosol partitioning model.* Atmospheric Chemistry and Physics, 2009. **9**(4): p. 1431-1449.
63. Herner, J.D., et al., *Dominant mechanisms that shape the airborne particle size and composition distribution in central California.* Aerosol Science and Technology, 2006. **40**(10): p. 827-844.
64. Businger, P.A., *MONITORING NUMERICAL STABILITY OF GAUSSIAN ELIMINATION.* Numerische Mathematik, 1971. **16**(4): p. 360-&.
65. Businger, J.A., et al., *FLUX-PROFILE RELATIONSHIPS IN ATMOSPHERIC SURFACE LAYER.* Journal of the Atmospheric Sciences, 1971. **28**(2): p. 181-&.

66. Myrup, L.O. and A.J. Ranzieri, *A consistent scheme for estimating diffusivities to be used in air quality models*. 1976, Federal Highway Administration Interim Report No. FHWA-CA-76-32.
67. Businger, J.A., *HEIGHT OF MIXED LAYER IN STABLY STRATIFIED PLANETARY BOUNDARY-LAYER.* Transactions-American Geophysical Union, 1974. **55**(3): p. 135-135.
68. Shir, C.C., *PRELIMINARY NUMERICAL STUDY OF ATMOSPHERIC TURBULENT FLOWS IN IDEALIZED PLANETARY BOUNDARY-LAYER.* Journal of the Atmospheric Sciences, 1973. **30**(7): p. 1327-1339.
69. Maaz, T.M., et al., *Inconsistencies undermine the conclusion that agriculture is a dominant source of NOx in California.* Science Advances, 2018. **4**(9).
70. Rasool, Q., J. Bash, and D. Cohan, *Mechanistic representation of soil nitrogen emissions in the Community Multi-scale Air Quality (CMAQ) model v 5.1.* Geoscientific Model Development, 2018. **in review**.
71. Van Drecht, G., et al., *Global modeling of the fate of nitrogen from point and nonpoint sources in soils, groundwater, and surface water.* Global Biogeochemical Cycles, 2003. **17**(4).
72. San Joaquin Valley Unified Air Pollution Control District, *2018 Plan for the 1997, 2006, and 2012 PM2.5 Standards*. 2018.